Final Report

Quantitative X-Ray Diffraction and Microstructural Analyses of Cementitious Materials

FDOT Contract Number: BDV25-977-15

Date: September 2017

Submitted to

Research Center (Research.center@dot.state.fl.us)

The Florida Department of Transportation

Research Center

605 Suwannee Street, MS 30

Tallahassee, FL 32399

c/o Dr. Harvey DeFord

Structural Materials Research Specialist

State Materials Office

5007 NE 39th Avenue

Gainesville, FL 32609

Phone: (352)955-6671

Email: Harvey.deford@dot.state.fl.us

Submitted by

Principal Investigator: Dr. A. Zayed

Department of Civil and Environmental Engineering

University of South Florida

4202 E Fowler Avenue; ENB 118

Tampa, FL 33620-5350

Email: zayed@usf.edu

DISCLAIMER

The opinions, findings, and conclusions expressed in this publication are those of the authors and not necessarily those of the State of Florida Department of Transportation (FDOT) or the U.S. Department of Transportation (USDOT) or the Federal Highway Administration (FHWA).

Approximate Conversions to SI Units (from FHWA)				
Symbol	**When You Know**	**Multiply By**	**To Find**	**Symbol**
Length				
in	inches	25.4	millimeters	mm
ft	feet	0.305	meters	m
yd	yards	0.914	meters	m
mi	miles	1.61	kilometers	km
Area				
in^2	square inches	645.2	square millimeters	mm^2
ft^2	square feet	0.093	square meters	m^2
yd^2	square yard	0.836	square meters	m^2
mi^2	square miles	2.59	square kilometers	km^2
Volume				
fl oz	fluid ounces	29.57	milliliters	mL
gal	gallons	3.785	liters	L
ft^3	cubic feet	0.028	cubic meters	m^3
yd^3	cubic yards	0.765	cubic meters	m^3
NOTE: volumes greater than 1000 L shall be shown in m^3				
Mass				
oz	ounces	28.35	grams	g
lb	pounds	0.454	kilograms	kg
Temperature (exact degrees)				
°F	Fahrenheit	5 (F-32)/9 or (F-32)/1.8	Celsius	°C
Illumination				
fc	foot-candles	10.76	lux	lx
fl	foot-Lamberts	3.426	candela/m^2	cd/m^2
Force and Pressure or Stress				
lbf	pound-force	4.45	newtons	N
lbf/in^2	pound-force per square inch	6.89	kilopascals	kPa

Technical Report Documentation Page

1. Report No.	2. Government Accession No.	3. Recipient's Catalog No.
4. Title and Subtitle Quantitative X-Ray Diffraction and Microstructural Analyses of Cementitious Materials		5. Report Date September 2017 6. Performing Organization Code
7. Author(s) A. Zayed and Yuriy Stetsko		8. Performing Organization Report No.
9. Performing Organization Name and Address Department of Civil and Environmental Engineering University of South Florida 4202 E Fowler Avenue; ENG 118 Tampa, FL 33620-5350		10. Work Unit No. 11. Contract or Grant No. BDV25-977-15
12. Sponsoring Agency Name and Address Florida Department of Transportation		13. Type of Report and Period Covered Final Report; 9/15/2014-9/30/2017 14. Sponsoring Agency Code
15. Supplementary Notes None		

16. Abstract

This study was initiated to establish a protocol that can be used on a routine basis to identify and quantify the mineralogy of portland cements (PC) and blended portland cements. For the latter, quantification of the supplementary cementitious materials (SCMs) content in a binary blended system was also an identified need. Towards satisfying the objectives, quantitative x-ray diffraction as well as optical microscopy were conducted. Two approaches for the data analyses of the collected x-ray diffraction scans were used; namely, calibration curves as well as Rietveld refinement coupled with Partial or No Known Crystal Structures (PONKCS) analyses. Three binary blended systems were studied here: PC-limestone, PC-ground granulated blast furnace slag (slag), and PC-Class F fly ash. Additionally, several commercial PCs, clinkers, limestones, slags, and Class F fly ash were analyzed. The findings indicate that quantitative x-ray diffraction using Rietveld refinement coupled with PONKCS analyses for amorphous phase quantification can render phase quantification of SCMs in the blended system with an accuracy within 1 wt.%. A protocol for routine analyses of blended binary systems has been established on laboratory binary blends. The outlined protocol was then tested on several binary commercial systems and found to be accurate in quantifying the SCM content in the blended systems studied here.

17. Keywords.	18. Distribution Statement
Clinker, portland cement, supplementary cementitious materials, X-ray diffraction, crystalline phases, amorphous content, phase quantification, Rietveld refinement, internal standard method, external standard method, calibration curve method, PONKCS method, scanning electron microscopy, optical microscopy.	No restrictions.

19. Security Classification (this report)	20. Security Classification (this page)	21. Pages	22. Price
Unclassified	Unclassified	181	

Form DOT F 1700.7 (8-72) Reproduction of completed page authorized

Acknowledgments

This work has been sponsored by the Florida Department of Transportation (FDOT). The Principal Investigator appreciates the valuable discussions with Dr. Harvey DeFord, Project Manager, and Mr. Michael Bergin, PE. The authors would like to thank Mr. Richard DeLorenzo with the FDOT State Materials Office (SMO) for his assistance with this research. The authors would like also to thank Dr. Natallia Shanahan, Post-Doctoral Scholar, in the Construction Materials Program at the Department of Civil and Environmental Engineering- University of South Florida for editing the report. The following technologist and students are also acknowledged for their contributions to this research through preparing and analyzing samples for optical microscopy: Ms. Delia De Leon Guajardo, Ms. Tanya Anisimova and Mr. Anthony Fromen.

EXECUTIVE SUMMARY

E1 Background

The mineralogical composition of portland cements is dependent on the composition of the raw materials used and the thermal processes employed in producing portland cement clinker. Since the raw materials and thermal processing used by cement plants can vary considerably, it follows that the mineralogical composition of cements can vary over time, for a given cement plant, and substantially for cements produced at different plants. The quality and durability of concrete elements depend to a large extent on the properties of the cement and cementitious materials used in concrete mixtures. Durability of concrete structures can therefore be improved by appropriately verifying and characterizing the mineralogical composition of the cementitious system used in structural concrete.

The importance of accurately determining cement composition cannot be overstated – development of concrete plastic and hardened properties is based on cement hydration, which is a physico-chemical process that is controlled by the phases present, their reactivity, and their chemical and mineralogical composition. With the use of chemical and mineral admixtures, phase composition of cement becomes even more important, as some admixtures are prone to generate undesirable interactions with some of the cement compounds, such as the aluminates.

The main purpose of this study was to establish a protocol to quantify accurately the mineralogy of portland cement and blended portland cement constituents using appropriate analytical technique(s) in order to improve the structural durability of concrete elements in the state of Florida.

E2 Research Objectives

The objectives of this investigation were to identify appropriate analytical techniques that can be adopted to routinely quantify the mineralogical characteristics of cementitious systems. Part of this process involved the establishment of protocols for routine characterization and quantification of portland cements and blended binary cementitious systems incorporating Class F fly ash, ground granulated blast furnace slag, and limestone. The objectives of this study were established to provide the Florida Department of Transportation (FDOT) with the tools necessary to conduct the mineralogical analyses needed to reliably qualify cementitious materials for use on

FDOT projects in the state of Florida, and to ensure adequate quality control of cementitious systems. This would place the State Materials Office (SMO) in a position to tailor the durability of concrete mixture designs and to develop and manage performance-based specifications. Without this research, the SMO will be limited in its ability to ensure the quality and durability of future Florida concrete structural elements.

E3 Main Findings

The findings of this study indicate that:

1. X-ray diffraction, coupled with Rietveld Refinement and PONKCS analyses, renders accurate quantification of slag and fly ash contents in blended cements with high precision and accuracy.
2. A step-by-step protocol was established for the quantification and analyses of portland cements, and the binary blends of portland cement-fly ash, portland cement-ground granulated blast furnace slag, and portland cement-limestone.

E4 Recommendations

Adoption of the outlined protocol for blended cementitious systems is highly recommended for the verification of the constituents of blended portland cement-SCM systems. This should directly enhance the durability of concrete elements in the infrastructure system of the state of Florida.

E5 Recommendations for Implementation of Results from this Study

Implementation of the results could be accomplished by the following:

1. Change FDOT specifications to require quantitative XRD analyses (QXRDA) of all cementitious materials as part of the acceptance program and for Quality Assurance procedures.
2. Coordinate with the Construction Materials Group in the Department of Civil and Environmental Engineering of the University of South Florida to host workshops for the characterization and phase analyses of portland cements and blended cementitious systems used by the state of Florida Department of Transportation.

The training received would enable FDOT personnel to perform QXRDA on cementitious raw materials at the State Materials Office (SMO).

TABLE OF CONTENTS

LIST OF FIGURES

LIST OF TABLES

Chapter 1. Literature Review

1.1 Introduction

Concrete performance and durability is known to be affected by its binder; namely, portland cement. Portland cement is a multiphase material, and as such, its properties and performance are primarily controlled by its constituents. While the main phases present in ordinary portland cement (OPC) have been well studied for about a century, variation and modification in its manufacturing technology and clinkering process continue to impose challenges on phase quantification.

The main and most predominately used phase identification and quantification technique of OPC is powder x-ray diffraction (XRD). Over the last decade, Rietveld refinement has become the most popular method for phase quantification, and current literature is replete with publications on application of this method to quantification of OPC [1-13], as well as supplementary cementitious materials (SCMs) [10, 14-27]. While the accuracy of cement quantification using Rietveld refinement is significantly higher than the traditional Bogue method [28] or the modified Bogue method [29, 30], there is still a debate in the literature [2, 4] regarding the accuracy of phase amounts obtained by Rietveld refinement. Frequently, it is said that the values obtained by Rietveld refinement represent the relative phase abundance rather than absolute values of phase content. While traditional single-peak methods allow each phase to be determined independently, the Rietveld method requires all phases present in the sample to be identified and included in the analysis. Presence of minor phases in OPC that may have been excluded from the analysis, and the presence of amorphous content in blended cements violate this underlying assumption of the Rietveld method, resulting in incorrect phase quantification. A number of methods have been proposed to overcome these issues, such as the use of an internal or external standard. A discussion of these methods, including their advantages and disadvantages, is presented in this literature review.

1.2 Powder X-ray Diffraction

Prior to discussing various methods of XRD data analysis, it is important to understand the inherent limitations and possible errors associated with collection of x-ray diffractograms in OPC

samples. It should be noted that aberrations associated with Bragg-Brentano parafocusing geometry, which is used by most commercial diffractometers, are not included in this discussion. A review of these aberrations and their effect on the collected diffractograms can be found in [31].

The XRD technique is based on the constructive interference of the diffracted beam by the ordered lattice structure of various crystalline phases in a material [31]. Since amorphous materials do not have an ordered structure, they cannot be directly identified by this technique. Although the presence of amorphous content in OPC is still a point of debate in the literature, this clearly presents a challenge in the analysis of blended cements, where a significant amorphous fraction is contributed by the addition of SCMs.

1.2.1 Phase Identification

Quantification of cement phases relies on identification of mineralogical phases in cement, and is typically performed by matching diffraction peaks produced by the sample to a database of powder diffraction files (PDF). Phase identification in portland cements is not a trivial problem. Main peaks for the major clinker phases suffer from severe peak overlap in the region of 31 to 35° 2θ (CuKα radiation). Moreover, identification of the correct crystal structure for each of the cement phases is complicated by 1) the existence of polymorphs for alite (C_3S), belite (C_2S), and C_3A, and 2) the typical variability of the C_4AF composition.

1.2.1.1 Extractions

The problem of peak overlap can be partially solved by performing selective dissolution (extraction) of clinker phases [13]. Combining selective dissolution with powder XRD has been shown to improve identification and quantification of phases present in low amounts in cementitious materials [32].

Gutteridge [33] proposed a procedure to dissolve aluminates and ferrites in an aqueous solution of sucrose and potassium hydroxide (KOSH extraction), which leaves a residue of C_3S, C_2S, alkali sulfates, and MgO [32]. Takashima [34] introduced a method of dissolving the silicates in a solution of salicylic acid in methanol (SAM), which leaves a residue of the aluminates, ferrites, and minor phases, such as periclase, carbonates, alkali sulfates, and double-alkali sulfates [32, 33].

Subsequently, Hjorth and Laurén [35] showed that solution concentration can be adjusted to dissolve most of the alite, leaving a residue containing belite in addition to aluminates and ferrites (modified SAM extraction). A combination of KOSH and modified SAM extractions can be used to isolate the belite phase. Silicate dissolution in a solution of maleic acid in methanol has also been proposed [36]; however, in the case of the presence of water in methanol, this method may involve problems with ettringite formation [37].

1.2.1.2 Polymorphism

C_3S is known to have seven (7) polymorphs: triclinic T1, T2, T3, monoclinic M1, M2, M3, and the rhombohedral high-temperature polymorph R [30]. The structure of the different alite polymorphs is complicated by the disorderly orientation of silicate ions [8]. However, industrial cements typically contain M1 and M3 polymorphs, which are stabilized at room temperature by the presence of sulfate or magnesium impurities [38]. Cements and clinkers can have almost pure M1 [39] or M3 [40] polymorphs, as well as a mixture of both polymorphs [8]. Although their diffraction patterns are very similar, Courtial et al. [41] suggested a procedure for visual identification of the alite polymorph based on observing the peak shape in several 2θ angular windows: 24.5° – 28.5°, 31.5° – 33.5°, 36° – 38°, and 51° – 53°. Maki and Goto [38] indicated that the alite polymorphs primarily depend on the relative amount of MgO and SO_3 in clinker. As was shown by Le Saoût *et al*. [8], increasing the SO_3 content in clinker causes an increase of the M1 polymorph content in the M1-M3 mixture, while MgO fosters formation of the M3 polymorph. Additionally, a recent investigation [42] showed that an increase in MgO content in clinker causes an increase of the total amount of alite phase in contrast to belite. Specifically, alite and belite contents are linearly related to the SO_3/MgO ratio.

C_2S has five (5) polymorphs: γ, β, α'_L, α'_H, and α [30]. In industrial clinkers, C_2S is typically present in the β-C_2S form, although the presence of α- and α'-C_2S polymorphs have also been reported [43, 44]. Gies and Knöfel [43] state that formation of α- and α'-C_2S is more likely in the alkali-rich clinkers, especially in the absence of sulfates. γ-C_2S can also be present in the kiln, although its formation on cooling is highly undesirable as it leads to "dusting" [30]. Although it is generally considered that the presence of even small amounts of impurities is sufficient to stabilize the β-C_2S polymorph and prevent its conversion to γ-C_2S on cooling, occurrence of kiln

dust is still a common phenomenon in the clinkering process. The C_2S polymorphs can be distinguished by observing the peaks in the 29 to 35° 2θ range [30, 32] on a belite-enriched extraction residue, as belite peaks in this range are overlapped by alite peaks.

Although pure C_3A has no polymorphs (it is cubic), some of the sodium ions can substitute for the calcium ions in C_3A structure during the clinkering process resulting in a compound with a general formula $Na_{2x}Ca_{3-x}Al_2O_6$ [30]. The cubic structure is maintained up to 2.4% Na_2O substitution, and changes to orthorhombic and subsequently monoclinic with increasing sodium content. Commercial clinkers can contain the cubic or orthorhombic forms of C_3A or a combination of both; occurrence of monoclinic C_3A has not been reported. As with the silicates, the diffraction patterns of the C_3A polymorphs are very similar, although they can be distinguished in the regions of 18-22° and 32-36° 2θ [30, 32]. Due to severe overlap with silicates in the 32-36° 2θ range, reliable polymorph identification requires the examination of SAM extraction residues.

The ferrite phase exists as a solid solution series with a general formula $Ca_2(Al_xFe_{1-x})_2O_5$, where $0<x<0.7$ [30]. Stutzman [32] lists brownmillerite ($Ca_2(Al,Fe)_2O_5$), srebrodol'skite ($Ca_2Fe_2O_5$), and $Ca_2Al_{1.38}Fe_{0.62}O_5$ as the most typical ferrite forms present in commercial clinkers. These compounds can be distinguished from differences in the diffraction peaks in the 12 to 34° 2θ range.

1.2.2 Phase Quantification

Quantitative XRD analysis of cements was initially based on comparison of measured intensities with pre-calculated x-ray reflection constants of pure clinker minerals using one or more reflections for each phase [36, 45, 47]. However, these simple approaches could not give reliable and accurate quantitative phase determination of cements. Cement phases suffer from overlapping peaks for a large number of reflections, and do not have enough distinct peaks for accurate phase quantification. This shortcoming was overcome by Rietveld [48, 49], who proposed a phase refinement based on a full-profile fitting procedure. This method was originally developed for neutron powder diffraction patterns; however, since this approach does not depend on the source of diffraction data, the Rietveld refinement technique was soon applied to powder x-ray diffraction [50, 51].

1.2.2.1 Full Pattern Quantification Methods – Rietveld Refinement

In the Rietveld method, a theoretical x-ray diffraction pattern is calculated based on the crystal structures of phases input by the user. The calculated pattern also includes the background calculation and various diffractometer parameters. The refinement is based on iterative comparison of the experimental pattern with the calculated one. The iterative process begins from presumed amounts of phases, and then all or part of the parameters can be adjusted during the refinement process to minimize the difference between the calculated intensity I_c and experimentally measured intensity I_m by least-squares fitting. The parameter $\sum_i (I_{mi} - I_{ci})^2 / I_{mi}$ is the subject of minimization. This parameter sums the normalized squared discrepancies, $(I_{mi} - I_{ci})^2$, over all points *i* along the angular range 2θ. Calculated intensity is a function of the following parameters: Rietveld scale factor S_p, structure factor F_K, peak profile function Φ_K, and preferred orientation function P_K. At the end of this iterative refinement process, the weight fraction W_p of each phase *p* is calculated according to:

$$W_p = \frac{S_p(ZMV)_p}{\sum_j S_j(ZMV)_j} 10^2 (\text{wt.}\%) \qquad \text{Equation 1-1}$$

where

S_p = the Rietveld scale factor

Z = are the number of formula units per unit cell

M = the mass of the formula unit

V = the unit-cell volume

j = the number of phases in the analysis [52, 53].

As can be seen from Equation 1-1, accurate calculation of the weight fraction of each phase requires all phases to be identified and included in the analysis. Omitting minor phases from the analysis can lead to overestimation of the phase abundance of the remaining structures. Therefore, all the phases must be identified prior to Rietveld quantification.

Peaks of minor phases present in small amounts will have low intensities and may be challenging to distinguish from the background. Statistical significance of a peak is determined by calculating the random counting error:

$$\sigma(N) = \sqrt{(R \cdot t)} \qquad \text{Equation 1-2}$$

where:

$\sigma(N)$ = the random counting error of x-ray quanta N

R = the counting rate (counts/s)

t = counting time (s).

From here, the 95% confidence interval (2σ) can be computed. Peak intensities of at least 2σ above the background are considered statistically significant [54]. The presence of minor phases may be missed in the analysis, especially if scans are collected with short counting times, which would increase $\sigma(N)$. The ability to resolve minor phases can be improved by preferentially dissolving some of the major clinker phases. Selective dissolutions, which are described earlier, can significantly improve identification of minor phases.

Overestimation of phase contents can also result from the presence of amorphous material. It has been suggested that amorphous content in OPC in excess of a few percent can be the result of the grinding process [55]. For blended cements, the supplemental cementitious materials added typically have high contents of amorphous material, and this content must be accounted for in order to obtain accurate phase composition values.

1.2.2.1.1. Amorphous/Unidentified Content Correction

Phase composition of cements determined by Rietveld refinement can only be considered as relative phase composition due to the presence of amorphous material. Various methods have been proposed to account for the presence of amorphous/unidentified content and account for amorphous content.

1.2.2.1.2. Internal Standard Method

The internal standard method is perhaps the most popular method of determining the amorphous/unidentified content of a sample [56, 57]. In this method, a material of high purity and known crystal structure is selected and mixed with the sample in known proportions. Madsen et al. [57] recommend using a material with a mass absorption coefficient similar to that of the sample to minimize microabsorption effects. Ideally, the material selected for use as an internal standard

should be completely crystalline, but could have a very low amorphous content. De La Torre et al. [58] determined that corundum is the best internal standard that does not introduce the additional amorphous content to the test material.

During the initial Rietveld refinement, the amount of internal standard is determined, together with the phases, according to Equation 1-1. Since the Rietveld method normalizes the amounts of crystalline phases included in the analysis to 100%, the amount of internal standard will be either overestimated compared to the amount added to the sample, or correctly determined. Overestimation indicates the presence of amorphous or unidentified content in the sample, while a correct amount of internal standard indicates that the sample is completely crystalline, and that all the phases have been identified and included in the analysis. It is possible to obtain an underestimated amount of internal standard; however, this indicates an error in the analysis [57]. In the case of overestimation, corrected weight percentages for each phase can be calculated:

$$Corr\left(W_p\right) = W_p \frac{STD_{known}}{STD_{measured}} \qquad \text{Equation 1-3}$$

where

Corr (W_p) = corrected weight percent of phase *p*

W_p = weight percent of phase *p* determined by Rietveld refinement

STD_{known} = weighed percentage of internal standard in the sample

$STD_{measured}$ = weight percentage of internal standard determined by Rietveld refinement

The amorphous or undetermined crystalline content ($W_{unknown}$) of the sample can then be calculated:

$$W_{unkown} = 100 - \sum_{j=1}^{n} W_j \qquad \text{Equation 1-4}$$

Several disadvantages of this method have been pointed out in the literature. First, because the internal standard has to be mixed in with the sample, homogenization, formation of additional amorphous content, and cement hydration during the mixing process can be of concern [9, 59, 60]. Proper mixing protocols should be followed to avoid homogenization issues and formation of amorphous content, such as one listed in ASTM C1365 [61]. Care should be taken to ensure that reagents used as a mixing medium are free from water to prevent hydration.

Second, Rietveld analysis can be affected when the mass absorption coefficients of the sample and standard materials differ significantly [57, 62]. Although most software packages allow the user to correct for microabsorption, incorrect application of microabsorption corrections have been shown to have a significant effect on phase quantification [63].

Third, small errors in determination of the amount of internal standard by Rietveld refinement ($STD_{measured}$) can translate into large errors in determination of small amorphous content [4]. Due to this, it is uncertain whether amorphous contents below 10% can be determined with any accuracy [4, 9, 64]. In order to minimize the effect of Rietveld error on the amorphous content determination, Westphal et al. [65] proposed increasing the amount of internal standard up to 50% for samples with low suspected amorphous contents. They showed that the optimal internal standard amount (W_s) is a function of the amorphous content ($W_{unknown}$):

$$W_S = \frac{100 - W_{unknown}}{200 - W_{unknown}}\ 10^2 (\text{wt.}\%) \qquad \text{Equation 1-5}$$

Equation 1-5 shows that 50% of internal standard is optimal for a sample with 1-10% of amorphous material. However, the downside of such high internal standard addition is dilution of the sample, which would significantly complicate identification of minor phases, thus potentially increasing the unidentified content of the sample. This can be overcome by performing an analysis on the actual sample to refine all the crystalline phases and then applying the determined parameters to the mixture of the sample with an internal standard [11, 58].

1.2.2.1.3. External Standard Method

Another commonly used method for correcting for amorphous/unidentified content is the use of an external standard. Again, a standard material is selected, although for the external standard method it can be a pure phase or a mixture with a known content of selected material [57]. An external standard is measured separately from the sample and is used to determine the experimental calibration factor (G) [9, 11, 57, 66]

$$G = \frac{S_S \rho_S V_S^2 \mu_S^*}{W_S} \qquad \text{Equation 1-6}$$

where S_S, ρ_S, V_S, μ_S^*, and W_S are respectively the Rietveld scale factor, density, unit cell volume, mass absorption coefficient, and crystalline weight fraction of the standard material in the external standard. Madsen et al. [57] state that this calibration factor "is dependent only on the instrumental and data collection conditions and is independent of individual phase and overall sample-related parameters." The calibration factor G is then used to determine the weight fractions of crystalline phases from Rietveld analysis of the sample

$$W_p = \frac{S_p \rho_p V_p^2 \mu^*_{Sample}}{G} \text{ (wt. \%)} \qquad \text{Equation 1-7}$$

where μ^*_{sample} is the mass absorption coefficient of the sample, which must be determined independently of the Rietveld analysis [9, 11]. Typically, μ^*_{sample} is calculated using the tabulated elemental mass absorption coefficients for oxides present in the sample as determined by x-ray fluorescence spectroscopy [9], although Compton scattering has also been suggested [67]. Loss on ignition content is treated as water, unless the presence of limestone is known, in which case it is attributed to CO_2 [56]. As in the case of internal standard, the amorphous/unidentified content is calculated by subtracting the sum of identified crystalline phases from 100% (Equation 1-4).

It can be seen from Equation 1-6 and Equation 1-7 that errors in determining the mass absorption coefficients of the external standard, the sample, or both can lead to errors in calculated phase amounts and in the amorphous/undermined content. Madsen et al. [57] reported that the accuracy of the external standard method in determining the amorphous content is significantly lower than that of the internal standard method. They found that a value of approximately 2% was obtained for the amorphous content by the external method when applied to a completely crystalline sample, while the internal standard yielded a value of 0.5%.

1.2.2.1.4. PONKCS Method

While internal and external methods provide an indirect measurement of amorphous/unidentified content, Scarlet and Madsen developed a direct method for quantification of phases with **p**artial **o**r **n**o **k**nown **c**rystal **s**tructure (PONKCS) [68]. As the name suggests, this method can be applied to quantify phases with partially-known structures, structures that deviate from published data, and phases with no known structures. The advantage of this method over the

indirect methods is that it potentially enables the user to separate the contribution of different phases to the amorphous/unidentified content. The following conditions must be met for the PONKCS method application: the unknown phase can be defined "as a related series of peaks" and the phase must be available in the pure form or as a major part of the sample. Peak intensities of the unknown phase are characterized by the empirical structure factors calculated via the Le Bail et al. curve fitting method [69], and a calibration mixture of the unknown phase with internal standard is prepared to determine the ZMV value for the unknown phase. In this method, $(ZMV)_{unknown}$ is treated as a "phase constant" and is calculated from the calibration by

$$(ZMV)_{unknown} = \frac{W_{unknown}}{W_s} \cdot \frac{S_s}{S_{unknown}} \cdot (ZMV)_s \qquad \text{Equation 1-8}$$

where

$W_{unknown}$ = known weight fraction of the unknown phase,

W_s = known weight fraction of the internal standard,

S_s = refined Rietveld scale factor for the internal standard, and

$S_{unknown}$ = refined Rietveld scale factor for the unknown phase.

After determining the phase constant for the unknown phase, a simulated crystal structure is created that can be used in the Rietveld analysis for quantification. Creation of the PONKCS phases database, in addition to the crystal structure databases, is highly important for direct phase quantification of all components of the sample [70]. This method is more applicable to blended cements than OPCs, since the amorphous content in OPCs cannot be described by a series of peaks, and the crystal structures are known for the minor phases. It can, however, be used in blended cements to quantify the contribution of SCMs to amorphous content [27].

1.2.2.1.5. Degree of Crystallinity

Degree of Crystallinity (DOC) is a standardless approach of determining the amorphous content, which was originally developed for samples with the same chemical composition containing both amorphous and crystalline fractions, although a correction has been proposed to account for differences in chemical composition [71]. This method separates the contribution of crystalline and amorphous material to peak intensities:

$$I^{corr}(s) = I_{cr}^{corr} + I_{amorphous}^{corr}(s) \quad \text{Equation 1-9}$$

where

$I^{corr}(s)$ = total intensity corrected for absorption and polarization

I_{cr}^{corr} = contribution of crystalline material to corrected intensities

$I_{amorphous}^{corr}$ = contribution of amorphous material to corrected intensities.

Crystalline and amorphous intensities are then integrated to obtain areas and the DOC is calculated as a ratio of crystalline to total area [57, 71]. A downside of this method is that all the crystalline phases are treated as one phase and so are the amorphous phases. A completely amorphous sample is highly desirable in order to separate amorphous scattering from Compton scattering, disorder and thermal scattering of the crystalline phase, and possible fluorescence of the crystalline phase. Since the chemical composition of cement phases is highly variable, this method has not found wide application in the analysis of cements and SCMs.

1.2.2.2 Single-Peak Quantification Methods

Although the traditional single-peak quantification methods have mostly been replaced by Rietveld refinement, they can be used to verify the accuracy of Rietveld quantification for one or several major clinker phases. As in the case of the internal standard method, overestimation of the weight fraction by Rietveld refinement can serve as an indication that amorphous/unidentified content is present in the sample.

1.2.2.2.1. Internal Standard Calibration Curve

The main disadvantage of the single-peak methods, as mentioned earlier, is an overlap of the main peaks of the clinker phases. Identification is especially difficult for low-intensity peaks, which can be hard to distinguish from the background noise and, therefore, the intensities are subject to counting errors [72]. However, counting time can be adjusted to minimize the random counting error according to Equation 1-2.

As in the Rietveld internal standard method, an internal standard material is selected and a known amount of internal standard is mixed with the sample. The analysis is based on the principle that the peak intensity of a phase, determined either as peak height or peak area, is directly

proportional to the amount of this phase in the sample, as described by the following equation [53, 73]:

$$\frac{I_{ij}}{I_{ks}} = K\frac{x_j}{x_s} \qquad \text{Equation 1-10}$$

where

I_{ij} = intensity of peak i of phase j

I_{ks} = intensity of peak k of the internal standard

x_j and x_s = weight fraction of the phase j and the internal standard respectively

K = constant.

Prior to sample analysis, a calibration curve is prepared by mixing known amounts of the phase of interest with the internal standard, where x_s, I_{ij}, and I_{ks} are plotted against x_j. At least three mixtures should be prepared with the expected minimum and maximum amounts of the phase of interest as well as a point halfway between the other points. If the mass absorption coefficients of the phase mixture and the internal standard are similar, the calibration curve will be linear. In the case of large differences in the mass absorption coefficients, the calibration curve will be nonlinear. In all cases, the calibration curve should pass through the (0,0) and (1,1) points [73].

1.2.2.2.2. Analysis by Dilution

Instead of preparing a calibration curve, a phase of interest can be quantified by adding a known amount of this phase in a pure form to the sample. This method is particularly suitable for quantification of phases present in small amounts. However, the challenge still exists with respect to successfully obtaining appropriate material for the phase of interest.

1.3 Other Quantification Techniques – Scanning Electron Microscopy and Optical Microscopy

Microscopy has been used in the quantification of clinker and cements. The literature indicates disagreement in the quantification of the aluminates and aluminoferrites in cements and clinker, using optical or scanning electron microscopy versus Rietveld-XRD quantitative analysis [74, 75]. This can be due to the difficulty in resolving the fine matrix using microscopy in addition

to resolving amorphous content [67]. Though microscopy gives information about the texture, size, and distribution of clinker and cement phases, it has limitations on the particle size that can be detected, in addition to the spatial resolution of energy dispersive spectroscopy.

1.4 Conclusions

Powder XRD, together with Rietveld (XRD-Rietveld) refinement analysis, has several important advantages compared to the other quantitative techniques of phase determination of cements in terms of repeatability and between-laboratory reproducibility [6, 7, 75], reliability and accuracy [1, 5, 8], rapidness, and accessibility.

1.5 References

[1] L. P. Aldridge, "Accuracy and precision of phase analysis in portland cement by Bogue, microscopic and X-ray diffraction methods," *Cem. Concr. Res.*, vol. 12, no. 3, pp. 381–398, 1982.

[2] J. C. Taylor and L. P. Aldridge, "Full-profile Rietveld quantitative XRD analysis of Portland cement : Standard XRD profiles for the major phase tricalcium silicate (C_3S: $3CaO.SiO_2$)," *Powder Diffr.*, vol. 8, no. 3, pp. 138–144, 1993.

[3] G. Walenta, T. Füllmann, and M. Gimenez, "Quantitative Rietveld analysis of cement and clinker," *Int. Cem. Rev.*, 2002.

[4] J. C. Taylor, L. P. Aldridge, C. E. Matulis, and I. Hinczak, "X-ray powder diffraction analysis of cements," in *Structure and Performance of Cements*, Second Edition., J. Bensted and P. Barnes, Eds. Spon Press, 2002, pp. 420–441.

[5] A. G. De La Torre and M. A. G. Aranda, "Accuracy in Rietveld quantitative phase analysis of Portland cements," *J. Appl. Crystallogr.*, vol. 36, pp. 1169–1176, 2003.

[6] P. E. Stutzman, "Powder diffraction analysis of hydraulic cements: ASTM Rietveld round-robin results on precision," *Powder Diffr.*, vol. 20, no. 02, pp. 97–100, Mar. 2005.

[7] L. León-Reina, A. G. De La Torre, J. M. Porras-Vázquez, M. Cruz, L. M. Ordonez, X. Alcobé, F. Gispert-Guirado, A. Larrãaga-Varga, M. Paul, T. Fuellmann, R. Schmidt, and

M. A. G. Aranda, “Round robin on Rietveld quantitative phase analysis of Portland cements,” *J. Appl. Crystallogr.*, vol. 42, pp. 906–916, 2009.

[8] G. Le Saoût, V. Kocaba, and K. Scrivener, “Application of the Rietveld method to the analysis of anhydrous cement,” *Cem. Concr. Res.*, vol. 41, no. 2, pp. 133–148, 2011.

[9] D. Jansen, C. Stabler, F. Goetz-Neunhoeffer, S. Dittrich, and J. Neubauer, “Does Ordinary Portland Cement Contain Amorphous Phase? A Quantitative Study Using an External Standard Method,” *Powder Diffr.*, vol. 26, no. 01, pp. 31–38, Mar. 2012.

[10] G. Walenta and T. Füllmann, “Advances in quantitative XRD analysis for clinker, cements, and cementitious additions,” *Powder Diffr.*, vol. 19, no. 01, pp. 40–44, Mar. 2012.

[11] M. A. G. Aranda, A. G. De la Torre, and L. Leon-Reina, “Rietveld Quantitative Phase Analysis of OPC Clinkers, Cements and Hydration Products,” *Reviews in Mineralogy and Geochemistry*, vol. 74, no. 1. pp. 169–209, 2012.

[12] N. V. Y. Scarlett, I. C. Madsen, C. Manias, and D. Retallack, “On-line X-ray diffraction for quantitative phase analysis: Application in the Portland cement industry,” *Powder Diffr.*, vol. 16, no. 02, pp. 71–80, Mar. 2012.

[13] R. Snellings, A. Bazzoni, and K. Scrivener, “The existence of amorphous phase in Portland cements: Physical factors affecting Rietveld quantitative phase analysis,” *Cem. Concr. Res.*, vol. 59, pp. 139–146, May 2014.

[14] T. Westphal, G. Walenta, T. Füllmann, M. Gimenez, E. Bermejo, K. L. Scrivener, and H. Pöllmann, “Characterisation of cementitious materials,” *Int. Cem. Rev.*, pp. 47–51, 2002.

[15] E. Sakai, S. Miyahara, S. Ohsawa, S. H. Lee, and M. Daimon, “Hydration of fly ash cement,” *Cem. Concr. Res.*, vol. 35, pp. 1135–1140, 2005.

[16] S. Hoshino, K. Yamada, and H. Hirao, “XRD/Rietveld Analysis of the Hydration and Strength Development of Slag and Limestone Blended Cement,” *J. Adv. Concr. Technol.*, vol. 4, no. 3, pp. 357–367, 2006.

[17] A. Korpa, T. Kowald, and R. Trettin, “Phase development in normal and ultra high performance cementitious systems by quantitative X-ray analysis and thermoanalytical methods,” *Cem. Concr. Res.*, vol. 39, no. 2, pp. 69–76, Feb. 2009.

[18] P. Termkhajornkit, T. Nawa, Y. Yamashiro, and T. Saito, “Self-healing ability of fly ash–cement systems,” *Cem. Concr. Compos.*, vol. 31, no. 3, pp. 195–203, Mar. 2009.

[19] M. Narmluk and T. Nawa, “Effect of fly ash on the kinetics of Portland cement hydration at different curing temperatures,” *Cem. Concr. Res.*, vol. 41, no. 6, pp. 579–589, Jun. 2011.

[20] K. De Weerdt, K. O. Kjellsen, E. Sellevold, and H. Justnes, “Synergy between fly ash and limestone powder in ternary cements,” *Cem. Concr. Compos.*, vol. 33, no. 1, pp. 30–38, 2011.

[21] K. De Weerdt, M. Ben Haha, G. Le Saout, K. O. Kjellsen, H. Justnes, and B. Lothenbach, “Hydration mechanisms of ternary Portland cements containing limestone powder and fly ash,” *Cem. Concr. Res.*, vol. 41, no. 3, pp. 279–291, 2011.

[22] H. Sun, B. Hohl, Y. Cao, C. Handwerker, T. S. Rushing, T. K. Cummins, and J. Weiss, “Jet mill grinding of portland cement, limestone, and fly ash: Impact on particle size, hydration rate, and strength,” *Cem. Concr. Compos.*, vol. 44, pp. 41–49, 2013.

[23] S. Kumar, A. Bandopadhyay, V. Rajinikanth, T. C. Alex, and R. Kumar, “Improved processing of blended slag cement through mechanical activation,” *J. Mater. Sci.*, vol. 39, pp. 3449–3452, 2004.

[24] S. Kumar, R. Kumar, A. Bandopadhyay, T. C. Alex, B. Ravi Kumar, S. K. Das, and S. P. Mehrotra, “Mechanical activation of granulated blast furnace slag and its effect on the properties and structure of portland slag cement,” *Cem. Concr. Compos.*, vol. 30, pp. 679–685, 2008.

[25] Y. Nakanishi, H. Tanaka, and M. Yamashita, “Rapid Determination of Blast-Furnace Slag Content in Portland Blast-Furnace Slag Cement Using Powder XRD-Rietveld Analysis,” *Cem. Sci. Concrete Technol.*, no. 64, pp. 582–587, 2010.

[26] V. Kocaba, E. Gallucci, and K. L. Scrivener, “Methods for determination of degree of reaction of slag in blended cement pastes,” *Cem. Concr. Res.*, vol. 42, no. 3, pp. 511–525, 2012.

[27] R. Snellings, A. Salze, and K. L. Scrivener, “Use of X-ray diffraction to quantify amorphous supplementary cementitious materials in anhydrous and hydrated blended cements,” *Cem. Concr. Res.*, vol. 64, pp. 89–98, 2014.

[28] R. H. Bogue, “Calculation of the compounds in Portland Cement,” *Ind. Eng. Chem. Anal. Ed.*, vol. 1, no. 4, pp. 192–197, 1929.

[29] H. Taylor, “Modification of the Bogue Calculation,” *Adv. Cem. Res.*, vol. 2, no. 6, pp. 73–77, 1989.

[30] H. F. W. Taylor, *Cement Chemistry*, 2nd ed., London, UK: Thomas Telford Publishing, 1997.

[31] Y. Leng, *Materials Characterization: Introduction to Microscopic and Spectroscopic Methods*, 2nd ed., Singapore: Wiley-VCH, 2013, p. 376.

[32] P. E. Stutzman, “Guide for X-Ray Powder Diffraction Analysis of Portland Cement and Clinker,” Gaithersburg, MD, 1996.

[33] W. A. Gutteridge, “On the Dissolution of the Interstitial Phases in Portland Cement,” *Cem. Concr. Res.*, vol. 9, no. 3, pp. 319–324, 1979.

[34] S. Takashima, “Systematic dissolution of calcium silicate in commercial Portland cement by organic acid solution,” *Rev. 12th Gen. Meet. Cem. Assoc. Japan, Tokyo*, pp. 12–13, 1958.

[35] L. Hjorth and K. Laurén, “Belite in portland cement,” *Cem. Concr. Res.*, vol. 1, pp. 27–40, 1971.

[36] A. A. Tabikh and R. J. Weht, “An X-ray diffraction analysis of Portland cement,” *Cem. Concr. Res.*, vol. 2, no. 1, p. 159, 1972.

[37] L. Struble, “The effect of water on maleic acid and salicylic acid extractions,” *Cem. Concr. Res.*, vol. 15, pp. 631–636, 1085.

[38] I. Maki and K. Goto, “Factors influencing the phase constitution of alite in Portland cement clinker,” *Cem. Concr. Res.*, vol. 12, no. 3, pp. 301–308, 1982.

[39] M.-N. de Noirfontaine, F. Dunstetter, M. Courtial, G. Gasecki, and M. Signes-Frehel, “Polymorphism of tricalcium silicate, the major compound of Portland cement clinker,” *Cem. Concr. Res.*, vol. 36, no. 1, pp. 54–64, Jan. 2006.

[40] Á. G. De La Torre, S. Bruque, J. Campo, and M. A. G. Aranda, “The superstructure of C_3S from synchrotron and neutron powder diffraction and its role in quantitative phase analyses,” *Cem. Concr. Res.*, vol. 32, no. 9, pp. 1347–1356, 2002.

[41] M. Courtial, M.-N. de Noirfontaine, F. Dunstetter, G. Gasecki, and M. Signes-Frehel, “Polymorphism of tricalcium silicate in Portland cement: a fast visual identification of structure and superstructure,” *Powder Diffr.*, vol. 18, no. 1, pp. 7–15, 2003.

[42] X. Li, W. Xu, S. Wang, M. Tang, and X. Shen, “Effect of SO_3 and MgO on Portland cement clinker: Formation of clinker phases and alite polymorphism,” *Constr. Build. Mater.*, vol. 58, pp. 182–192, May 2014.

[43] A. Gies and D. Knöfel, “Influence of alkalies on the composition of belite-rich cement clinkers and the technological properties of the resulting cements,” *Cem. Concr. Res.*, vol. 16, no. 3, pp. 411–422, 1986.

[44] S. N. Ghosh, P. B. Rao, A. K. Paul, and K. Raina, “The chemistry of dicalcium silicate mineral,” *J. Mater. Sci.*, vol. 14, no. 7, pp. 1554–1566, 1979.

[45] É. Péter, “Die quantitative bestimmung der klinkermineralien mit dem diffraktometer,” *Cem. Concr. Res.*, vol. 1, no. 1, pp. 105–111, 1971.

[46] M. Kristmann, “Portland cement clinker: Mineralogical and chemical investigations: Part I Microscopy, X-ray fluorescence and X-ray diffraction,” *Cem. Concr. Res.*, vol. 7, no. 6, pp. 649–658, 1977.

[47] T. Knudsen, “Quantitative analysis of the compound composition of cement and cement clinker by X-Ray Diffraction,” *Bull. Am. Ceram. Soc.*, vol. 55, no. 12, pp. 1052–1054, 1976.

[48] H. M. Rietveld, “Line profiles of neutron powder-diffraction peaks for structure refinement,” *Acta Crystallogr.*, vol. 22, pp. 151–152, 1967.

[49] H. M. Rietveld, “A Profile Refinement Method for Nuclear and Magnetic Structures,” *J. Adv. Concr. Technol.*, vol. 2, pp. 65–71, 1969.

[50] G. Malmros and J. D. Thomas, “Least squares structure refinement based on powder film intensity data,” *J. Appl. Crystallogr.*, vol. 10, pp. 107–111, 1977.

[51] R. A. Young, D. Mackie, and R. B. von Dreele, “Application of the pattern fitting structure refinement method to X-ray powder diffractometer pattern,” *J. Appl. Crystallogr.*, vol. 10, pp. 262–269, 1977.

[52] R. Hill and C. Howard, “Quantitative phase analysis from neutron powder diffraction data using the Rietveld method,” *J. Appl. Crystallogr.*, vol. 20, pp. 467–474, 1987.

[53] R. L. Snyder and D. L. Bish, “Quantitative Analysis,” in *Modern Powder Diffraction*, D. L. Bish and J. E. Post, Eds. Reviews in Mineralogy, 20, Mineralogical Society of America, 1989, pp. 101–144.

[54] R. Jenkins, “Experimental Procedures,” in *Modern Powder Diffraction*, D. L. Bish and J. E. Post, Eds. Washington, DC: The Mineralogical Society of America, 1989, pp. 47–71.

[55] J. P. Cline, R. B. Von Dreele, R. Winburn, P. W. Stephens, and J. J. Filliben, “Addressing the amorphous content issue in quantitative phase analysis: the certification of NIST standard reference material 676a.,” *Acta Crystallogr. A.*, vol. 67, no. Pt 4, pp. 357–67, Jul. 2011.

[56] R. Snellings, A. Bazzoni, and K. Scrivener, “The existence of amorphous phase in Portland cements: Physical factors affecting Rietveld quantitative phase analysis,” *Cem. Concr. Res.*, vol. 59, pp. 139–146, 2014.

[57] I. C. Madsen, N. V. Y. Scarlett, and A. Kern, “Description and survey of methodologies for the determination of amorphous content via X-ray powder diffraction,” *Zeitschrift für Krist.*, vol. 226, no. 12, pp. 944–955, Dec. 2011.

[58] A. G. De La Torre, S. Bruque, and M. A. G. Aranda, “Rietveld quantitative amorphous content analysis,” *J. Appl. Crystallogr.*, vol. 34, pp. 196–202, 2001.

[59] D. Jansen, F. Goetz-Neunhoeffer, C. Stabler, and J. Neubauer, “A remastered external standard method applied to the quantification of early OPC hydration,” *Cem. Concr. Res.*, vol. 41, no. 6, pp. 602–608, Jun. 2011.

[60] D. Jansen, S. T. Bergold, F. Goetz-Neunhoeffer, and J. Neubauer, “The hydration of alite: A time-resolved quantitative XRD approach using the G-factor method compared with heat release,” *J. Appl. Crystallogr.*, vol. 44, pp. 895–901, 2011.

[61] ASTM Standard C1365 2006 (2011), *Standard Test Method for Determination of the Proportion of Phases in Portland Cement and Portland-Cement Clinker Using X-Ray Powder Diffraction Analysis*. West Conshohocken, Pa.: ASTM International, 2012.

[62] H. Hermann and M. Ermrich, “Microabsorption Correction of X-Ray Intensities Diffracted by Multiphase Powder Specimens,” *Powder Diffr.*, vol. 4, no. 4, pp. 189–195, 1989.

[63] I. C. Madsen, N. V. Y. Scarlett, L. M. D. Cranswick, and T. Lwin, “Outcomes of the International Union of Crystallography Commission on Powder Diffraction Round Robin on Quantitative Phase Analysis: samples 1a to 1h,” *J. Appl. Crystallogr.*, vol. 34, no. 4, pp. 409–426, Jul. 2001.

[64] G. Le Saoût, T. Füllmann, V. Kocaba, and K. L. Scrivener, “Quantitative study of cementitious materials by X-ray diffraction/ Rietveld analysis using an external standard,” *Proc. 12th Int. Congr. Chem. Cem. Montréal, Canada*, pp. TH2–07.01, 2007.

[65] T. Westphal, T. Füllmann, and H. Pöllmann, “Rietveld quantification of amorphous portions with an internal standard—Mathematical consequences of the experimental approach,” *Powder Diffr.*, vol. 24, no. September, pp. 239–243, 2009.

[66] B. H. O’Connor and M. D. Raven, “Application of the Rietveld Refinement Procedure in Assaying Powdered Mixtures,” *Powder Diffr.*, vol. 3, no. 01, pp. 2–6, Jan. 1988.

[67] P. M. Suherman, A. van Riessen, B. O’Connor, D. Li, D. Bolton, and H. Fairhurst, “Determination of amorphous phase levels in Portland cement clinker,” *Powder Diffr.*, vol. 17, no. 3, pp. 178–185, 2002.

[68] N. V. Y. Scarlett and I. C. Madsen, “Quantification of phases with partial or no known crystal structures,” *Powder Diffr.*, vol. 21, no. 4, pp. 278–284, Mar. 2006.

[69] A. Le Bail, H. Duroy, and J. L. Fourquet, “Ab-initio structure determination of LiSbWO6 by X-Ray powder diffraction,” *Mat. Res. Bull.*, vol. 23, pp. 447–452, 1988.

[70] M. Leoni, “Uniting Electron Crystallography and Powder Diffraction,” *Uniting Electron Crystallogr. Powder Diffr.*, pp. 173–182, 2012.

[71] P. Riello, “Quantitative Analysis of Amorphous Fraction in the Study of the Microstructure of Semi-crystalline Materials,” in *Diffraction Analysis of the Microstructure of Materials*, E. Mittemeijer and P. Scardi, Eds. Springer, 2004, pp. 167–186.

[72] I. C. Madsen and N. V. Y. Scarlett, “Cement: Quantitative Phase Analysis of Portland Cement Clinker,” in *Industrial Applications of X-Ray Diffraction*, F. H. Chung and D. K. Smith, Eds. New York, NY: Marcel Dekker, 2000, pp. 415–440.

[73] H. P. Klug and L. E. Alexander, *X-Ray Diffraction Procedures*, Second Edition. Wiley Interscience, 1974, p. 966.

[74] P. Stutzman, G. Lespinasse and S. Leigh, "Compositional Analysis and Certification of NIST Reference Material Clinker 2686a," US Department of Commerce, 2008.

[75] P. Stutzman and S. Leigh, “Phase analysis of hydraulic cements by X-ray powder diffraction: precision, bias, and qualification,” *J. ASTM Int.*, vol. 4, pp. 1–11, 2007.

Chapter 2. General Methodologies for Sample Preparation and Refinement

2.1 Introduction

Quantitative x-ray diffraction analysis of clinkers, cements, SCMs and other materials consists of several steps: preparation of a powdered sample from the material of interest, data collection, and Rietveld refinement analysis. These steps have some specific demands and features. The powder sample preparation requires the grinding of the as-received materials to a fineness of about 1 - 10 μm to minimize the Brindley micro absorption effect [1]. The back-loading technique [2] of powders into the sample holder minimizes preferred orientation effects for some specific phases. Sample spinning, in a direction normal to the sample surface, during data collection, enhances particle statistics for better reproducibility of the measured intensity [3]–[6]. Several approaches for Rietveld analysis have been proposed in the literature [5]–[8]. These approaches have some common and specific features in the order and number of parameters that should be refined; namely, scale factors, lattice parameters, zero shift or specimen displacement, polynomial or Chebyshev polynomial coefficients for background fitting, preferred orientation for some specific phases, and peak shape parameters. This chapter describes the methodologies common for most powder x-ray diffraction studies, while the specific methodologies are given in subsequent chapters.

2.2 Methodology of Sample Preparation

2.2.1 Powder Sample Preparation

The as-received materials used in this study were: clinkers, portland cements (PC), Class F fly ash, ground granulated blast furnace slag, limestones, and blended cements (PC-Class F fly ash, PC-slag, and PC- limestone). Initially, the as-received materials were ground using a mortar and pestle to obtain a powder finer than 45 microns (passing #325 sieve). All materials were ground for about 10 minutes to a particle size less than 10 μm in a McCrone Micronizing Mill with the addition of approximately 2 ml of nonaqueous solvent (200 proof ethanol) for each gram of powdered sample.

2.2.2 Mixtures of Materials

To ensure proper mixture homogeneity, the ASTM C1365-06 protocol [9], was adopted here. Powdered specimens containing more than one material and/or mixtures containing the internal standard, corundum SRM 676*a*, were mixed for approximately 10 minutes using a Micronizing Mill with the addition of approximately 5 ml of a nonaqueous solvent (200 proof ethanol) for each gram of powder.

2.2.3 Selective Extraction of Clinkers and Portland Cements

Selective dissolution is typically adopted in the mineralogical analyses of the crystalline phases of clinkers and portland cements. It has been indicated that peak profile parameters and lattice constants are better acquired through the use of selective dissolution of the aluminate and silicate phases, as well as phases that are present in minor amounts, such as alkali sulfates [10]. The main extraction procedures typically used in phase analyses of cements and clinkers are presented in the following sections.

2.2.3.1 Potassium Hydroxide/Sugar (KOSH) Extraction

The KOSH extraction dissolves the aluminate and ferrite phases and leaves a residue of silicate phases (alite, belite) and some minor phases. The KOSH extraction procedure adopted from reference [10] is:

(i) Prepare a KOSH solution of 30 g of potassium hydroxide and 30 g of sucrose in 300 ml of deionized water as follows: place 30 g of potassium hydroxide (Fisher Scientific, CAS#1310-58-3) and 30 g of sucrose (Fisher Scientific, CAS#57-50-1) into a flask and fill it with 300 ml of deionized water, then mix the solution (in a fume hood) using a stirring rod until completely dissolved and there are no solids in solution;

(ii) Heat the solution up to 95°C using a hot plate with a magnetic stirring bar, mixing the solution as it heats;

(iii) Add about 9 grams of the as-received cement into the solution, then use a stopper to close the flask and mix the solution for 1 minute;

(iv) Vacuum filter the solution, for about 0.5 – 3 hours at ~ 340 mm Hg, using a 0.45 μm filter (Durapore membrane filter, Merck Millipore LTD) and Buchner funnel;

(v) Wash the residue with 50 ml of water followed by 100 ml of methanol (reagent grade 99.8 pure, Alfa Aesar, CAS#67-56-1). Then dry the residue at 60°C for about 24 hours, and store in a vacuum desiccator.

The KOSH extraction retains the following phases: alite, belite, periclase, brucite, magnesite, merwinite, akermanite, monticellite, portlandite, calcite, dolomite, lime, quartz, wollastonite, rankinite, ternesite, ellesteadite, and fluorellestadite. The chemical formulas, PDF and ICSD codes of the KOSH clinker and cement residue phases are shown in Table 2-1 [5], [6], [10].

Table 2-1: KOSH Residue Structures

Phase	Formula	Crystal System	PDF codes	ICSD Code
Alite	**Ca_3SiO_5-Mg, Al**	**Monoclinic/M3**	**01-070-8632**	**94742**
	Ca_3SiO_5	Monoclinic/M3	01-085-1846	64759
	Ca_3SiO_5	Monoclinic	01-086-0402	81100
	Ca_3SiO_5	Triclinic/T1	01-070-1846	4331
Belite	**Ca_2SiO_4**	**Monoclinic/β**	**01-086-0398**	**81096**
	Ca_2SiO_4	Monoclinic/β	01-083-0460	79550
	Ca_2SiO_4	Orthorhombic/α	01-086-0399	81097
	Ca_2SiO_4	Orthorhombic/γ	01-086-0397	81095
Periclase	**MgO**	**Cubic**	**01-071-1176**	**9863**
	MgO	Cubic	00-045-0946	104844
Brucite	$Mg(OH)_2$	Rhombohedral	00-007-0239	28275
Magnesite	$CMgO_3$	Rhombohedral	00-008-0479	63663
Merwinite	$Ca_3Mg(SiO_4)_2$	Monoclinic	01-089-2432	43078
Akermanite	$Ca_2Mg(Si_2O_7)$	Tetragonal	00-035-0592	158177
Monticellite	$CaMg(SiO_4)$	Orthorhombic	00-035-0590	34591
Portlandite	**$Ca(OH)_2$**	**Rhombohedral**	**01-072-0156**	**15471**
	$Ca(OH)_2$	Rhombohedral	00-004-0733	43433
Calcite	**CaCO3**	**Rhombohedral**	**01-086-0174**	**80869**
	CaCO3	Rhombohedral	01-083-0577	79673
Dolomite	**$CaMg(CO_3)_2$**	**Rhombohedral**	**01-075-1711**	**31277**
	$CaMg(CO_3)_2$	Trigonal	01-075-1761	31335
Lime	CaO	Cubic	01-071-4121	52783
	CaO	Cubic	00-043-1001	75785
	CaO	Cubic	00-037-1497	75785
Quartz	**SiO_2**	**Rhombohedral**	**00-046-1045**	**41414**
	SiO_2	Rhombohedral	01-083-2465	200721
Wollastonite	$CaSiO_3$	Monoclinic	00-043-1460	30884
Rankinite	$Ca_3Si_2O_7$	Monoclinic	01-070-1138	2282
Ternesite	$Ca_5(SiO_4)_2(SO_4)$	Orthorhombic	01-088-0812	85123
Ellesteadite	$Ca_{10}(SiO_4)_3(SO_4)_3Cl_2$	Hexagonal	00-041-0479	154205
Fluorellestadite	$Ca_{10}(SiO_4)_3(SO_4)_3F_2$	Hexagonal	01-072-7301	97203

The structures used in the Rietveld refinement analysis are indicated in Table 2-1 by bold letters.

2.2.3.2 Salicylic Acid/Methanol (SAM) Extraction

The SAM extraction dissolves the silicate phases and free lime, leaving a residue of aluminates, ferrites, and some minor phases. The SAM extraction procedure, as adopted from reference [10], is:

(i) Prepare a SAM solution of 20 g of salicylic acid (reagent grade 99% pure, Sigma-Aldrich, CAS#69-72-7) in 300 ml of methanol (reagent grade 99.8+ pure, Alfa Aesar, CAS#67-56-1) as follows: place 20 g of the salicylic acid and 300 ml of methanol into a flask, then mix solution (in fume hood) using a standing mixer, operated at medium speed, until the solution is clear and there is no solid;

(ii) Add about 5 grams of the as-received cement into the solution, then stopper the flask and mix the solution for two hours using a standing mixer at medium speed;

(iii) Allow the solution to settle for about 15 minutes;

(iv) Vacuum filter (for about 0.5 – 3 hours) the solution (~ 340 mm Hg) using a 0.45 μm filter (Durapore membrane filter, Merck Millipore LTD) and Buchner funnel;

(v) Wash the residue using enough methanol to cover the residue and mix until the residue is suspended. Move the residue onto a glass plate, dry at 90°C for about 24 hours, and store in a vacuum desiccator.

The SAM residue can include the following phases: aluminate, ferrite, periclase, srebrodolskite, calcite, dolomite, diopside, arcanite, potassium sulfate (alpha), aphthitalite, Ca-langbenite, syngenite, metathenardite, thenardite, mirabilite, potassium calcium sulfate, brucite, magnesite, gypsum, hemihydrate, soluble anhydrite, anhydrite, anhydrite-III, and anhydrite-II. The chemical formulas, PDF numbers, and ICSD codes of the SAM clinker and cement residue phases are shown in Table 2-2 [5], [6], [10].

Table 2-2: SAM Residue Structures

Phase	Formula	Crystal System	PDF codes	ICSD Code
Aluminate	**$Ca_3Al_2O_6$**	**Cubic**	**01-070-0839**	**1841**
	$Ca_{8.5}NaAl_6O_{18}$	Orthorhombic	01-083-1359	100220
	$Ca_{8.5}NaAl_6O_{18}$	Orthorhombic	00-032-0150	1880
	$Ca_{8.25}Na_{1.5}Al_6O_{18}$	Monoclinic	01-083-1360	100221
Ferrite	**Ca_2AlFeO_5**	**Orthorhombic**	**01-071-0667**	**9197**
Srebrodolskite	$Ca_2Fe_2O_5$	Orthorhombic	00-038-0408	14296
Calcite	**CaCO3**	**Rhombohedral**	**01-086-0174**	**80869**
	CaCO3	Rhombohedral	01-083-0577	79673
Dolomite	**$CaMg(CO_3)_2$**	**Rhombohedral**	**01-075-1711**	**31277**
Diopside	**$CaMgSi_2O_6$**	**Monoclinic**	**01-071-1067**	**9672**
Arcanite	**K_2SO_4**	**Orthorhombic**	**01-083-0681**	**79777**
	K_2SO_4	Orthorhombic	01-070-1488	2827
Potassium Sulfate (α)	K_2SO_4	Hexagonal	00-025-0681	2408
Aphthitalite	**$K_3Na(SO_4)_2$**	**Rhombohedral**	**01-074-0398**	**26018**
Ca-Langbenite	$Ca_2K_2(SO_4)_3$	Orthorhombic	01-074-0404	40989
Syngenite	**$K_2Ca(SO_4)_2H_2O$**	Monoclinic	**00-028-0739**	**157072**
Metathenardite	**Na_2SO_4**	Hexagonal	**01-078-1883**	**63077**
Thenardite	Na_2SO_4	Orthorhombic	00-037-1465	81506
Mirabilite	$H_{20}Na_2O_{14}S$	Monoclinic	00-011-0647	15867
Potassium Calcium Sulfate	**$Ca_2K_2O_{12}S_3$**	**Orthorhombic**	**00-020-0867**	**40989**
Periclase	**MgO**	**Cubic**	**01-071-1176**	**9863**
	MgO	Cubic	00-045-0946	104844
Brucite	$Mg(OH)_2$	Rhombohedral	00-007-0239	28275
Magnesite	$CMgO_3$	Rhombohedral	00-008-0479	63663
Quartz	**SiO_2**	**Rhombohedral**	**00-046-1045**	**41414**
	SiO_2	Rhombohedral	01-083-2465	200721
Gypsum	**$CaSO_4(H_2O)_2$**	**Monoclinic**	**00-033-0311**	**151692**
Hemihydrate	**$CaSO_4(H_2O)_{0.5}$**	**Monoclinic**	**01-083-0438**	**79528**
	$CaSO_4(H_2O)_{0.5}$	Monoclinic	00-041-0224	380286
Anhydrite	**$CaSO_4$**	**Orthorhombic**	**01-086-2270**	**40043**
Anhydrite-III	**$CaSO_4$**	**Hexagonal**	**01-073-1942**	**24473**
Anhydrite-II	$CaSO_4$	Orthorhombic	01-072-0916	16382

The structures used in the Rietveld refinement analysis are indicated in Table 2-2 by bold letters.

2.3 XRD Data Collection and Analysis.

XRD scans for all materials studied here were collected in accordance with ASTM C1365-06 specifications. The following identifies the diffractometer settings used in data collection:

2.3.1 Instrument Settings

- Diffractometer: Phillips X'Pert PW3040 Pro
  Goniometer: θ - 2θ , radius 240 mm
  Source: CuKα radiation, line focus
  Generator: 45 kV, 40 mA

- Sample:
  Surface diameter: 16 mm
  Spinning rate (rpm) 30
  Preparation: Back-loading

- Incident optics:
  Programmable divergence slit: 5 mm (automatic)
  Soller slit: 0.04 radians
  Mask (horizontal divergence slit): 10 mm

- Receiving optics:
  Programmable anti-scatter slit: 5 mm (automatic)
  Soller slit: 0.02 radians
  Detector: X'Celerator Scientific

- Scan info:
- Angular range (2θ): 7 - 70°
  Step (2θ): 0.0167°
  Length of linear detector (2θ): 2.122°
  Counting time per step (s): 130.2

Automatic slits were used in the incident and receiving optics to reduce scattering from the metal holder that can occur when using fixed slit settings at the low angular 2θ range of about 5 - 20° [11]. The peak fit procedure, the crystalline phases search and match procedure, and the

Rietveld refinement analysis of the collected x-ray scans were all performed using versions 3.0 and 4.5 of HighScore Plus software.

2.3.2 Crystalline Phases Search and Match Procedure/Strategy

The search and match procedure was used on the collected scans to identify potential phases present in the as-received materials, [5], [9]. The crystalline phase candidates can then be examined by the Rietveld refinement analysis for subsequent phase quantification. The HighScore Plus software peak search and match procedure is as follows:

(i) open the experimental XRD file;

(ii) convert the automatic divergent slit scan (ADS) to the fixed divergent slit scan (FDS) using the ***Treatment*** option, then ***Corrections***, then ***Convert Divergence Slit***, then ***Convert ADS to FDS***, and finally ***Replace*** the scan;

(iii) determine the background by using the ***Treatment*** option, then ***Determine Background*** (using values of 20 for the ***Granularity*** and 0 for the ***Bending factor***), and finally ***Accept*** the background;

(iv) perform peak search by using the ***Treatment*** option, then ***Search Peaks*** (with 2.00 ***Minimum significance***, 0.05 ***Minimum tip width [2Th.]***, 0.50 ***Maximum tip width [2Th.]***, 2.00 ***Peak base width [2Th.]***, and ***Minimum 2nd derivative*** in ***Method***), and finally ***Accept*** the search peaks;

(v) load the phase subset to the candidate list by using ***Pattern List*** pane, then right-click the ***Candidates*** sub-pane ***Load Subset to Candidate List***. For this step, a subset file or files (with the extension "SUB") with PDF codes should be created first. A subset file can be created by opening a new file in HighScore selecting ***New*** from the ***Fil***e menu. Then, click on ***Reference Pattern*** menu, ***Retrieve Pattern*** and ***Reference Code***. A window (***Retrieve Pattern by Reference Code***) will appear. Enter the PDF number for the desired phases and press the ***Save as Subset*** button;

(vi) begin the match procedure by choice of the minor phases and end by the choice of the major phases: by double-clicking the candidate phase, open the ***Reference Pattern*** file, then check 2θ positions of 3 to 5 of the most intense peaks, and if these positions correspond to the peaks on the experimental scan, drag this phase from

the ***Candidate*** sub-pane to the ***Accepted Pattern*** sub-pane. Repeat this procedure to match all peaks;

(vii) if at the end of step *(vi)* some of peaks are still unidentified, make a wider search and match of peaks by selecting ***Analysis*** option, then ***Search & Match***, then ***Execute Search & Match***, then select restriction set ***Cement*** or/and ***Minerals*** in ***Restrictions***, and finally click ***Search*** and ***OK***;

(viii) repeat step *(vi)* of the procedure to identify all peaks.

2.3.3 Rietveld Refinement Procedures/Strategies

Rietveld refinement is based on the iterative comparison (described in Chapter 1) of the experimentally collected diffraction pattern with the calculated pattern for a mixture of known phases. According to the literature [6, 12-17], the calculated intensity $I_c(S_p, F_K, \Phi_K, P_K)$ depends on the Rietveld scale factors S_p, which is proportional to the number of unit cells contributing to the scattering intensity normalized by the volume of the unit cell, the structure factor F_K, the peak profile function Φ_K, and preferred orientation function P_K. Here, the subscript K is the plane indices of the x-ray reflection [6].

The accuracy of the fitting procedure for overlapping and/or single peaks depends on the shape of the profile function Φ_K used in the refinement. The diffraction profiles are well described by the pseudo-Voigt function [6],

$$\Phi_K = (1-\eta)G(H_K) + \eta L(H_K) \qquad \text{Equation 2-1}$$

which is the linear combination of the Gaussian $G(H_K)$ and the Lorentzian $L(H_K)$ with the adjustable pseudo-Voigt mixing parameter η and the peak width H_K. The pseudo-Voigt function mixing parameter η is expressed as:

$$\eta = \eta_1 + \eta_2(2\theta) + \eta_3(2\theta)^2 \qquad \text{Equation 2-2}$$

where η_1, η_2, and η_3 [11] are free variables. It has been indicated that using $\eta = \eta_1 = 0.6$ results in good refinement for the crystalline phases in clinkers, cements, and SCMs [6, 18]. However, some specific cases, described in Chapter 8, require the refinement of η_1, η_2, and η_3. To have a chance to fit the wide variety of peak shapes, including the asymmetric shapes, Caglioti et al. [19]

proposed a quadratic dependence of the peak width H_K with adjustable parameters *U*, *V*, and *W*. In the simplified form, proposed by Rietveld [12], the peak width is given by:

$$H_K^2 = U\tan^2\theta + V\tan\theta + W \qquad \text{Equation 2-3}$$

The parameter *W* describes the symmetrical profile shape, while the *U* and *V* parameters introduce the peak asymmetry.

Typical refinement parameters include the following:

(i) appropriate polynomial [5, 7, 17, 20, 21] or Chebyshev polynomial [7, 8, 22-26] with different numbers of refined coefficients. A fourth-order polynomial or Chebyshev polynomial is adequate for background fitting in samples with relatively low amorphous content, less than about 10 wt.%. However, if the amorphous content is high, the number of coefficients may have to be increased, and in some instances up to 23;

(ii) the weight fraction scale factors for all phases;

(iii) pattern shift: zero shift [5, 7, 21, 25-28];

(iv) the lattice parameters for all phases;

(v) preferred orientation: alite-M3 (-101), gypsum (010), hemihydrate (001), portlandite (001), calcite (104), basanite (001), anhydrite (001), dolomite (001), and ettringite (001) [5, 7, 8, 20, 25]. Indices for preferred orientation indicated in the parentheses should be set up at the beginning of the Rietveld refinement in the ***Preferred Orientation*** sub-pane of the ***Selected object: Phase*** section in the ***Object Inspector*** pane;

(vi) peak shape parameters for crystalline phases: the Caglioti parameters *W*, *V* and *U* [19] for major phases and *W* parameter for minor phases [6, 8].

2.3.3.1 Materials of Low Amorphous Content

For materials with relatively low amorphous content, such as clinkers, portland cements, limestones, gypsums, and standard reference materials, the Rietveld refinement procedure can begin in the ***Manual Mode*** with the background fitting fourth-order polynomial, followed by:

(i) flat background;

(ii) scale factors of all phases;

(iii) zero shift;

(iv) 1 – 4 polynomial coefficients;

(v) lattice parameters of all phases. (Note: During lattice parameter refinement, minor phases that have weak peaks that overlap with strong peaks of major phases should initially be excluded from the refinement. Later, the lattice parameter refinement of the minor phases could be individually done while visually inspecting the peak shape during refinement);

2.3.3.2 Materials with High Amorphous Content

For materials with relatively high amorphous content, such as supplementary cementitious materials and blended cements, background fitting is conducted using Chebyshev polynomials, the orders of which are established individually for each material studied. The main steps used in the refinement mode are as follows:

(i) select the Chebyshev I polynomial for background: go to ***Refinement Control*** pane click on ***Global Variables*** and select ***Chebyshev I*** option in the ***Method*** of ***Background*** of the ***Object Inspector***. Click the option ***Use Extended Background Terms*** if the order of Chebyshev polynomial exceeds 5;

(ii) refine the flat background in ***Chebyshev I Background Polynomial*** of the ***Global Variables***;

(iii) refine scale factors of all phases;

(iv) refine zero shift;

(v) refine Chebyshev I polynomial coefficients;

(vi) refine lattice parameters of phases. (Note: During lattice parameters refinement, minor phases that have weak peaks that overlap with strong peaks of major phases should initially be excluded from refinement initially. Later, the lattice parameters refinement of the minor phases could be individually done while visually inspecting the peak shape during refinement).

2.3.3.2.1. Refinement Procedure (*I*): Single Phase Materials

(i) begin the refinement according to section 2.3.3.1 or section 2.3.3.2 depending on the expected amorphous content;

(ii) refine Caglioti parameter *W* of the phase;

(iii) add Caglioti *V* and make refinement;

(iv) add Caglioti *U* and make refinement;

(v) add preferred orientation parameter, if necessary, and make refinement.

2.3.3.2.2. Refinement Procedure (*II*): Materials with Two Major Phases (with Strong Peak Overlap)

(i) begin the refinement according to section 2.3.3.1 or section 2.3.3.2;

(ii) simultaneously refine parameter *W* of these phases;

(iii) add parameter *V* and make refinement;

(iv) add parameter *U* and make refinement;

(v) add preferred orientation parameters, if necessary, and make refinement.

Refinement Procedure (*II*) can also be utilized for two major phases without overlapping or with minor peak overlapping. However, in these cases phases can be refined separately.

2.3.3.2.3. Refinement Procedure (*III*): Material with Two Phases (without Strong Overlap)

(i) begin the refinement according to section 2.3.3.1 or section 2.3.3.2;

(ii) if both phases have a content above 20% (major phase), apply procedure (*II*) for these phases;

(iii) if the weight percentage of the second phase is between 5-20 wt.% (minor phase), apply Refinement Procedure (*I*) for the major phase. Turn off the refined *W*, *V*, *U*, and preferred orientation parameters, then apply procedure (*I*) for the minor phase. This step should be accompanied by visual observation of the strong peak(s) of this minor phase. If during *w* refinement, the value of this parameter increases dramatically (more than about 10 times) and the width of the calculated peak becomes more than the collected profile, the last step of refinement should be cancelled by ***Undo Profile/Rietveld Refinement*** in the ***Edit*** mode. After that, the

successive fit of the experimental profile could be done by setting the range of change of this parameter (click on parameter w in ***Refinement Control*** mode and then set the value (in %) in ***Set Value Range*** in ***Object Inspector***);

(iv) if the content of the second phase is less than about 5 wt.%, only refine parameter *W*;

(v) if the content of the minor phase is about 1 wt.% or less, the peak refinement of this phase could be omitted. However, if the strong peak(s) of this phase is clearly observed, parameter *w* can be refined with visual observation.

2.3.3.2.4. Refinement Procedure (*IV*): Material with Three or More Phases

(i) begin the refinement according to section 2.3.3.1 or section 2.3.3.2;

(ii) perform Refinement Procedure (*II*) for major phases with strong peak overlapping, if any;

(iii) turn off parameters *W, V, U,* and preferred orientation for the major phases in order to minimize the number of refinement parameters;

(iv) perform Refinement Procedure (*III*) for the next major phase if there is no peak overlap;

(v) turn off parameters *W, V, U,* and preferred orientation for the major phase, to minimize the number of the refined parameters;

(vi) repeat steps *(iv)* and *(v)* for each following phase.

2.3.3.2.5. Refinement Procedure (*V*): Mixture Analysis with Internal-Standard Material

(i) begin the refinement according to section 2.3.3.1 or section 2.3.3.2;

(ii) perform procedure (*IV*) for the mixture;

(iii) perform procedure (*I*) for internal standard material.

2.3.3.2.6. Refinement Procedure (*VI*): Material (PC-SCM Mixtures and PC-SCM-Internal Standard Mixture) following KOSH and SAM Extraction and SCM Preliminary Refinement

Refinement of the KOSH and SAM residue as well as the SCMs should be done using Refinement Procedures (*IV*) or (*V*); the end result of those procedures should be a fitted structure

with refined lattice constants and parameters *W*, *V* and *U* for peak profiles. The fitted structures are saved in the ".CRY" ICSD format and then used as the starting structures for refinement (cement-SCM mixtures and/or their mixtures with an internal standard) as follows:

(i) insert fitted ".CRY" structures (and the internal standard structure for mixture with the internal-standard material);

(ii) begin the refinement for alite and belite, then aluminate and ferrite using Procedure *II*;

(iii) perform Refinement Procedure (*IV*) for cement-SCM mixtures and Refinement Procedure (*V*) for their mixtures with internal-standard material;

(iv) turn off parameters *W*, *V*, *U*, and preferred orientation for all structures;

(v) turn on the refinement for one of the minor phases in the ***Refinement Control*** pane;

(vi) perform Refinement Procedure (*III*) for the remaining phases;

(vii) perform Refinement Procedure (*I*) for the internal standard.

2.4 References

[1] G. W. Brindley, "The effect of grain or particle size on X-ray reflections from mixed powders and alloys considered in relation to the quantitative determination of crystalline substances by X-ray methods," *Phil. Mag.*, vol. 36, pp. 347–369, 1945.

[2] J. C. Taylor, L. P. Aldridge, C. E. Matulis, and I. Hinczak, "X-ray powder diffraction analysis of cements," in *Structure and Performance of Cements*, Second edi., J. Bensted and P. Barnes, Eds. Spon Press, 2002, pp. 420–441.

[3] A. G. De La Torre and M. A. G. Aranda, "Accuracy in Rietveld quantitative phase analysis of Portland cements," *J. Appl. Crystallogr.*, vol. 36, pp. 1169–1176, 2003.

[4] M. Criado, A. Fernández-Jiménez, A. G. de la Torre, M. A. G. Aranda, and A. Palomo, "An XRD study of the effect of the SiO_2/Na_2O ratio on the alkali activation of fly ash," *Cem. Concr. Res.*, vol. 37, no. 5, pp. 671–679, May 2007.

[5] M. A. G. Aranda, A. G. De la Torre, and L. Leon-Reina, "Rietveld Quantitative Phase Analysis of OPC Clinkers, Cements and Hydration Products," *Rev. Mineral. Geochemistry*, vol. 74, no. 1, pp. 169–209, May 2012.

[6] G. Le Saoût, V. Kocaba, and K. Scrivener, “Application of the Rietveld method to the analysis of anhydrous cement,” *Cem. Concr. Res.*, vol. 41, no. 2, pp. 133–148, Feb. 2011.

[7] R. Snellings, A. Bazzoni, and K. Scrivener, “The existence of amorphous phase in Portland cements: Physical factors affecting Rietveld quantitative phase analysis,” *Cem. Concr. Res.*, vol. 59, pp. 139–146, May 2014.

[8] W. Wilson, K. J. Krakowiak, and F.-J. Ulm, “Simultaneous assessment of phase chemistry, phase abundance and bulk chemistry with statistical electron probe micro-analyses: Application to cement clinkers,” *Cem. Concr. Res.*, vol. 55, pp. 35–48, Jan. 2014.

[9] C1365-06, “Standard Test Method for Determination of the Proportion of Phases in Portland Cement and Portland-Cement Clinker Using X-Ray Powder Diffraction Analysis,” *Annu. B. ASTM Stand. ASTM Int. West Conshohocken, PA*, vol. Vol. 4.01, pp. 1–10, 2011.

[10] P. E. Stutzman, “Guide for X-Ray Powder Diffraction Analysis of Portland Cement and Clinker,” *NISTIR 5755*, 1996.

[11] V. Pecharsky and P. Zavalij, *Fundamentals of Powder Diffraction and Structural Characterization of Materials.*, Second Edi. Springer, 2009.

[12] H. M. Rietveld, “A Profile Refinement Method for Nuclear and Magnetic Structures,” *J. Adv. Concr. Technol.*, vol. 2, pp. 65–71, 1969.

[13] G. Malmros and J. D. Thomas, “Least squares structure refinement based on powder film intensity data,” *J. Appl. Crystallogr.*, vol. 10, pp. 107–111, 1977.

[14] R. A. Young, D. Mackie, and R. B. von Dreele, “Application of the pattern fitting structure refinement method to X-ray powder diffractometer pattern,” *J. Appl. Crystallogr.*, vol. 10, pp. 262–269, 1977.

[15] B. H. O’Connor and M. D. Raven, “Application of the Rietveld Refinement Procedure in Assaying Powdered Mixtures,” *Powder Diffr.*, vol. 3, no. 1, pp. 2–6, Jan. 1988.

[16] R. A. Young, *The Rietveld Method*. Oxford University Press, Oxford, 1993.

[17] L. B. McCusker, R. B. Von Dreele, D. E. Cox, D. Louër, and P. Scardi, “Rietveld refinement guidelines,” *J. Appl. Crystallogr.*, vol. 32, no. 1, pp. 36–50, Feb. 1999.

[18] Q. I. Roode-Gutzmer and Y. Ballim, “Phase composition and quantitative X-ray powder

diffraction analysis of Portland cement and clinker," in *Materials Science of Concrete VI*, J. Skalny, Ed. The American Ceramic Society, 2001, pp. 1–48.

[19] G. Caglioti, A. P. Paoletti, and R. F., "Choice of collimators for a crystal spectrometer for neutron diffraction," *Nucl. Instruments*, vol. 3, pp. 223 – 228, 1958.

[20] G. Le Saoût, T. Füllmann, V. Kocaba, and K. L. Scrivener, "Quantitative study of cementitious materials by X-ray diffraction/ Rietveld analysis using an external standard," *Proc. 12th Int. Congr. Chem. Cem. Montréal, Canada*, p. TH2-07.01, 2007.

[21] R. Jadhav and N. C. Debnath, "Computation of X-ray powder diffractograms of cement components and its application to phase analysis and hydration performance of OPC cement," *Bull. Mater. Sci.*, vol. 34, no. 5, pp. 1137–1150, Dec. 2011.

[22] V. K. Peterson, A. S. Ray, and B. A. Hunter, "A comparative study of Rietveld phase analysis of cement clinker using neutron, laboratory X-ray, and synchrotron data," *Powder Diffr.*, vol. 21, no. 1, pp. 12–18, Mar. 2006.

[23] N. Marinoni, A. Pavese, M. Voltolini, and M. Merlini, "Long-term leaching test in concretes: An X-ray powder diffraction study," *Cem. Concr. Compos.*, vol. 30, no. 8, pp. 700–705, Sep. 2008.

[24] J. P. Cline, R. B. Von Dreele, R. Winburn, P. W. Stephens, and J. J. Filliben, "Addressing the amorphous content issue in quantitative phase analysis: the certification of NIST standard reference material 676a.," *Acta Crystallogr. A.*, vol. 67, no. Pt 4, pp. 357–67, Jul. 2011.

[25] M. L. Gualtieri, M. Romagnoli, P. Miselli, M. Cannio, and A. F. Gualtieri, "Full quantitative phase analysis of hydrated lime using the Rietveld method," *Cem. Concr. Res.*, vol. 42, no. 9, pp. 1273–1279, Sep. 2012.

[26] M. De Schepper, K. De Buysser, I. Van Driessche, and N. De Belie, "A Hydration Study by XRD / Rietveld Analysis of Cement Regenerated from Completely Recyclable Concrete," *IJRET*, vol. 3, no. 13, pp. 129–134, 2014.

[27] R. Snellings, G. Mertens, Ö. Cizer, and J. Elsen, "Early age hydration and pozzolanic reaction in natural zeolite blended cements: Reaction kinetics and products by in situ synchrotron X-ray powder diffraction," *Cem. Concr. Res.*, vol. 40, no. 12, pp. 1704–1713,

Dec. 2010.

[28] S. A. Speakman, “Fundamentals of Rietveld Refinement II . Refinement of a Single Phase The Rietveld Method,” *Mater. Sci.*, 2010.

Chapter 3. Evaluation of X-Ray Diffraction Refinement Approach for Phase Quantification

3.1 Introduction

Based on the literature review, selected x-ray diffraction quantification methodologies were assessed on cements with known composition and known mixtures of pure phases. Each methodology was evaluated as to its accuracy and precision, and analysis procedures were established for the quantification of crystalline cement phases.

Additionally, it is of interest to assess the lower limit for detecting the amorphous content in mixtures and to identify the best methodology for amorphous content quantification. This is of special significance as one of the objectives of this study was to assess the amount of SCMs in blended cements. Towards satisfying this objective, several standard materials were acquired from the National Institute of Standards and Testing (NIST). Corundum (SRM 670a) has a certified crystalline content of more than 99%, (Appendix A). It was used as an internal and external standard throughout the current study. TiO_2 and Cr_2O_3 (SRM 674b) were also used to verify the procedures for mixtures containing amorphous content from 4% up to 10%. Titania has a certified amorphous content of about 10% while chromium oxide has about 4% according to the NIST certification, Appendix B. Several standard clinkers were then used for the quantification of the crystalline phases using Rietveld analysis and the results were compared to the NIST certification. The software used in the current study was Panalytical HighScore Plus V4.5. Sample preparation, selective dissolution, x-ray measurements, and Rietveld refinement analysis of the materials followed the general procedures outlined previously in Chapter 2 with specifics of refinement presented here.

3.2 Rietveld Refinement Procedures

3.2.1 Standard Single-Phase Materials and their Combinations

The single-phase standard materials examined here were SRM 676a, and SRM 674b. The refinement procedure is carried out in the ***Manual*** mode from the ***Refinement Control*** pane and consists of the following successive refinement steps.

(i) Insert the crystal structures from a database for the phases identified during the Search and Match procedure conducted according to the steps described in section 2.3.2.

(ii) Refine flat background in the ***Background Polynomial*** submenu under the ***Global Variables*** menu.

(iii) Refine scale factors of all phases.

(iv) Refine ***Zero Shift (2θ)*** under ***Global Variables***.

(v) Click on the ***Background Polynomial*** submenu under ***Global Variables*** to open the ***Object Inspector*** pane and select ***Polynomial*** under ***Method***. Refine coefficients 1 – 4 under the ***Background Polynomial***.

(vi) Refine lattice parameters. Minor phases should be excluded from refinement in this step. The lattice parameters for these phases can be refined individually.

(vii) For a mixture of phases, where both phases are present in large proportions, refinement can be performed simultaneously for both phases.

(viii) Refine the *Caglioti W* parameter.

(ix) Refine the *Caglioti V* parameter.

(x) Refine the *Caglioti U* parameter.

(xi) Refine preferred orientation if necessary.

(xii) Uncheck the *Caglioti W, V, U* parameters and preferred orientation for the refined phase and repeat steps *(vii)* - *(x).* For minor phases, such as anatase present in a small quantity in TiO_2, only refine the *W* parameter.

3.2.2 Portland Cement Clinkers with Corundum

The major difference in the refinement of the single phases described above and refinement of clinkers is the strong peak overlap between alite and belite phases, and aluminate and ferrite. The refinement steps for the clinkers are as follows:

(i) Perform KOSH and SAM extractions as described in section 2.2.3.

(ii) Open the collected XRD scan for each extraction residue.

(iii) Insert crystal structure identified during the Search and Match procedure described in section 2.3.2.

(iv) For the refinement of extraction residues, select the ***Polynomial*** profile function in the ***Background*** of the ***Object Inspector*** pane.

(v) Refine flat background.

(vi) Refine scale factors of all phases.

(vii) Refine zero shift.

(viii) Click on the ***Background Polynomial*** submenu and select ***Polynomial*** under ***Method***. Refine coefficients 1 – 4 under the ***Background Polynomial***.

(ix) Refine lattice parameters for all phases. For the minor phases (below 5%) refinement of lattice parameters at this point should be omitted.

(x) Simultaneously refine the *W* parameters for alite and belite for the KOSH extraction residue, or aluminate and ferrite for the SAM residue.

(xi) Simultaneously refine the *V* parameters for alite and belite or aluminate and ferrite.

(xii) Simultaneously refine the *U* parameters for alite and belite or aluminate and ferrite.

(xiii) Refine preferred orientation for alite (KOSH extraction). Care should be taken to enter the correct hkl value for the direction of the preferred orientation in the ***Object Inspector*** pane.

(xiv) Uncheck *W, V, U,* and preferred orientation parameters for the refined phases to exclude them from further refinement.

(xv) Consider the next most dominant phase. If refinement of lattice parameters for this phase was omitted in step *(ix)*, refine all the lattice parameters with visual observation. If peak shift beyond the collected pattern is observed, the lattice parameters for this phase should be excluded from refinement.

(xvi) If the phase considered in step *(xv)* is present in amounts above 5 wt.%, refine *W*, *V*, *U* parameters one at a time. For phases present in weight fractions of approximately 5-20%, this step should be accompanied by visual observation. If during refinement of one of the parameters the value of this parameter increases dramatically and the shape of the calculated profile broadens beyond the collected profile, undo this refinement step and limit the ***Set Value Range (%)*** for the *W* parameter in the ***Object Inspector*** pane. This may be repeated several times until good agreement between the simulated and the collected pattern is observed. This should be done during *V* and *U* refinement as well.

(xvii) Refine preferred orientation if necessary.

(xviii) Uncheck *W, V, U* and preferred orientation parameters for the refined phase.

(xix) If the phase considered in step *(xv)* is present in amounts of approximately 1-5%, only refine the *W* parameter. However, if a strong, non-overlapped peak of this minor phase can be clearly observed in the collected pattern, *V* and *U* parameters can be refined as well with visual observation. For phases present in amounts below 1%, refinement of *W, V, U* and preferred orientation parameters can be omitted.

(xx) Repeat steps *(xv) – (xix)* until all the phases have been considered.

(xxi) Uncheck all refined parameters for all phases and save the refined structures as a .cry file.

(xxii) Open the collected XRD scan for the clinker and insert the .cry structures created during the KOSH and SAM residue refinements.

(xxiii) Select the ***Polynomial*** profile function in the background ***Object Inspector*** pane.

(xxiv) Repeat steps *(v) – (ix).*

(xxv) Repeat steps *(x) – (xii)* for alite and belite.

(xxvi) Repeat steps *(x) – (xii)* for aluminate and ferrite.

(xxvii) Refine the *W* parameter for the next most abundant phase.

(xxviii) Refine the *V* parameter.

(xxix) Refine the *U* parameter.

(xxx) Uncheck the *W, V, U* parameters for the refined phase and repeat steps *(xxvii) - (xxix)* for the remaining phases.

(xxxi) If the weight percentage of one of the phases is between 5-20 wt.%, visually observe the strong peak(s) of this phase. If during refinement of one of the parameters the value of this parameter increases dramatically and the shape of the calculated profile broadens beyond the collected profile, undo this refinement step and limit the ***Set Value Range*** (%) for the *W* parameter in the ***Object Inspector*** pane. This may be repeated several times until good agreement between the simulated and the collected pattern is observed. This should be done during *V* and *U* refinement as well.

(xxxii) For phases present in amounts of approximately 1-5%, only refine the *W* parameter. However, if a strong, non-overlapped peak of this minor phase can be clearly

observed in the collected pattern, *V* and *U* parameters can be refined as well with visual observation.

(xxxiii) For phases present in amounts below 1%, refinement of *W, V, U* and preferred orientation parameters can be omitted.

3.3 Results and Discussion

3.3.1 Sample Preparation and its Effect on Phase Quantification

In order to assess the effects of repacking powder in the XRD sample holder, rescanning without repacking, and sample preparation procedures on the quantification of crystalline phases, a mixture of 50% TiO_2 (Aldrich) and 50% CaF_2 (Aldrich) was prepared. First, three specimens were prepared and scanned. Then, one of the three specimens was scanned three times without repacking and quantification was conducted on each scan and averaged. The last set used one specimen that was repacked and scanned 3 times. For each set of the outlined sets, Rietveld analysis using HighScore Plus was conducted on each scan for the quantification of the crystalline content. The results presented in Table 3-1 indicate that rescanning, repacking, or preparing new mixtures introduced error that did not exceed 0.4 weight percent error in crystalline weight fraction quantification.

Table 3-1: Standard mixtures used for Verification of Specimen Preparation Procedures

Measurement	Weight Fraction (*W*t.%)		
	TiO_2 (Rutile)	TiO_2 (Anatase)	CaF_2 (Fluoride)
3 Scans (one pack)	47.0 (0.1)	2.9 (0.1)	50.1 (0.2)
3 Scans (with Repacking)	47.2 (0.3)	2.9 (0.1)	49.9 (0.4)
3 Replicate Mixtures	47.1 (0.4)	2.8 (0.1)	50.1 (0.4)

3.3.2 Crystalline/Amorphous Content in Standard Reference Materials

NIST standard reference materials 674b TiO_2 and Cr_2O_3 (see Appendix B) were used together with corundum 676a (see Appendix A) to quantify the crystalline content in known certified standards using both internal and external standard materials procedures. The 674b certification indicates a crystalline content of 89.47% ± 0.62% for TiO_2 and 95.91% ± 0.6% for

chromium trioxide. Corundum (SRM 676a) has the highest certified crystalline content of 99.02% ± 1.1%; therefore, it was used in implementing the internal and external standard protocol in the current work. The mixtures used for specimen preparation using the internal standard method included 50% of the internal standard, as suggested by Westphal et al. [1], for mixtures with low amorphous content. Mixtures of 50:50 Al_2O_3-TiO_2, and Al_2O_3-Cr_2O_3 were prepared and analyzed using Rietveld refinement. For the external standard method, pure corundum, titania, and chromium trioxide patterns were collected and analyzed using Rietveld refinement. In the current study, the crystalline weight fraction of corundum, 99.02%, was used in Equation 1-6 to determine the *G* calibration factor for corundum. The same instrumental and data collection conditions adopted for corundum were used in pattern collection for 674b, as the calibration factor "is dependent on the instrumental and data collection conditions" [2]. The calibration factor *G* was then used to determine the crystalline weight fractions in TiO_2 and Cr_2O_3 samples. Table 3-2 shows the mass absorption coefficient values used for all oxides in the current study.

Table 3-2: Mass Absorption Coefficients for Elemental Oxides

Oxide	**Mass Absorption Coefficient (MAC), (cm^2/g)**
SiO_2	34.84
Al_2O_3	30.91
Fe_2O_3	220.77
CaO	120.47
MgO	27.88
SO_3	42.48
Na_2O	24.28
K_2O	116.82
TiO_2	121.97
P_2O_5	38.59
Mn_2O_3	196.9
SrO	100.36
LOI	9.76
Cr_2O_3	176.40

X-ray diffraction scans of TiO_2 revealed the presence of anatase in small amounts. The NIST certificate does not indicate if anatase was considered in quantification of the crystalline content reported for titania. Using the external standard method to quantify the crystalline/amorphous content for pure preparations of titania, and the internal standard methods

of quantification for a 50:50 mixture of Al_2O_3 and TiO_2 yielded similar crystalline/amorphous content results with no significant differences between both methods and with similar errors as depicted in Table 3-3.

As indicated previously, a second standard material, Cr_2O_3, was also used to verify the appropriateness of both external and internal standard procedures in quantifying the crystalline/amorphous content of mixtures. The individual values used for calculating the G factors necessary for the external standard procedure are listed in Table 3-4. The results depicted in Table 3-5 indicate that for materials with a low amorphous content of about 4%, both procedures yielded results in good agreement with the certified values.

Table 3-3: Crystalline (Rutile) Content in TiO_2 (SRM 674b)

Quantification Method	**SRM Certified Crystalline Content (%)**	**Rutile Crystalline Content (%)**
Internal Standard	89.47	89.9 (0.1)
External Standard	89.47	90.1

Table 3-4: Structure Parameters used for Calibration Parameter "G" Calculations for the External Standard Method

Property	**Rutile**	**Corundum**	**Eskolaite (Cr_2O_3)**
Volume (cm^3)	62.41	254.87	289.37
Density (g/cm^3)	4.25	3.99	5.23
Mass Absorption Coefficient(cm^2/g)	121.97	30.91	176.4

Table 3-5: Crystalline Content Quantification for SRM 674b Cr_2O_3 using Internal and External Standard Methods

Quantification Method	**SRM Certified Crystalline Content (%)**	**Eskolaite Crystalline Content (%)**
Internal Standard	95.91	95.9
External Standard	95.91	95.6

The findings indicate that for Rietveld analysis, both internal and external methods yield results in good agreement with NIST SRM certification for both titanium oxide and chromium oxide. It was therefore concluded that either protocol could be used in the current study. The

findings also indicate that an amorphous content as low as about 4.0% can be determined accurately using the outlined methodology.

3.3.3 Phase Analysis of Standard NIST Clinkers

NIST clinkers were used in the current study for verifying phase quantification procedures using Rietveld analyses. Three clinkers were used here; namely, SRM 2686, 2687, and 2688 (see Appendices C, D and E, respectively). The results of the Rietveld refinement for the 3 NIST clinkers are presented in Table 3-6 through Table 3-8. It is to be noted that the NIST certified values are based on quantification methods using optical microscopy and Rietveld analysis. The results depicted here indicate agreement between the analysis conducted in this current study and the ASTM C1365 [3] specified limits on portland cement clinker phase quantification.

Table 3-6: Rietveld Analysis for NIST-SRM 2686 Clinker

Measurement	*Wt.* (%)				
	Alite	Belite	Aluminate	Ferrite	Periclase
Scan 1 Scan 2	54.3 54.8	26.0 25.7	3.2 3.1	14.0 13.9	2.6 2.5
Average	54.6 (0.4)	25.9 (0.2)	3.2 (0.1)	14.0 (0.1)	2.6 (0.1)
NIST SRM 2686 Certificate	58.6 ± 4.0	23.3 ± 2.8	2.3 ± 2.1	14.1 ± 1.4	3.3 ± 1.9
ASTM C1365 (maximum difference)	5.93	3.70	2.14	2.46	0.85

Table 3-7: Rietveld Analysis for NIST-SRM 2687 Clinker

Measurement	*Wt.* (%)				
	Alite	Belite	Aluminate	Ferrite	Arcanite
Scan 1 Scan 2	72.4 72.3	12.8 12.7	12.8 13.0	1.2 1.3	0.7 0.8
Average	72.4 (0.1)	12.8 (0.1)	12.9 (0.1)	1.3 (0.1)	0.8 (0.1)
NIST SRM 2687 Certificate	71.24 ± 1.27	12.57 ± 1.22	11.82 ± 1.03	2.81 ± 0.68	0.92 ± 0.15
ASTM C1365 (maximum difference)	5.93	3.70	2.14	2.46	0.85

Table 3-8: Rietveld Analysis for NIST-SRM 2688 Clinker

Measurement	*Wt.* (%)			
	Alite	Belite	Aluminate	Ferrite
Scan 1 Scan 2	64.0 64.0	18.9 18.7	5.3 5.4	11.9 11.9
Average	64.0 (0.0)	18.8 (0.1)	5.4 (0.1)	11.9 (0.0)
NIST SRM 2688 Certificate	64.95 ± 1.04	17.45 ± 0.96	4.99 ± 0.5	12.2 ± 0.84
ASTM C1365 (maximum difference)	5.93	3.70	2.14	2.46

3.4 Conclusions

The findings in this chapter indicate that the amorphous content can be determined with accuracy for mixtures that contain an amorphous content as low as approximately 4%. Additionally, the findings indicate that the Rietveld refinement protocol implemented on the certified SRM clinkers gives results in agreement with the NIST certification as well as in compliance with ASTM C1365 requirements.

3.5 References

[1] T. Westphal, G. Walenta, T. Füllmann, M. Gimenez, E. Bermejo, K. L. Scrivener, and H. Pöllmann, "Characterisation of cementitious materials," *Int. Cem. Rev.*, pp. 47–51, 2002.

[2] I. C. Madsen, N. V. Y. Scarlett, and A. Kern, "Description and survey of methodologies for the determination of amorphous content via X-ray powder diffraction," *Zeitschrift für Krist.*, vol. 226, no. 12, pp. 944–955, Dec. 2011.

[3] ASTM Standard C1365 2006 (2011), *Standard Test Method for Determination of the Proportion of Phases in Portland Cement and Portland-Cement Clinker Using X-Ray Powder Diffraction Analysis*. West Conshohocken, Pa.: ASTM International, 2012.

Chapter 4. XRD Analyses of Commercial Portland Cement and Clinker

4.1 Introduction

Powder x-ray diffraction quantitative analysis was conducted on commercial PC and clinker obtained from the FDOT approved list of construction materials suppliers. Rietveld refinement of the crystalline phases and the total amorphous/unidentified content (A/uC) was conducted on the as-received materials according to procedures outlined earlier in Chapter 2. Three portland cements, PC1, PC2, and PC3, in addition to 3 clinkers, C1, C2, and C3, were selected for quantitative analysis using x-ray diffraction coupled with Rietveld refinement.

4.2 Rietveld Refinement Procedures

4.2.1 Refinement of KOSH and SAM Extraction Residues

Since clinkers and cements contain a number of phases that suffer from peak overlap and contain minor phases that may be difficult to identify, it is useful to perform selective dissolution (extraction). In this study, KOSH and SAM extractions were used to refine the crystal structure of silicates, aluminates, ferrites, and minor phases, which were then used in the refinement of the as-received cements. Refinement of extraction residues can be carried out as follows:

(i) Open the scan file for the extraction residue and insert crystal structures from a database for the phases identified in the extraction residue during the Search and Match procedure.

(ii) Select ***Polynomial*** as the profile function in the ***Background*** of the ***Object Inspector*** pane.

(iii) Refine the flat background.

(iv) Refine scale factors for all phases.

(v) Refine zero shift.

(vi) Refine background coefficients 1-4.

(vii) Refine lattice parameters. Minor phases, especially those with peak overlap, should be excluded from refinement in this step. The lattice parameters for these phases can be refined individually.

(viii) Refinement of *W*, *V*, *U*, and preferred orientation parameters should first be performed for the major phases with strong peak overlap, for example, for alite and belite in the KOSH residue, and for aluminate and ferrite in the SAM residue.

(ix) Simultaneously refine the *W* parameters for the major phases with strong peak overlap.

(x) Simultaneously refine the *V* parameters.

(xi) Simultaneously refine the *U* parameters.

(xii) Refine preferred orientation if necessary. Care should be taken to enter the correct hkl value for the direction of the preferred orientation in the ***Object Inspector*** pane.

(xiii) Uncheck the *W*, *V*, *U*, and preferred orientation parameters for the refined phases.

(xiv) Consider the next most dominant phase. If refinement of lattice parameters for this phase was omitted in step *(vii)*, refine all the lattice parameters with visual observation. If peak shift beyond the collected pattern is observed, the lattice parameters for this phase should be excluded from refinement.

(xv) If the phase considered in step *(xiv)* is present in amounts above 5 wt.%, repeat steps *(viii)* – *(xiii)*. For phases present in weight fractions of approximately 5-20%, this step should be accompanied by visual observation. If, during refinement of one of the parameters, the value of this parameter increases dramatically and the shape of the calculated profile broadens beyond the collected profile, undo this refinement step and limit the ***Set Value Range (%)*** for the *W* parameter in the ***Object Inspector*** pane. This may be repeated several times until good agreement between the simulated and the collected pattern is observed. This should be done during *V* and *U* refinement as well. For phases present in amounts of approximately 1-5%, only refine the *W* parameter. However, if a strong, non-overlapped peak of this minor phase can be clearly observed in the collected pattern, *V* and *U* parameters can be refined as well with visual observation. For phases present in amounts below 1%, refinement of *W*, *V*, *U*, and preferred orientation parameters can be omitted.

(xvi) Repeat steps *(xiv)* and *(xv)* until all the phases have been considered.

(xvii) Uncheck all refined parameters for all phases and save the refined structures as a .cry file.

4.2.2 Refinement of Commercial Clinkers and Cements

(xviii) Open the collected scan of a clinker or cement and insert the refined crystal structures obtained from the KOSH and SAM residue refinement (step *(xvii)* above). It was observed that although a gypsum structure is refined as part of the SAM extraction residue, the use of this refined gypsum structure in cement analysis results in overestimation of the gypsum content. Therefore, gypsum structure should be added from the database. Calcite structure was taken from the KOSH residue refinement, as formation of additional calcite was observed during SAM extraction. Periclase structure was taken from the SAM residue refinement since there is less peak overlap compared to the KOSH residue.

(xix) Repeat steps *(ii) – (vii)*.

(xx) Repeat steps *(viii) – (xiii)* first for alite and belite, then for aluminate and ferrite.

(xxi) Repeat steps *(xiv) – (xvi)* for calcite and gypsum. It may not be necessary to further refine the rest of the phases.

(xxii) When refinement is performed for materials with an internal standard, the internal standard peak parameters should be refined last. After refinement of the internal standard, open the ***Object Inspector*** pane for the internal standard phase, and enter the actual crystalline content of the internal standard under ***Standard Weight Percentage*** in order to calculate amorphous/unidentified content. If the wt.% of internal standard is displayed with the rest of the phases in the ***Analyze View***, select ***Program Settings*** from the ***Customize*** menu, select ***Fitting/Rietveld*** tab, and change the ***Show Weight Percentages*** drop-down menu to ***As Received***. The program will then recalculate the wt.% for the as-received material without the internal standard and the internal standard phase will no longer be visible in the ***Analyze View***.

4.3 Results and Discussion

The sample preparation, selective dissolution, data collection, and analyses for cements and clinkers were conducted according to the methodologies described in detail in Chapter 2. For the crystalline and amorphous/unidentified content determination, the cements and clinkers were mixed with 20 wt.% corundum as an internal-standard material [1]–[6]. The corundum content was selected to compare the results of the alite and belite weight fraction determination using an additional methodology of phase quantification, a calibration curve method, that will be presented later in Chapter 5.

4.3.1 Cements

4.3.1.1 PC1 Cement

The phase search and match procedure and the Rietveld refinement showed the presence of the following minor phases in PC1 cement: portlandite and syngenite. The content of portlandite and syngenite was low, less than 1 wt.%. Calcite and gypsum in the cement were about 5 wt.%. The amorphous/unidentified content in the PC1 cement was about 2 wt.%. The amount of ferrite slightly exceeded that of the aluminate. The complete phase analysis for the PC1 cement is shown in Table 4-1.

Table 4-1: PC1 Cement Mineralogical Analysis

Phase	Sample P1-S1	Sample P2-S1	Sample P3-S1	AVERAGE (STDEV)
Alite	46.7	46.4	46.8	46.6 (0.2)
Belite	24	24.5	24.8	24.4 (0.4)
Aluminate	4.8	4.9	4.7	4.8 (0.1)
Ferrite	9.9	9.7	9.8	9.8 (0.1)
Portlandite	0.9	0.8	0.7	0.8 (0.1)
Syngenite	0.9	1	0.7	0.9 (0.2)
Calcite	4.9	4.7	4.8	4.8 (0.1)
Gypsum	5	5	4.9	5.0 (0.1)
Hemihydrate	1.1	1	0.7	0.9 (0.2)
A/uC	1.7	2	2	1.9 (0.2)

Abbreviations: P – pack, S – scan. AVERAGE and STDEV are the average and the standard deviation for P1 – P3 packs, respectively.

4.3.1.2 PC2 Cement

Rietveld refinement indicates the minor phases in the PC2 cement were: anhydrite, aphthitalite, and syngenite, and were present at less than 1 wt.%. The main difference between PC2 and PC1 cements was that the PC2 cement had a much higher calcite content, about 11 wt.%. The amorphous/unidentified content in PC2 cement was about 10 wt.%. The crystalline and amorphous/unidentified contents in PC2 cement are shown in Table 4-2.

Table 4-2: Mineralogical Analysis of PC2 cement

Phase	Sample P1-S1	Sample P2-S1	Sample P3-S1	AVERAGE (STDEV)
Alite	48.1	47.8	47.1	47.7 (0.5)
Belite	14.5	14.2	14.8	14.5 (0.3)
Aluminate	1.7	1.8	1.6	1.7 (0.1)
Ferrite	10.9	11.2	11.3	11.1 (0.2)
Aphthitalite	0.0	0.1	0.1	0.1 (0.1)
Syngenite	1.0	1.0	0.7	0.9 (0.2)
Calcite	9.7	11.2	11.1	10.7 (0.8)
Gypsum	1.0	0.9	1.1	1.0 (0.1)
Hemihydrate	2.0	2.1	1.9	2.0 (0.1)
Anhydrite	0.0	0.0	0.1	0.0 (0.1)
A/uC	10.8	9.8	10.2	10.3 (0.5)

4.3.1.3 PC3 Cement

The phase search and match procedure and the Rietveld refinement analysis showed the presence of the following minor phases in PC3 cement: periclase, aphthitalite, and syngenite. The contents of these phases were less than 1 wt.%. The calcite content in the cement was about 5 wt.%. The total amount of gypsum and hemihydrate in cement was about 3 - 3.5 wt.%. The amorphous/unidentified content in PC3 cement was about 8 - 9 wt.%. The amount of ferrite notably exceeded that of the aluminate. The crystalline and amorphous/unidentified contents in PC3 cement are presented in Table 4-3.

Table 4-3: PC3 Cement Mineralogical Analysis

Phase	Sample P1-S1	Sample P2-S1	Sample P3-S1	AVERAGE (STDEV)
Alite	53.3	52.4	54.3	53.3 (1.0)
Belite	14.5	14.6	14.4	14.5 (0.1)
Aluminate	1.7	1.6	1.6	1.6 (0.1)
Ferrite	11.6	11.4	12.0	11.7 (0.3)
Periclase	0.2	0.1	0.2	0.2 (0.1)
Aphthitalite	0.1	0.0	0.1	0.1 (0.1)
Syngenite	1.0	0.9	0.7	0.9 (0.2)
Calcite	5.1	5.5	6.3	5.6 (0.6)
Gypsum	2.3	2.7	2.2	2.4 (0.3)
Hemihydrate	1.0	1.3	0.8	1.0 (0.3)
A/uC	9.0	9.5	7.4	8.6 (1.1)

4.3.2 Clinkers

The mineralogical composition of C1, C2, and C3 clinkers are presented in Tables 4-4 through 4-6. C3 clinker had a periclase content of about 2 - 3%, while C1 and C2 clinkers had no periclase content.

Table 4-4: Mineralogical Analysis of C1 clinker

Phase	Sample P1-S1	Sample P2-S1	Sample P3-S1	AVERAGE (STDEV)
Alite	49.5	49.4	49.1	49.3 (0.2)
Belite	29.3	29.0	29.0	29.1 (0.2)
Aluminate	5.2	5.4	5.4	5.3 (0.2)
Ferrite	10.6	10.6	10.7	10.6 (0.1)
Portlandite	0.5	0.6	0.6	0.6 (0.1)
Syngenite	1.6	1.4	1.6	1.5 (0.1)
A/uC	3.3	3.7	3.5	3.5 (0.2)

Table 4-5: Mineralogical Analysis of C2 Clinker

Phase	Sample P1-S1	Sample P2-S1	Sample P3-S1	AVERAGE (STDEV)
Alite	68.9	68.6	68.1	68.5 (0.4)
Belite	12.4	11.2	11.4	11.7 (0.6)
Aluminate	2.7	2.7	2.7	2.7 (0.0)
Ferrite	12.4	12.4	12.4	12.4 (0.0)
Lime	0.1	0	0.1	0.1 (0.1)
Aphthitalite	0.2	0.1	0.1	0.1 (0.1)
Syngenite	0	0.2	0.2	0.1 (0.1)
A/uC	3.4	4.8	5.0	4.4 (0.9)

Table 4-6: Mineralogical Analysis of C3 Clinker

Phase	Sample P1-S1	Sample P2-S1	Sample P3-S1	AVERAGE (STDEV)
Alite	57.0	56.8	55.4	56.4 (0.9)
Belite	16.9	17.4	17.1	17.1 (0.3)
Aluminate	11.2	11.2	11.0	11.1 (0.1)
Ferrite	6.4	6.5	6.4	6.4 (0.1)
Periclase	2.5	2.4	2.4	2.4 (0.1)
Lime	0.1	0.1	0.1	0.1 (0.0)
Arcanite	0.9	1.0	1.1	1.0 (0.1)
Aphthitalite	0.2	0.1	0.2	0.2 (0.1)
Portlandite	0.4	0.3	0.4	0.4 (0.1)
Syngenite	0.3	0.3	0.2	0.3 (0.1)
A/uC	4.1	3.9	5.7	4.6 (1.0)

The phase search and match procedures and the Rietveld refinement analyses showed the presence of the following minor phases in C1 clinker: portlandite and syngenite. Syngenite content was highest in this clinker compared to C2 and C3 clinkers. C3 clinker showed the presence of arcanite and aphthitalite, which were not detected in C1 clinker. Additionally, potassium calcium sulfate was identified in the SAM extraction for C3 clinker as a minor phase but was not reliably detected, due to its lower content, in the Rietveld refinement of the clinker.

4.4 Conclusions

(i) The cements and clinkers analyzed here contained from three to six minor phases. All commercial materials contained syngenite as a minor phase;

(ii) For PCs and clinkers studied here, the amorphous/unidentified content varied from about 2 wt.% to 10 wt.%;

(iii) Quantitative x-ray diffraction and Rietveld analyses showed high precision in quantifying the mineralogical phases in the commercial PCs and clinkers.

4.5 References

[1] M. A. G. Aranda, A. G. De la Torre, and L. Leon-Reina, "Rietveld Quantitative Phase Analysis of OPC Clinkers, Cements and Hydration Products," *Rev. Mineral. Geochemistry*, vol. 74, no. 1, pp. 169–209, May 2012.

[2] V. Pecharsky and P. Zavalij, *Fundamentals of Powder Diffraction and Structural Characterization of Materials.*, Second Edi. Springer, 2009.

[3] N. V. Y. Scarlett, I. C. Madsen, L. M. D. Cranswick, T. Lwin, E. Groleau, G. Stephenson, M. Aylmore, and N. Agron-Olshina, "Outcomes of the International Union of Crystallography Commission on Powder Diffraction Round Robin on Quantitative Phase Analysis: samples 2, 3, 4, synthetic bauxite, natural granodiorite and pharmaceuticals," *J. Appl. Crystallogr.*, vol. 35, no. 4, pp. 383–400, Jul. 2002.

[4] J. P. Cline, R. B. Von Dreele, R. Winburn, P. W. Stephens, and J. J. Filliben, "Addressing the amorphous content issue in quantitative phase analysis: the certification of NIST standard reference material 676a.," *Acta Crystallogr. A.*, vol. 67, no. Pt 4, pp. 357–67, Jul. 2011.

[5] G. Álvarez-Pinazo, A. Cuesta, M. García-Maté, I. Santacruz, E. R. Losilla, A. G. De la Torre, L. León-Reina, and M. A. G. Aranda, "Rietveld quantitative phase analysis of Yeelimite-containing cements," *Cem. Concr. Res.*, vol. 42, no. 7, pp. 960–971, Jul. 2012.

[6] R. Snellings, A. Bazzoni, and K. Scrivener, "The existence of amorphous phase in Portland cements: Physical factors affecting Rietveld quantitative phase analysis," *Cem. Concr. Res.*, vol. 59, pp. 139–146, May 2014.

Chapter 5. Optical Microscopy, XRD Calibration Curves, and Rietveld Refinement

5.1 Introduction

In this chapter, different experimental techniques that are commonly used in phase quantification of portland cements will be employed to evaluate their suitability for routine cement analysis. Three techniques were used here; namely, optical microscopy (OM), XRD calibration curves (XRD-CC) and XRD-Rietveld refinement (XRD-RF). The focus was on quantifying the silicate phases, alite and belite. Three commercial cements and one commercial clinker were studied and the results are presented in the following sections.

5.2 Materials and Methodology

5.2.1 Materials

In generating the alite and belite calibration curves, the following materials were selected:

(i) Alite and Belite purchased from a certified commercial laboratory;

(ii) Calcium fluoride, CaF_2, as a dilution material;

(iii) SRM 676*a* Corundum (at 20 weight percent), as an internal standard.

SRM 676*a* corundum was chosen as the internal-standard reference material, while the fluoride was chosen as a dilution material. Corundum content was maintained constant, while calcium fluoride was used to dilute alite and belite in the sample to generate data for calibration curves. The diluted values were close to the percentages of alite and belite typically encountered in commercial portland cement, approximately 40 to 60 wt.% for alite and 9 to 30 wt.% for belite. Three commercially available cements and one clinker were examined by both XRD-CC and XRD-RF, and the clinker was further examined by OM. The analyzed specimens were: PC1 cement, PC2 cement, PC3 cement, and C2 clinker. The cements used here were the same as in Chapter 4; however, the cements were heat treated prior to conducting calibration curve analysis to transform gypsum and hemihydrate to anhydrite to avoid interference with the belite peak in XRD-CC analysis.

5.2.2 XRD-CC Procedure/Strategy

The calibration curve method is based on the analysis of a single-peak intensity for the phases of interest in the analyzed material as well as in the internal-standard material. The single-peak intensity is the integrated area under the experimental or theoretical fitted peak [1]. The procedure for the single-peak intensity measurements involves two steps: fitting of the experimental peak, and calculating the integrated area under the fitted peak. The selected cements were calcined at 500°C for one hour to drive off the water and convert the gypsum and hemihydrate to anhydrite [2, 3]. This eliminates peak overlap since the gypsum and hemihydrate peaks interfere with belite, and provides a single resolvable belite diffraction peak for calibration curve measurements.

The calibration curve method is considered as part of the internal-standard method and is based on the analysis of single peak intensities, I_p and I_S, for the phase p and the internal-standard material [1, 2, 4, 5]. According to Klug and Alexander [1], the intensity ratio

$$\frac{I_p}{I_S} = k\frac{W_p}{W_S} = k' W_p \qquad \text{Equation 5-1}$$

eliminates the necessity to know the mass absorption coefficients of the phase p and the internal-standard material [1, 4]. Here, W_p and W_S are the weight fractions of the phase p and the internal-standard material, and k' is the calibration constant derived from the plot I_p/I_S versus W_p for a known weight fraction, W_S, of the internal-standard material. To get sufficient data for a calibration curve or the calibration constant k', a set of mixtures of the standard material with the phase of interest are prepared; at least three mixtures with known minimum, medium and maximum weight fractions of W_p should be prepared.

The XRD patterns from a set of at least three mixtures provide I_p/I_S versus W_p, and the linear fitting of these data points provides the calibration curve and the calibration coefficient k'. Then, these calibration curves can be used for the quantification of a single phase p in a multiphase material via measurement of the I_p/I_S ratio and using:

$$W_p = \frac{1}{k'}\frac{I_p}{I_S} \ . \qquad \text{Equation 5-2}$$

The relationship between the precision (standard deviation), s_W, of the weight fraction and the precision (standard deviation), s_I, of the intensity ratio is given by the following relationship:

$$s_W = \frac{1}{k'} s_I \quad . \qquad \text{Equation 5-3}$$

Within the calibration curve analysis, the precisions (s_W, standard deviation) of the weight fractions were determined according to Equation 5-3. The precision, s_I, of the intensity ratio is the sum of the precisions (standard deviations) $s_{I(invest)}$ and $s_{I(calibr)}$ of the investigation and calibration materials, respectively. In Equation 5-4, $s_{I(calibr)}$ is the average value of the intensity ratio standard deviations for the three mixtures of the calibration curve.

$$s_I = s_{I(invest)} + s_{I(calibr)} \qquad \text{Equation 5-4}$$

In establishing the calibration curves for alite and belite, the following peaks were selected:

(i) alite: $2\theta_{Alite} = 51.7^o$;

(ii) belite: $2\theta_{Belite} = 31^o$;

(iii) corundum SRM 676*a*: $2\theta_{Cor} = 43.3^o$

Corundum was added at 20 wt.% in the mixtures to provide an alite-to-corundum intensity ratio close to unity. The calibration curves for alite and belite quantification are presented in Figure 5-1 and Figure 5-2 as the average intensity ratios versus the weight fractions of W_{Alite} and W_{Belite}. The alite and belite calibration constants determined from the data were $k'_{Alite} = 0.0255$ and $k'_{Belite} = 0.0083$, respectively.

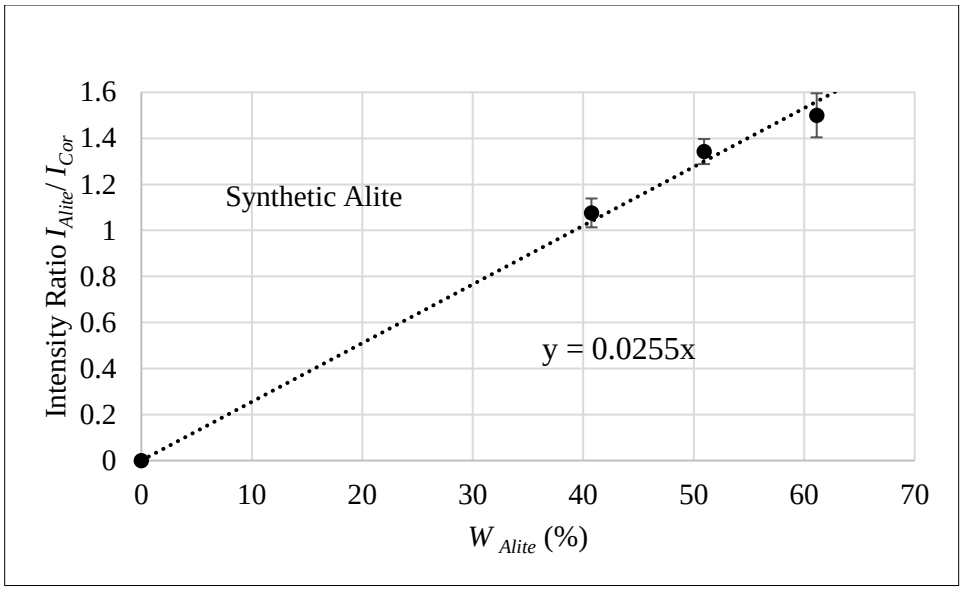

Figure 5-1: Alite calibration curve

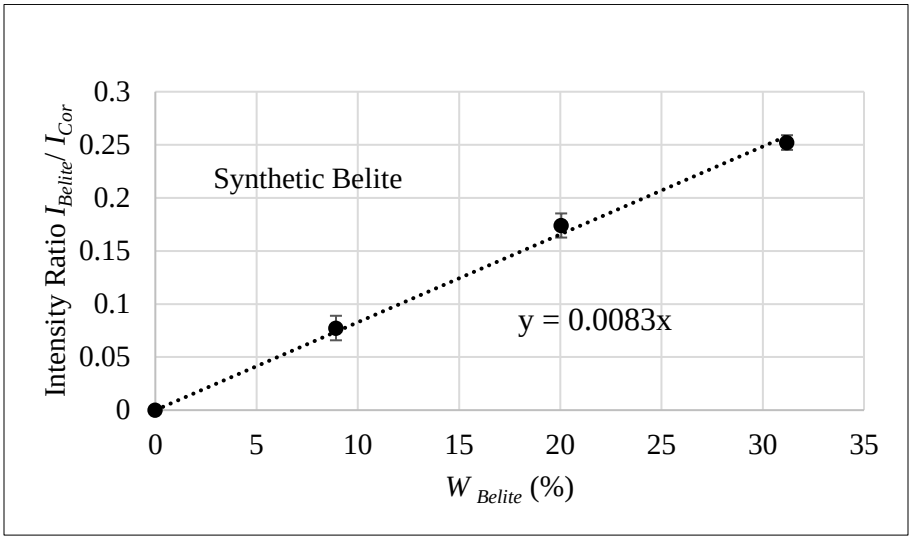

Figure 5-2: Belite calibration curve

5.2.3 OM Methodology

The comparative and complex studies of cements and clinkers made by different methods enabled the general conclusion that Rietveld refinement analysis is currently the most reliable and accurate way for phase quantification [6 - 8]. However, in combination with optical microscopy and spectroscopic microanalysis, these methods give more complete information concerning the composition, complex chemistry, and crystallography of phases [9].

Optical microscopy can provide qualitative and quantitative information about the microstructure of the clinker and cement, and can aid in the control of the clinker and cement quality [10]. Preparation of clinker and cement samples involves the following general steps [10]:

- crushing and grinding sample to usable particle size
- mounting sample and epoxy-impregnating
- grinding and polishing the sample, and
- etching the surface of the sample

The use of different etchants reveals the color and texture contrast of different phases for easier observation, investigation, and identification [10]. Phase identification is based on the relative sizes, shapes, colors, and textures of the cementitious grains. Point-count analysis can be used to estimate the phase volume fractions [11]. The point-counting procedure was done in accordance with the ASTM C1356-07 Standard [12]. In this procedure, the samples were moved with uniform steps on a grid pattern using a position-adjustable microscope stage. The grid pattern can be established with a grid reticle in the microscope eyepiece, or using a cross-hair in the eyepiece with a mechanical point-count microscope stage. The phase present at each grid point is identified and counted. The quantification of phases in the point-counting method is based on the principle that the areas of the phases on the polished section of the sample are proportional to their volumes in the sample [13]. However, this principle is valid for statistically isotropic samples, where the preferred orientation of phases is minimized. This condition is usually hard to satisfy, especially for clinker material. Several more factors strongly affect the phase quantification by the point-counting method in optical microscopy. For heterogeneous materials like clinkers, where grains can be composed of a single crystalline phase or a distribution of crystalline phases, accurate phase identification and quantification is difficult. Additionally, the quantification of aluminate

and ferrite phases by the point-counting method is often quite difficult because of their very small crystallite size within the microstructure [6, 14].

5.2.3.1 Sample Preparation

The sample preparation adopted from reference [10] is followed in preparing samples for optical study. In the following sections, the sample preparation procedures are outlined.

5.2.3.2 Sample Mounting

(i) Crush and grind clinker nodules using mortar and pestle to obtain sample fragments finer than 2.38 mm (passing #8 sieve);

(ii) Clean the sample fragments in 200 proof ethanol for 5 minutes using an Ultramet 2003 Sonic Cleaner;

(iii) Dry the sample fragments for 5 minutes using a hairdryer;

(iv) Place the sample fragments into a mounting cup coated with a release agent;

(v) Mix 25 g of epoxy resin (EPO-TEK 301A from Epoxy Technology Company) with 10 grams of hardener (EPO-TEK 301B). The viscosity at room temperature was reported by the manufacturer to be 100-200 cPs. Stir the mixture for 3 minutes;

(vi) Fill the mounting cup with activated epoxy resin half-way, prod with wire for about 1 minute to dislodge bubbles, and place the mounting cup into a Logitech Epvac Vacuum chamber to remove air-bubbles;

(vii) Fill the mounting cup with the remainder of the epoxy and repeat the previous de-airing step (*vi*);

(viii) Cure the impregnated clinker sample in an oven at 50°C for 3 hours.

5.2.3.3 Sample Surface Grinding and Polishing

(i) Cured samples were ground with Struers MD Piano (220, 500, 1200-grit) grinding disks using ethylene glycol as a lubricant in order to prevent hydration of the clinker particles overheating of the sample surface. The rotational speed of the disks ranged from about 150 - 300 rpm;

(ii) Initial polishing of the sample surface was accomplished with a Struers MD Dur polishing disk using 3µm diamond paste;

(iii) Final polishing was done with an MD Nap polishing disk with 0.05 µm Al_2O_3 powder.

5.2.3.4 Sample Surface Etching and Staining

(i) The freshly polished sample surface was etched with ammonium nitrate solution (1g NH_4NO_3 + 20 mL H_2O + 20 mL ethyl alcohol + 10 mL acetone + 150 mL isopropyl alcohol) for 15 seconds, cleaned with 200 proof ethanol, and dried with a hair dryer;

(ii) The sample surface was stained with salicylic acid stain (0.2g salicylic acid + 25 mL H_2O + 25 mL ethyl alcohol) for 10 seconds, cleaned with 200 proof ethanol, and dried with a hair dryer.

5.2.3.5 Typical Characteristics of Clinker Phases

Alite consists of trigonal, monoclinic, and triclinic modifications of impure tricalcium silicate, C_3S [10]. Alite generally occurs as a well-defined crystal with sharp edges and hexagonal morphology. When etched with ammonium nitrate, alite crystals reflect brown in polarized light, and after being stained with salicylic acid, alite crystals can reflect blue, brown, or light yellow (see Figure 5-3). Commonly, alite crystals can contain belite and matrix inclusions, and secondary belite coatings [10, 15]. Another common feature of alite crystals is structural variation that occurs due to selective inclusion of different ions during the alite formation process. This distinction is noticeable in the etched polished section, where the colors of alite crystals vary from brown to blue [15].

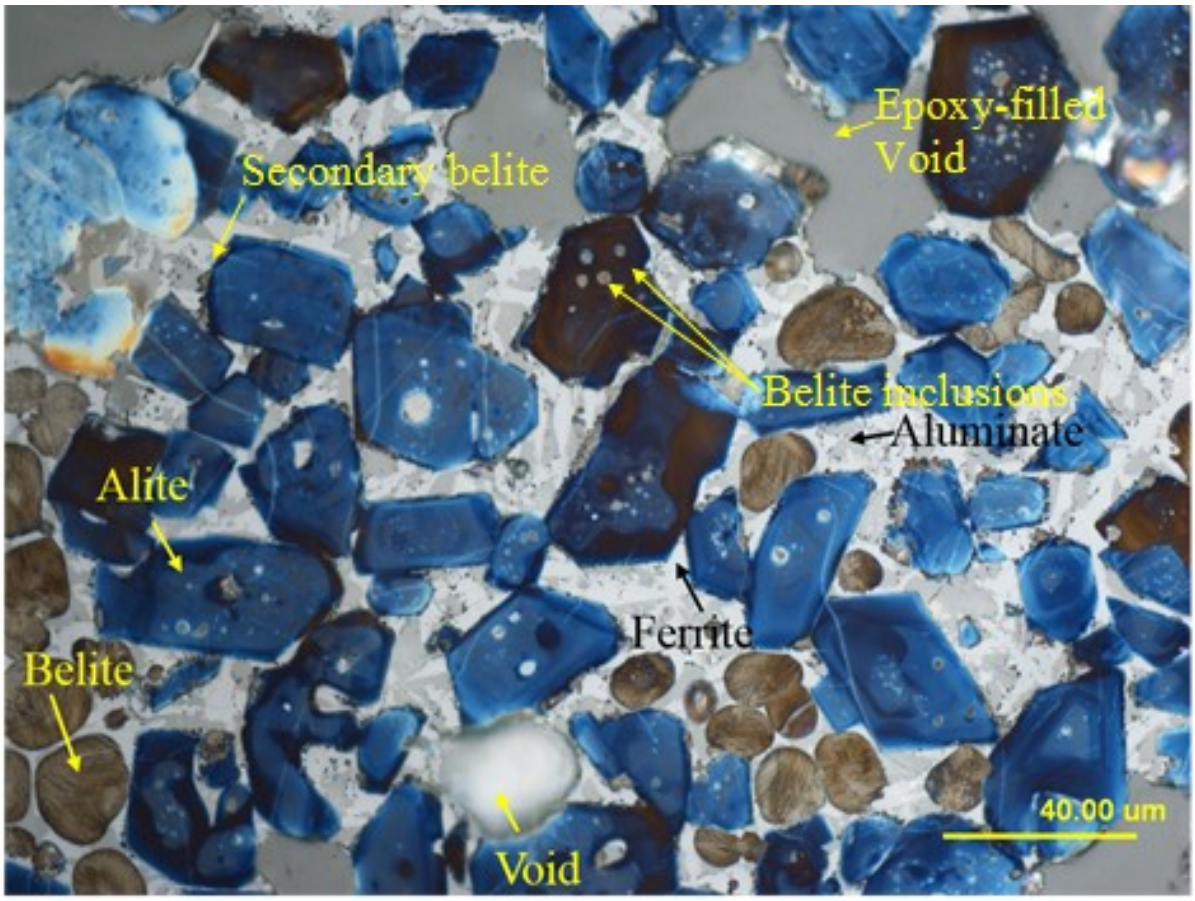

Figure 5-3: Optical image of clinker after etching and staining, 500x

Belite is a solid solution of impure dicalcium silicate, C_2S [10]. Belite crystals are typically of round morphology with cross lamellar structure. Belite crystals can also take on ragged shape, with lamellae extending into the matrix. After etching using ammonium nitrate and salicylic acid stain, belite crystals ranged from light to dark brown in color [10] (see Figure 5-3). At the clinkering temperature during production, alite and belite grains are typically surrounded by a liquid matrix phase that is mainly an iron-aluminum-calcium-silicate. During cooling, tricalcium aluminate, tetracalcium aluminoferrite, and secondary belite crystallize from the matrix. Minor phases of periclase and sulfate crystals can also form during cooling [15].

Tricalcium aluminate, C_3A, consists of xenomorphous to rectangular crystals of varying sizes. On a polished section, aluminate is visible as the light-gray areas of the solidified liquid phase. Ferrite, C_4AF, is an orthorhombic solid solution that typically forms a mesh in which C_3A crystallizes. Under polarized light, ferrite appears as a white network between alite and belite

crystals. Free lime is often present in contact with alite, but not in contact with belite because free lime and belite react to produce alite [15]. In clinkers and cements, expansive hydration produces popcorn-like crystals of calcium hydroxide that surround grains of free lime. Free lime occurs as grey, rounded grains that occur separately, in clusters, or as inclusions in aluminates or alite [10]. Periclase (cubic magnesium oxide) occurs as small triangular, octahedral, rectangular, or rounded grains, or as dendritic crystals. On a polished section, periclase has a pinkish, light-gray color.

5.2.3.6 Quantification of Clinker Phases

Point counting entails the identification and recording of the phase under cross-hair intersections or dots in an eyepiece reticle [10]. During the point count analysis, a grid is superimposed on the observed clinker surface. Grid dimensions are usually chosen in such a way that the cross-hair intersections do not fall on the same crystal, except for the few unusually large crystals. Figure 5-4 shows different grid proportions during the application of the point count method. Figure 5-4 (a) is an example of how grid dimensions should be used to get a more representative phase count because most of the cross-hairs fall on a different crystal. Figure 5-4 (b) is an example of underrepresentation of clinker phases because many of the phase crystals are missed by the crosshairs. Figure 5-4 (c) is an example of overrepresentation of clinker phases because many crosshairs fall on the same crystal.

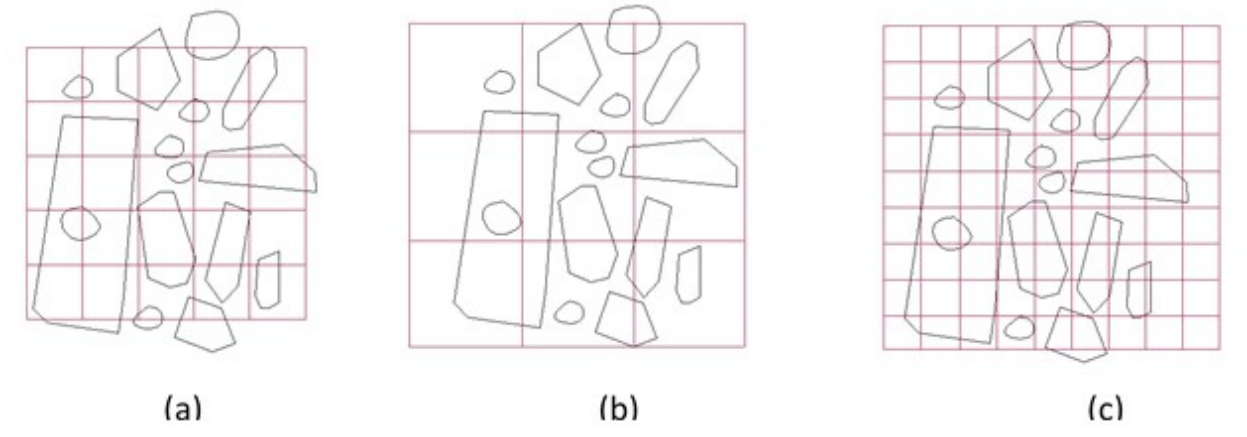

Figure 5-4: Illustration of different grid proportions

The volume fraction of each phase was calculated by dividing the number of points counted for that phase by the total number of points. This number multiplied by 100 yields the phase content

in volume percent (V) [12]. In order to find the weight percent W_p of each phase p, the volume percent of each phase (V_p) was multiplied by the respective phase density ρ_p and normalized by the total weight.

$$W_p = 100 \frac{V_p \rho_p}{\sum_p V_p \rho_p} (\%). \qquad \text{Equation 5-5}$$

Figure 5-5 through Figure 5-12 present some of typical variations in clinker morphology captured by optical microscopy. The polished clinker samples were prepared according to the procedures discussed previously in sections 5.2.4.1-5.2.4.4. The apparent heterogeneity in phase distributions, within each of the captured images, is noted.

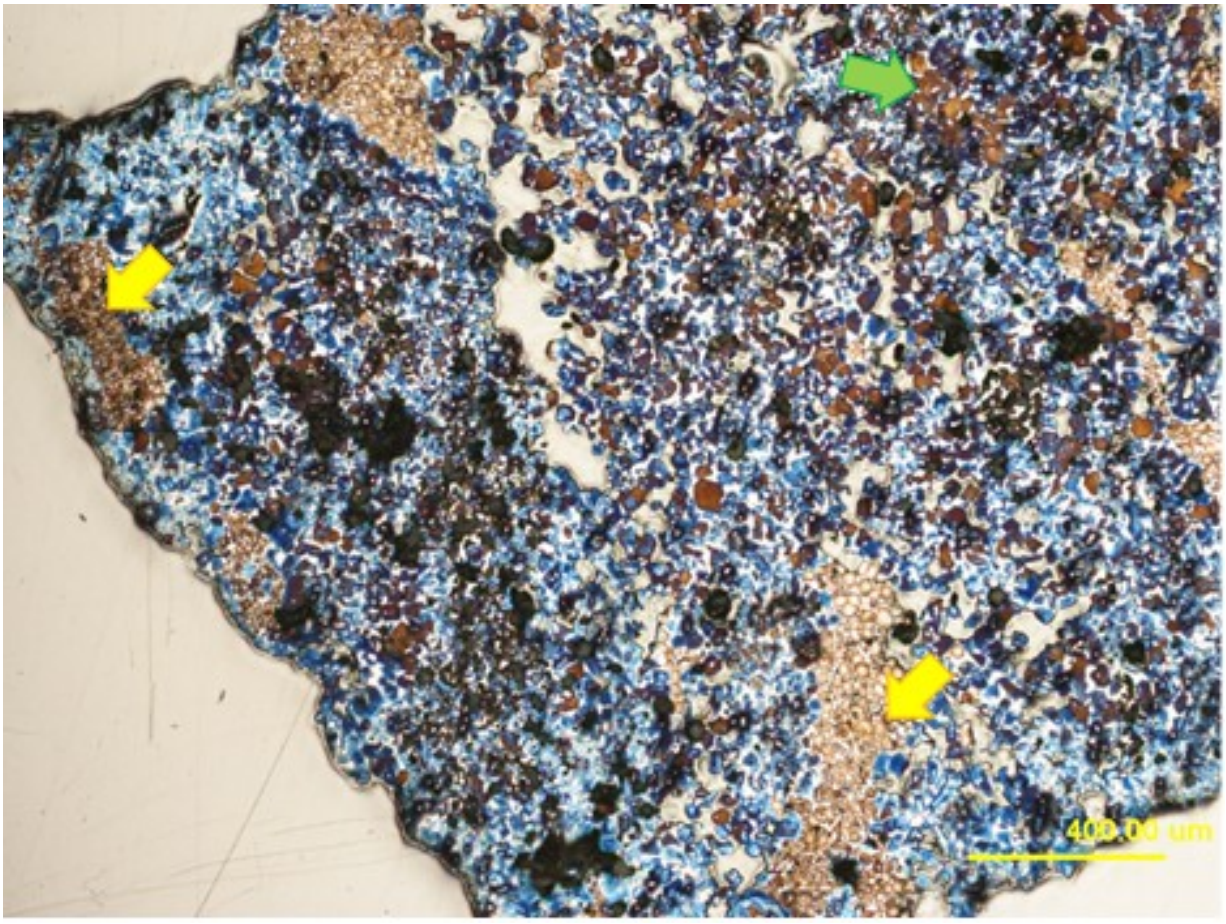

Figure 5-5: Optical micrograph (50x) of a polished clinker sample (15 second ammonium nitrate etch and 10 second salicylic acid stain)

In Figure 5-5 through Figure 5-7, large clusters of beige-brown belite crystals are noticeable along the edges of the clinker grain. Belite crystals have a rounded shape and appear to be light- to medium-beige with brown outlines (yellow arrows). These are not to be confused with the typically idiomorphous brown alite crystals (green arrow). A heterogeneous distribution of crystal phases in the porous clinker nodule can be seen in Figure 5-6. A wide size range of alite crystals, ranging in color from dark-blue to brown are observable. Clustering of beige-colored belite crystals is apparent in the top right corner and in the bottom center of the image. Small groups of round black grains of free lime are well dispersed throughout the nodule.

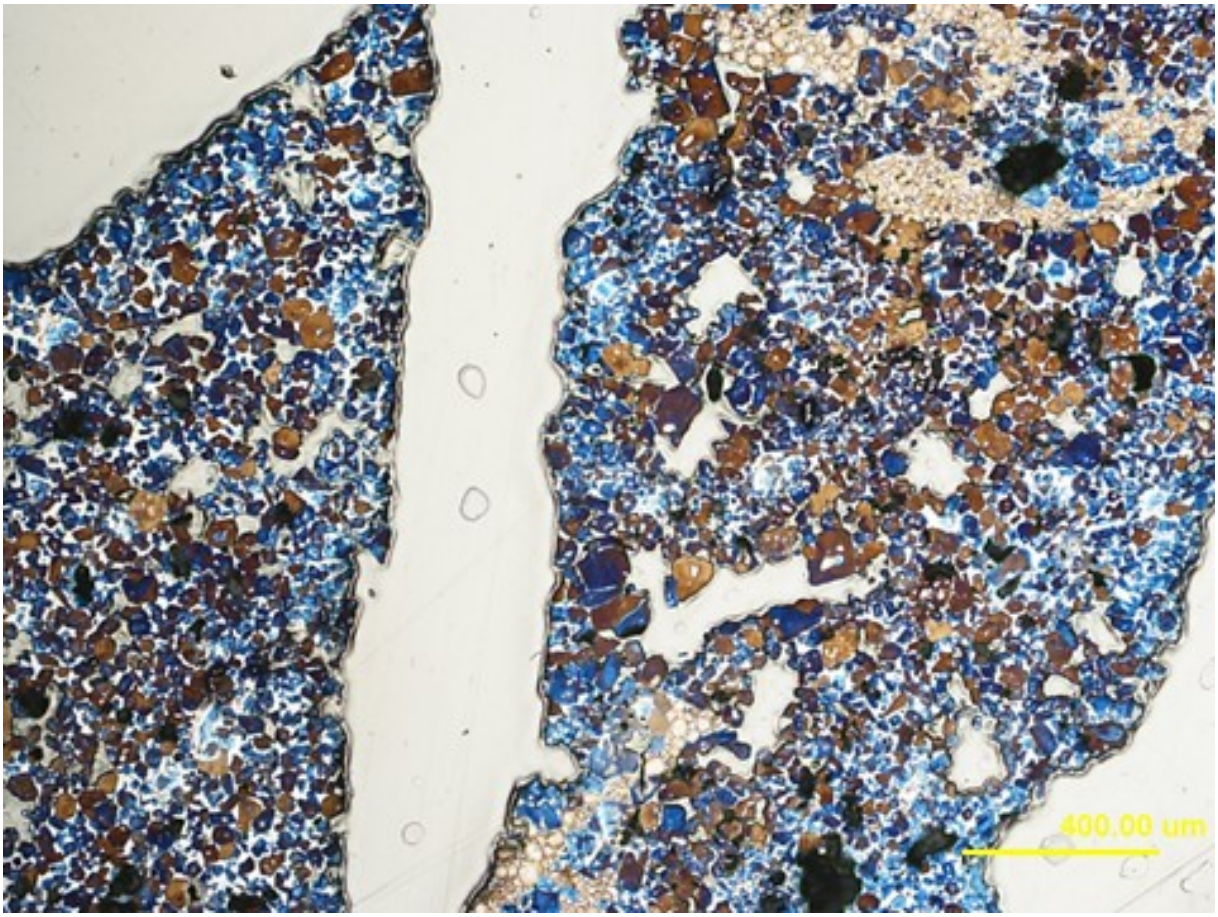

Figure 5-6: Optical micrograph (50x) of a polished clinker sample (15 second ammonium nitrate etch and 10 second salicylic acid stain)

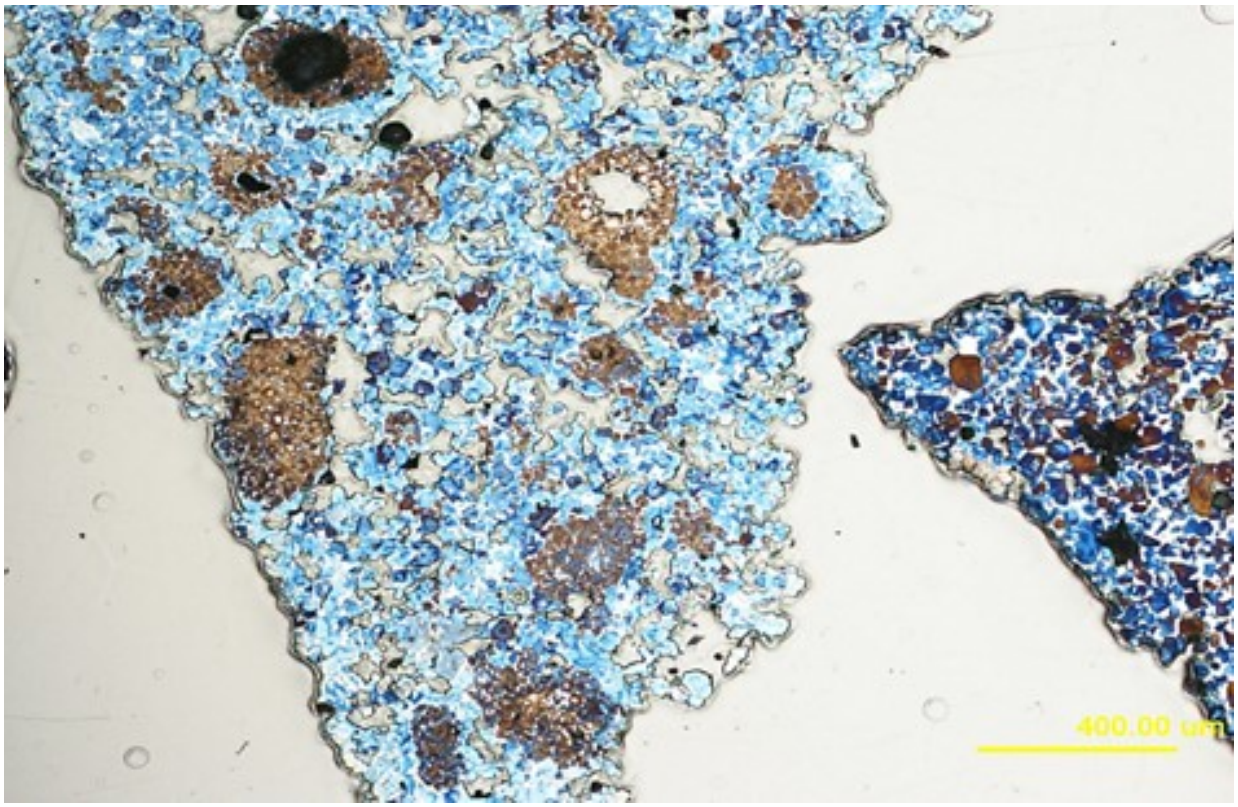

Figure 5-7: Optical micrograph (50x) of a polished clinker sample (15 second ammonium nitrate etch and 10 second salicylic acid stain)

The clinker nodule on the left in Figure 5-7 is porous with a heterogeneous distribution of crystal phases. It contains more light-blue alite crystals that were more reactive to the salicylic acid stain. Large clusters of brown belite appear to be common on the edges of voids and pores. The clinker nodule on the left of Figure 5-7 appears to have a slightly better distribution of belite than the nodule on the right, which also has darker alite crystals.

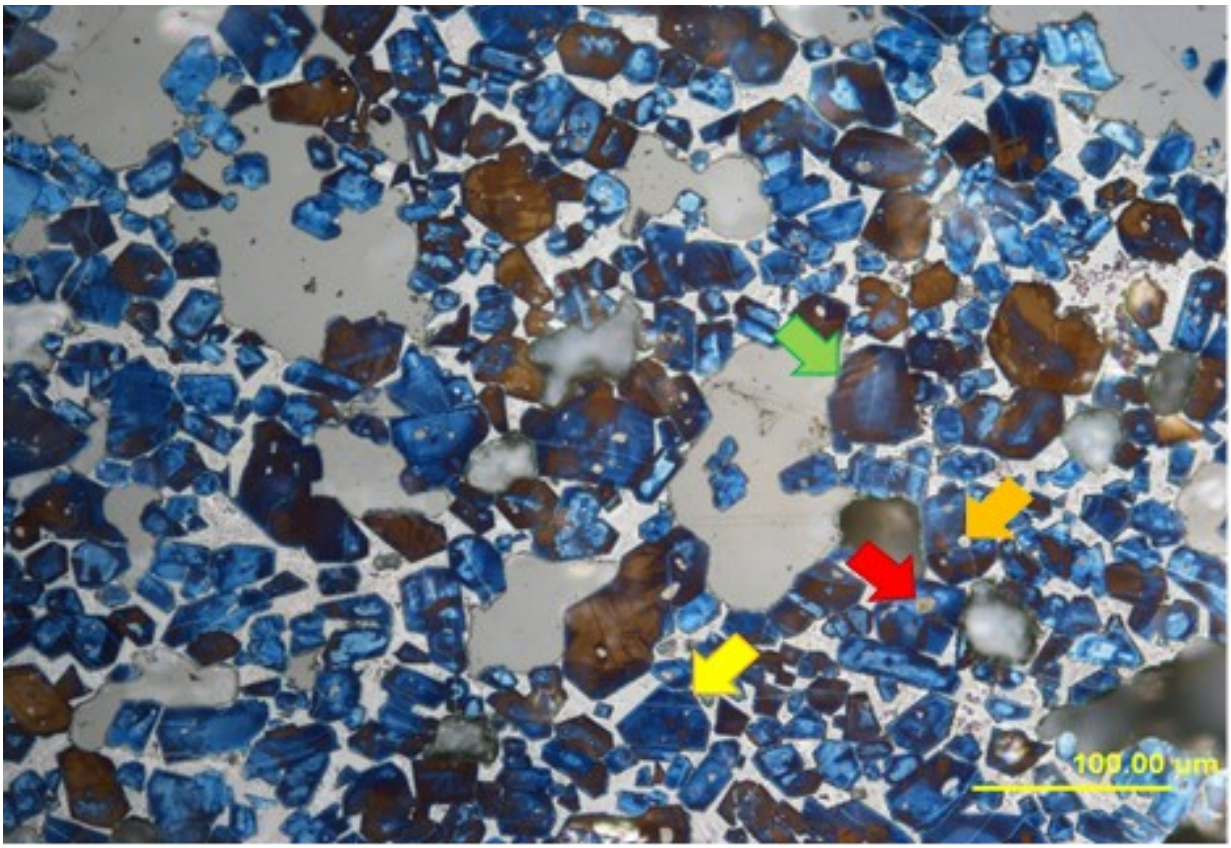

Figure 5-8: Optical micrograph (200x) of a polished clinker sample (15 second ammonium nitrate etch and 10 second salicylic acid stain)

Figure 5-8 shows a wide size range of alite crystals, from very small to large. The alite crystals are uniformly distributed and are mostly idiomorphous (yellow arrow) with some xenomorphous (green arrow) alite crystals. Alite crystals vary in color from medium blue to dark blue to brown. Other observations include a relatively low content of solidified liquid (matrix phase) containing a relatively dull ferrite phase and medium-sized aluminate grains, small round belite inclusions in the alite crystals (red arrow), and belite inclusions in the matrix (orange arrow). Care must be taken not to mistake belite inclusions in the alite for porosity. The inclusions are brown or white and at the same surface height as the crystals, whereas pores are recessed and appear grey-black. A trail of small, xenomorphous periclase crystals is visible in the upper left corner of Figure 5-8; small clusters and individual grains of free lime inconsistently occur at the top of pores and in the matrix phase.

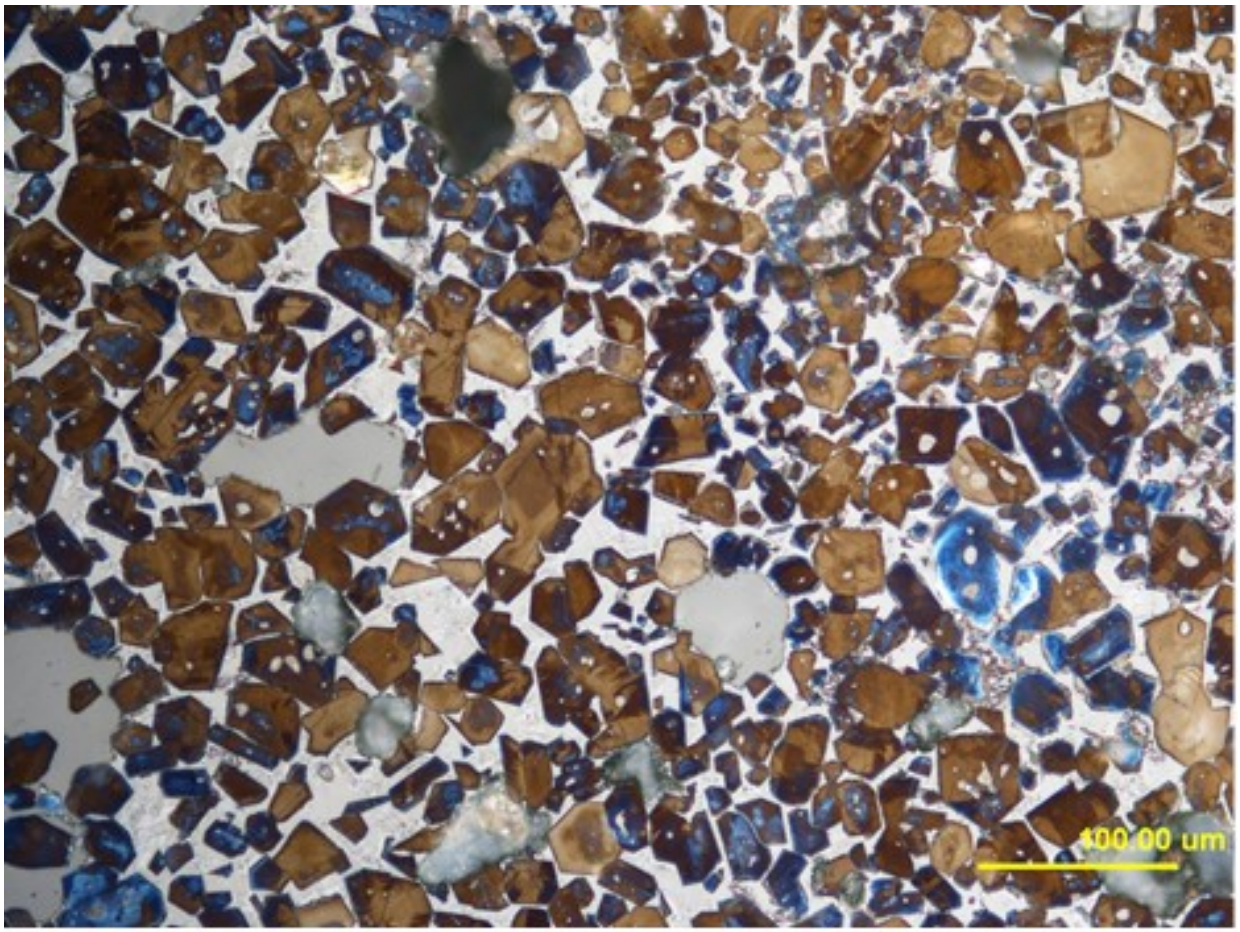

Figure 5-9: Optical micrograph (200x) of a polished clinker sample (15 second ammonium nitrate etch and 10 second salicylic acid stain)

Figure 5-9 shows a clinker nodule that is heterogeneous and moderately porous. The microstructure contains mainly alite grains with a range of sizes. The clinker also contains belite, matrix inclusions, and a low amount of free lime. Most of the alite crystals exhibit a brown color with an idiomorphous (typical) to xenomorphous shape. No belite can be seen; however, the matrix contains less-reflective ferrite and medium-sized aluminate inclusions.

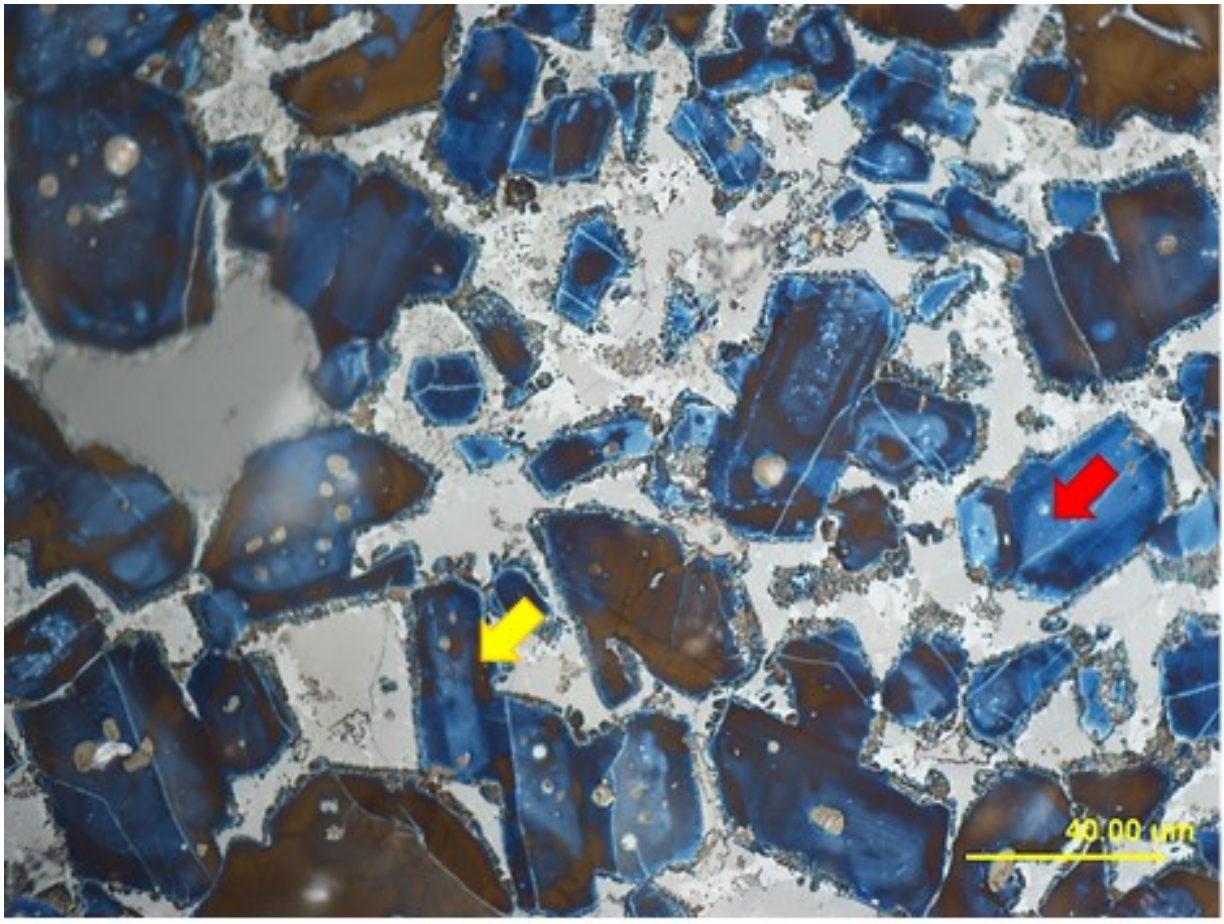

Figure 5-10: Optical micrograph (500x) of a polished clinker sample (15 second ammonium nitrate etch and 10 second salicylic acid stain)

In Figure 5-10, the alite crystal shape ranges from idiomorphous (yellow arrow) to subhedral or xenomorphous (red arrow), with a wide range of grain sizes. Belite occurs only as inclusions and secondary belite. Small belite and matrix inclusions are present in many of the alite crystals. A thick fringe of dendritic, brownish-gray, secondary belite is present on the edges of the alite crystals and inside the matrix phase. Cannibalism of idiomorphic alite crystals is common in this granule (yellow arrow). The microstructure contains a relatively low content of matrix phase, which contains very coarse, prismatic aluminate crystals and bright ferrite crystals. In addition, dendritic periclase crystals and secondary belite can be seen.

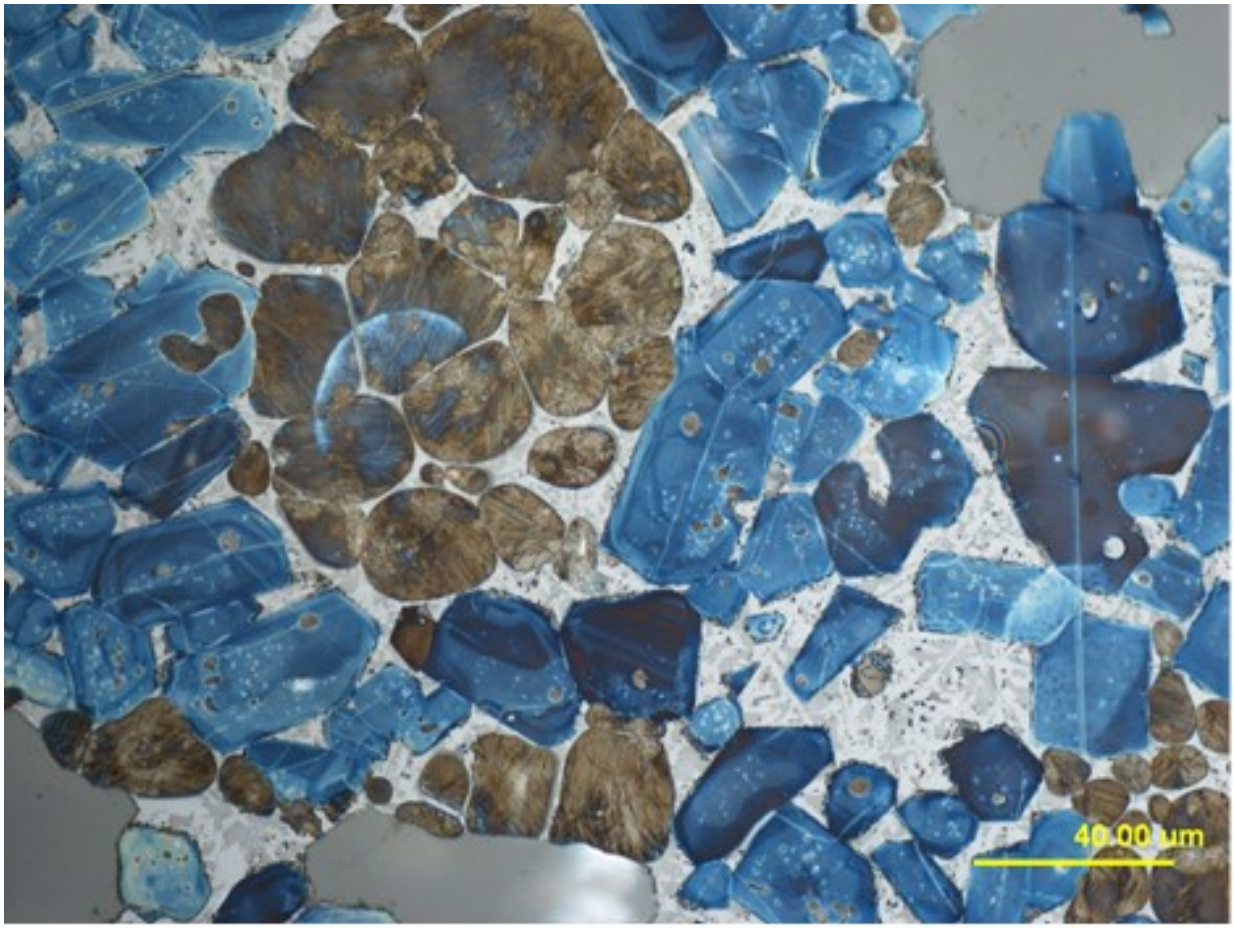

Figure 5-11: Optical micrograph (500x) of a polished clinker sample (15 second ammonium nitrate etch and 10 second salicylic acid stain)

The microstructure of the polished clinker sample shown in Figure 5-11 contains loosely packed alite and belite grains surrounded by a matrix containing aluminate and bright ferrite inclusions. The morphology of the alite grains ranges from subhedral to xenomorphous, and the rounded belite grains contain a cross-lamellar structure or have multidirectional lamellae. Many alite grains have belite inclusions. A thin fringe of secondary belite surrounds many of the alite grains. The large, gray, rounded areas visible in the bottom left, bottom center, and top right of the image are epoxy-filled holes in the clinker.

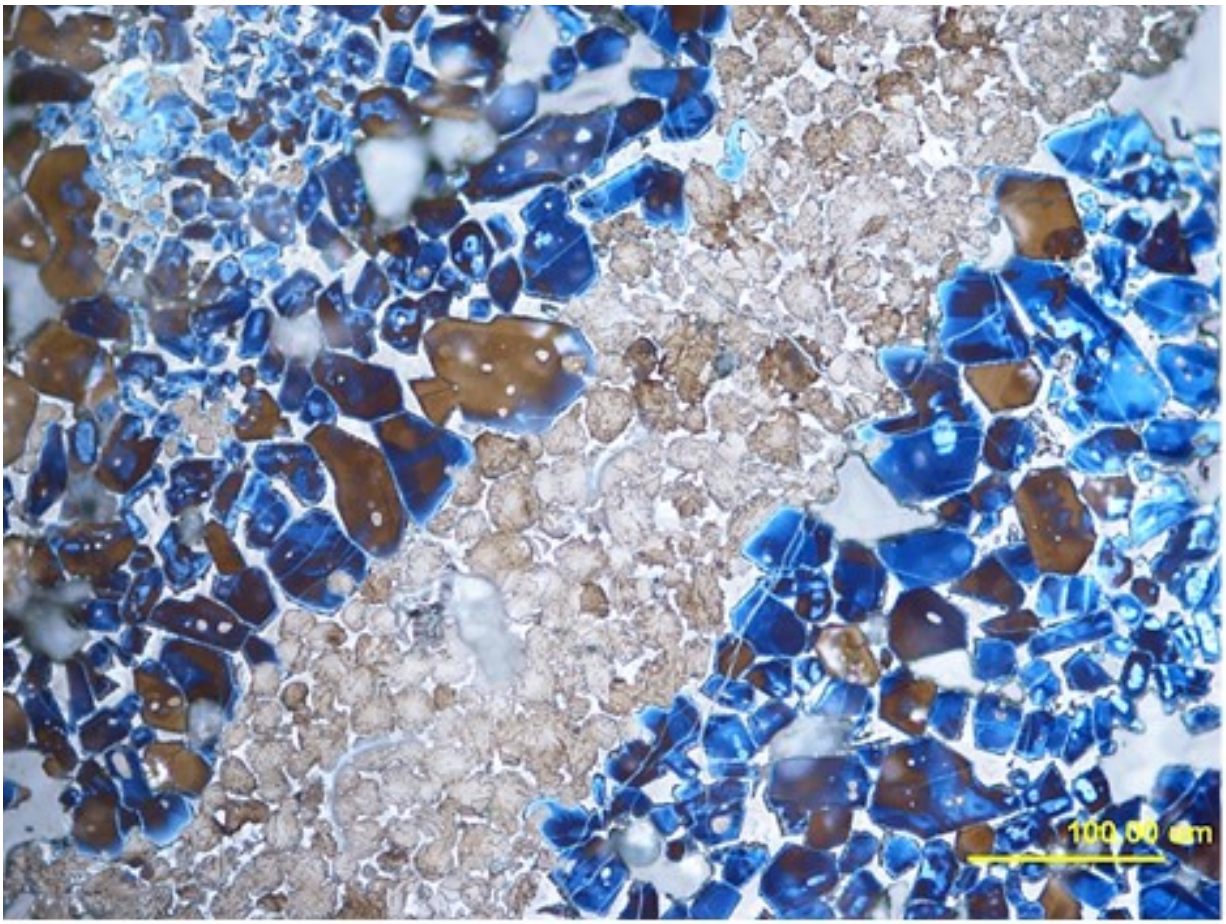

Figure 5-12: Optical micrograph (200x) of a polished clinker sample (15 second ammonium nitrate etch and 10 second salicylic acid stain)

A densely-packed vein of beige-brown, ragged belite grains can be seen diagonally traversing the clinker surface shown in Figure 5-12. The dark-blue to brown alite grains surrounding this vein of belite range from idiomorphous to xenomorphous, and appear to be larger next to the belite vein and temporarily decrease in size with distance from the vein. Free lime is visible on the pore surfaces.

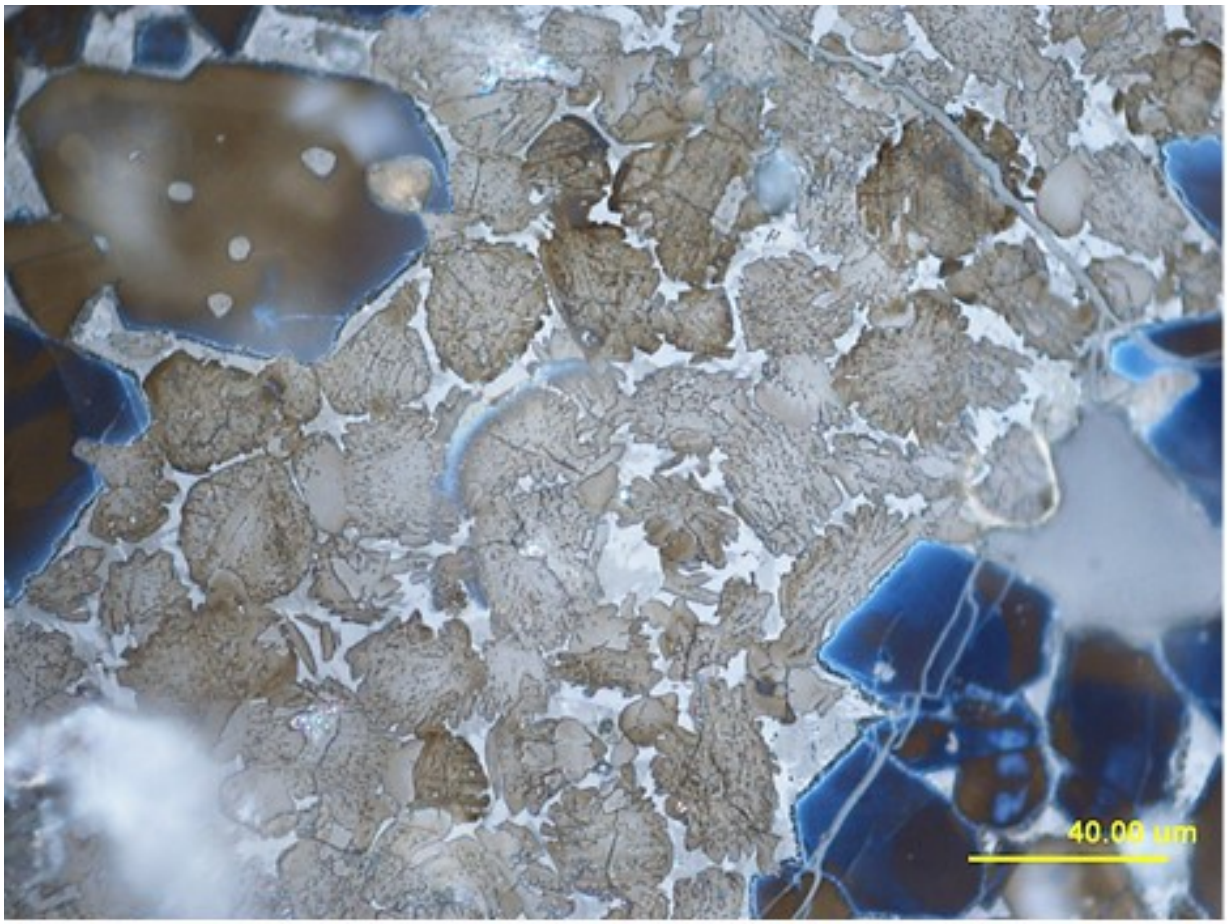

Figure 5-13: Higher magnification (500x) optical micrograph of the belite vein in the clinker microstructure shown in Figure 5-12

The densely packed belite vein from the microstructure in Figure 5-12 is shown at higher magnification in Figure 5-13, where the rough texture of the belite grains is easily seen. The presence of dendritic belite “fingers” can be seen extending into the matrix. The subhedral to xenomorphous alite grains, appearing dark blue to brown, can be seen at the edges of the belite vein. The matrix contains moderately bright ferrite and brighter aluminate inclusions.

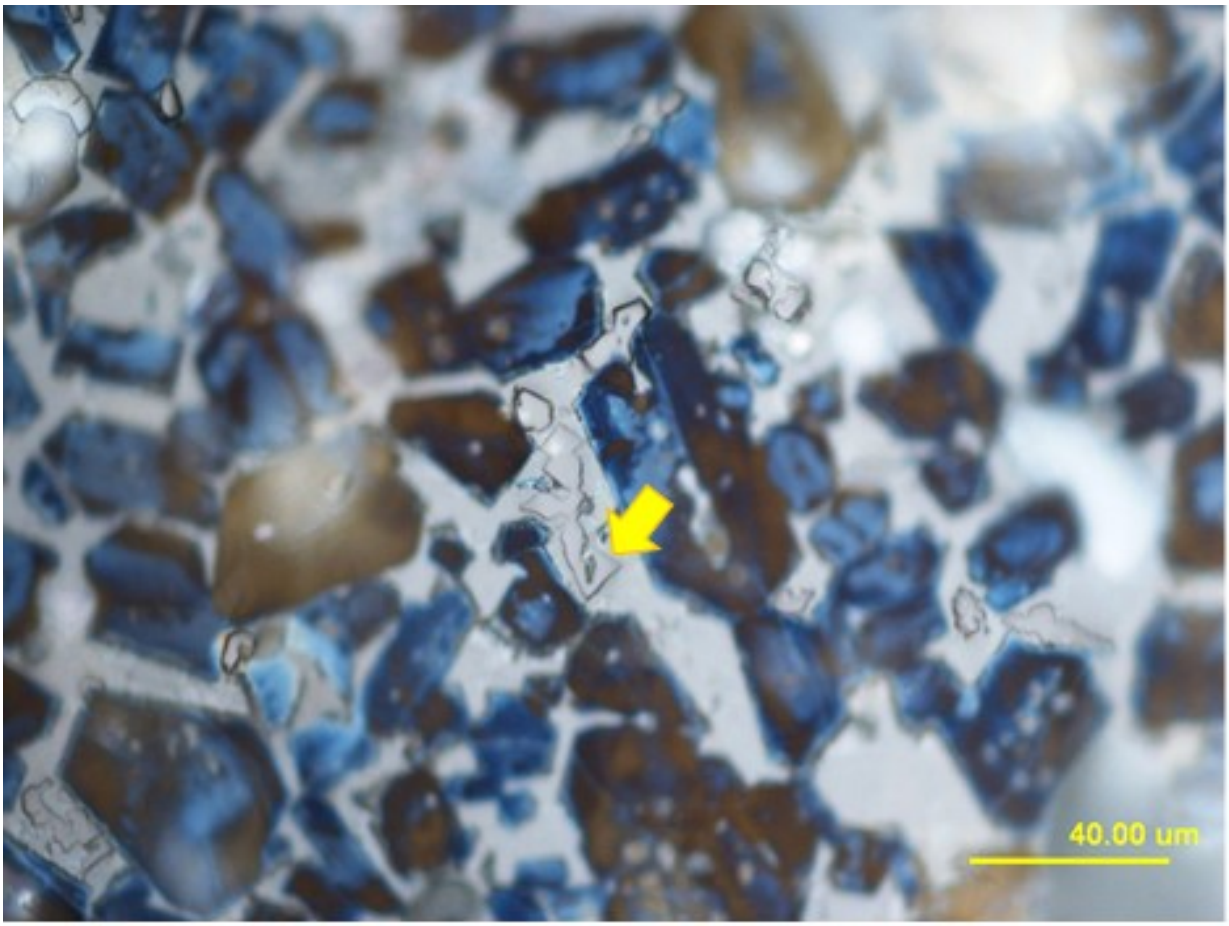

Figure 5-14: Optical micrograph (500x) of a polished clinker sample (15 second ammonium nitrate etch and 10 second salicylic acid stain)

The clinker microstructure presented in Figure 5-14 shows blue-brown, idiomorphous to xenomorphous alite grains, with rounded belite inclusions, surrounded by a matrix containing aluminate, dull ferrite, and periclase inclusions. A periclase crystal (yellow arrow) appears to be developing a dendritic structure. The periclase crystals are not level with the polished surface, indicating a difference in hardness.

5.3 Results and Discussion

As indicated previously, cements used in this part of the study were heat treated to transform gypsum and hemihydrate to anhydrite so as to avoid interference with the belite peak

used in XRD-CC analysis. The results for the 3 commercial cements PC1, PC2 and PC3, as well as C2 clinker are presented in Table 5-1.

Table 5-1: Silicate Phases Content in Cements and Clinker

Phase	PC1 Cement		PC2 Cement		PC3 Cement		C2 Clinker		
	XRD-RF	XRD-CC	XRD-RF	XRD-CC	XRD-RF	XRD-CC	XRD-RF	XRD-CC	OM
Alite	46.6(0.2)	43.0(4.8)	47.7(0.5)	44.1(3.3)	53.3(1.0)	57.4(3.4)	68.5(0.4)	65.4(3.3)	69.8
Belite	24.4(0.4)	20.5(2.0)	14.5(0.3)	13.8(2.3)	14.5(0.1)	11.4(1.5)	11.7(0.6)	6.6(2.2)	10.9

Comparing XRD-RF and XRD-CC indicates, in general, that the silicate phases' quantification using the calibration method yielded lower values than those determined through Rietveld refinement for all materials studied here. Additionally, the latter showed lower standard deviation than the former. Clinker phase analysis results using optical microscopy were in good agreement with those determined through Rietveld analysis. Again, quantification using XRD-CC resulted in lower values for the two silicate phases, alite and belite. However, it must be stated that no attempt was made to recalculate the phases (Rietveld analysis) based on eliminating the unidentified content in C2 clinker (Chapter 4). Recalculation would increase the crystalline phase content by about 5.7% for the XRD-RF samples. One of the concerns in using optical microscopy to determine phase volume fractions is the number of images that must be analyzed to ensure that a representative sampling of the microstructure has been analyzed. Due to the time-consuming nature of the image analysis process, it is not favored as a routine method for phase quantification.

5.4 Conclusions

(i) It is critical to select appropriate materials in establishing XRD-CC for phase quantification. For example, the materials used for establishing calibration curves, in this case alite and belite, should have crystal structures that are similar to the commercial materials that are to be quantified. Also, the materials used for calibration must be free from peak overlap in the 2θ angular range selected for establishing the calibration curve.

(ii) In satisfying the above, it might be necessary to resort to selective dissolution to separate the phase(s) of interest from the commercial cement/clinker. This could be very challenging and time consuming. Additionally, if there are changes in the kiln

burning conditions or raw feed, the process must be repeated, or at a minimum verified, to determine the effects of the burning conditions on the crystal structure of the clinker phases.

(iii) The comparative analysis of the Rietveld and calibration curve techniques showed that quantification of silicate phases using calibration curves yielded lower values than for Rietveld analysis.

(iv) Calibration curve development can be challenging in the event there is peak overlap.

(v) The calibration curve analysis showed, in general, a lower precision for determination of phase weight fractions than with the Rietveld refinement analysis. This was expected as Rietveld analysis minimizes differences between measured and analyzed patterns for the whole scan versus an individual peak.

(vi) Optical microscopy phase quantification can be affected by phase inhomogeneity in the clinker nodules. It requires a properly trained and dedicated petrographer.

(vii) For clinker or portland cement phase analyses, it appears that Rietveld refinement is the most practical method to adopt, especially since it can be automated in cement production plants as well as in regulatory agencies.

5.5 References

[1] H. P. Klug and L. E. Alexander, *X-Ray Diffraction Procedures*, Second Edi. Wiley Interscience, 1974.

[2] P. E. Stutzman, "Guide for X-Ray Powder Diffraction Analysis of Portland Cement and Clinker," *NISTIR 5755*, 1996.

[3] C1365-06, "Standard Test Method for Determination of the Proportion of Phases in Portland Cement and Portland-Cement Clinker Using X-Ray Powder Diffraction Analysis," *Annu. B. ASTM Stand. ASTM Int. West Conshohocken, PA*, vol. Vol. 4.01, pp. 1–10, 2011.

[4] L. Alexander and H. P. Klug, "Basic aspects of X-ray absorption in quantitative diffraction analysis of powder mixtures," *Anal. Chem.*, vol. 20, no. 10, pp. 886–889, 1948.

[5] J. I. Langford and D. Louer, "Powder diffraction," *Rep. Prog. Phys.*, vol. 59, pp. 131–234, 1996.

[6] P. Stutzman and S. Leigh, “Phase Composition Analysis of the NIST Reference Clinkers by Optical Microscopy and X-ray Powder Diffraction Reference Clinkers by Optical Diffraction,” *NIST Tech. Note 1441*, pp. 1–44, 2002.

[7] G. Walenta and T. Füllmann, “Advances in quantitative XRD analysis for clinker, cements, and cementitious additions,” *Powder Diffr.*, vol. 19, no. 1, pp. 40–44, Mar. 2004.

[8] G. Le Saoût, V. Kocaba, and K. Scrivener, “Application of the Rietveld method to the analysis of anhydrous cement,” *Cem. Concr. Res.*, vol. 41, no. 2, pp. 133–148, Feb. 2011.

[9] A. Crumbie, G. Walenta, and T. Füllmann, “Where is the iron? Clinker microanalysis with XRD Rietveld, optical microscopy/point counting, Bogue and SEM-EDS techniques,” *Cem. Concr. Res.*, vol. 36, no. 8, pp. 1542–1547, Aug. 2006.

[10] D. H. Campbell, *Microscopical Examination and Interpretation of Portland Cement and Clinker*, Second Edi. Portland Cement Association, 1999.

[11] F. Hofmänner, “Microstructure of Portland Cement Clinker,” *Rheintaler Druckerei un Verlag, Heerbrugg, Switz.*, p. 48, 1975.

[12] C1356-07, “Standard Test Method for Quantitative Determination of Phases in Portland Cement Clinker by Microscopical Point-Count Procedure,” *Annu. B. ASTM Stand. ASTM Int. West Conshohocken, PA*, pp. 1–6, 2007.

[13] M. A. Delesse, “Procédé mécanique pour déterminer la composition des roches,” *Compte-Rendu l’académie des Sci. Paris*, vol. 25, pp. 544–545, 1847.

[14] H. F. W. Taylor, *Cement Chemistry*, Second edi. Thomas Telford Publishing, 1997.

[15] “Chapter 2: Portland Cement Clinker,” in *“Holderbank” Cement Seminar 2000 Materials Technology II*, Holderbank Management & Consulting, 2000, pp. 433–486.

Chapter 6. Portland-Limestone Cements

6.1 Introduction

One of the main objectives of the current study is to identify and quantify constituents of commercial SCM-blended cements as well as portland-limestone cements (PLCs). In this chapter, phase quantification and analysis for limestone blended cements will be presented. Rietveld refinement of the crystalline phases and the total amorphous/unidentified content (A/uC) was conducted on portland-limestone cements as well as limestones that are currently being considered for use in different construction projects in the state of Florida. Two portland-limestone cements, PCL1 and PCL3, and three limestones, L1, L2 and L3, were selected for quantitative analysis using Rietveld refinement.

6.2 Methodology

6.2.1 Refinement Procedure for Limestone

The refinement of limestone was carried out using an internal standard.

(i) Open the collected XRD scan and insert crystal structures identified during the Search and Match procedure described in section 2.3.2 including the structure for the internal standard.

(ii) Select the ***Polynomial*** background function and refine flat background.

(iii) Refine scale factors of all phases.

(iv) Refine zero shift.

(v) Refine coefficients 1 – 4 under the ***Background Polynomial***.

(vi) Refine lattice parameters. Minor phases should be excluded from refinement in this step. The lattice parameters for these phases can be refined individually.

(vii) Successive refinement should be carried out for the phases with the largest content to the smallest.

(viii) Refine the *W* parameter. For phases present in amounts of approximately 5-20%, this step should be accompanied by visual observation. If during refinement of one of the parameters, the value of this parameter increases dramatically and the shape of the calculated profile broadens beyond the collected profile, undo this refinement step and

limit the ***Set Value Range (%)*** for the *W* parameter in the ***Object Inspector*** pane. This may be repeated several times until good agreement between the simulated and the collected pattern is observed. This should be done during *V* and *U* refinement as well. For phases present in amounts of approximately 1-5%, only refine the *W* parameter. However, if a strong, non-overlapped peak of this minor phase can be clearly observed in the collected pattern, the *V* and *U* parameters can be refined as well with visual observation. For phases present in amounts below 1%, refinement of *W*, *V*, *U* and preferred orientation parameters can be omitted.

(ix) Refine the *V* parameter.

(x) Refine the *U* parameter.

(xi) Refine preferred orientation if necessary.

(xii) Repeat steps *(viii)* through *(xi)* until all the phases have been considered.

6.2.2 Refinement Procedure for PC-Limestone Blends

(i) Perform KOSH and SAM extractions as described in section 2.2.3.

(ii) Open the collected XRD scan for each extraction residue.

(iii) Insert crystal structure identified during the Search and Match procedure.

(iv) For the refinement of extraction residues, select the ***Polynomial*** profile function in the background ***Object Inspector*** pane.

(v) Refine flat background.

(vi) Refine scale factors of all phases.

(vii) Refine zero shift.

(viii) Click on the ***Background Polynomial*** submenu and select ***Polynomial*** under ***Method***. Refine coefficients 1 – 4 under the ***Background Polynomial***.

(ix) Refine lattice parameters for all phases. For the minor phases (below 5%) refinement of lattice parameters at this point should be omitted.

(x) Simultaneously refine the *W* parameters for alite and belite for the KOSH extraction residue or aluminate and ferrite for the SAM residue.

(xi) Simultaneously refine the *V* parameters for alite and belite or aluminate and ferrite.

(xii) Simultaneously refine the *U* parameters for alite and belite or aluminate and ferrite.

(xiii) Refine preferred orientation for alite (KOSH extraction). Care should be taken to enter the correct hkl value for the direction of the preferred orientation in the ***Object Inspector*** pane.

(xiv) Uncheck *W*, *V*, *U* and preferred orientation parameters for the refined phases to exclude them from further refinement.

(xv) Consider the next most dominant phase. If refinement of lattice parameters for this phase was omitted in step *(ix)*, refine all the lattice parameters with visual observation. If peak shift beyond the collected pattern is observed, the lattice parameters for this phase should be excluded from refinement.

(xvi) If the phase considered in step *(xv)* is present in amounts above 5 wt.%, refine *W*, *V*, *U* parameters one at a time. For phases present in weight fractions of approximately 5-20%, this step should be accompanied by visual observation. If during refinement of one of the parameters the value of this parameter increases dramatically and the shape of the calculated profile broadens beyond the collected profile, undo this refinement step and limit the ***Set Value Range (%)*** for the *W* parameter in the ***Object Inspector*** pane. This may be repeated several times until good agreement between the simulated and the collected pattern is observed. This should be done during *V* and *U* refinement as well.

(xvii) Refine preferred orientation if necessary.

(xviii) Uncheck *W*, *V*, *U* and preferred orientation parameters for the refined phase.

(xix) If the phase considered in step *(xv)* is present in amounts of approximately 1-5%, only refine the *W* parameter. However, if a strong, non-overlapped peak of this minor phase can be clearly observed in the collected pattern, *V* and *U* parameters can be refined as well with visual observation. For phases present in amounts below 1%, refinement of *W*, *V*, *U* and preferred orientation parameters can be omitted.

(xx) Repeat steps *(xv) – (xix)* until all the phases have been considered.

(xxi) Uncheck all refined parameters for all phases and save the refined structures as a .cry file.

(xxii) Open the collected XRD scan for the PC-limestone blend and insert the .cry structures created during the KOSH and SAM residue refinements. It was observed that although a gypsum structure is refined as part of the SAM extraction residue,

the gypsum is altered by the extraction process, and the use of this refined gypsum structure results in overestimation of the gypsum content in as-received cement. Therefore, the gypsum structure to be used should be added from the database. The calcite structure was obtained from the KOSH residue refinement, as formation of additional calcite was observed during SAM extraction. The periclase structure was taken from the SAM residue refinement since there is less peak overlap compared to the KOSH residue.

(xxiii) Select the ***Polynomial*** profile function in the ***Background*** of the ***Object Inspector*** pane.

(xxiv) Repeat steps *(v) – (ix).*

(xxv) Repeat steps *(x) – (xii)* for alite and belite.

(xxvi) Repeat steps *(x) – (xii)* for aluminate and ferrite.

(xxvii) Refine the *W* parameter for the next most abundant phase.

(xxviii) Refine the *V* parameter.

(xxix) Refine the *U* parameter.

(xxx) Uncheck the *W, V, U* parameters for the refined phase and repeat steps *(xxvii) - (xxix)* for the remaining phases.

(xxxi) If the weight percentage of one of the phases is between 5-20 wt.%, visually observe the strong peak(s) of this phase. If, during refinement of one of the parameters, the value of this parameter increases dramatically and the shape of the calculated profile broadens beyond the collected profile, undo this refinement step and limit the ***Set Value Range (%)*** for the *W* parameter in the ***Object Inspector*** pane. This may be repeated several times until good agreement between the simulated and the collected pattern is observed. This should be done during *V* and *U* refinement as well.

(xxxii) For phases present in amounts of approximately 1-5%, only refine the *W* parameter. However, if a strong, non-overlapped peak of this minor phase can be clearly observed in the collected pattern, *V* and *U* parameters can be refined as well with visual observation.

(xxxiii) For phases present in amounts below 1%, refinement of *W, V, U* and preferred orientation parameters can be omitted.

6.3 Results and Discussion

In studying the minor phases in PLCs, scans of the extracted cement residue, as well as the scans of the accompanying limestones were used [1], [2] [3]–[6]. The literature indicates that the most commonly reported phases in limestone are: calcite, quartz, dolomite, mica, illite, microcline, muscovite, kaolinite, hematite, clinochlore, cristobalite, dolomite, siderite, and pyrite [3]–[6].

Typically, limestone blended with portland cements usually contains more than 75 wt.% calcite and less than 1 wt.% clay [7]. The chemical formulae, and the PDF and ICSD codes of the most predominant limestone crystalline phases are presented in Table 6-1 [3]–[6].

Table 6-1: Limestone Common Minerals

Phase	Formula	Crystal System	PDF codes	ICSD Code
Calcite	**$Ca(CO_3)$**	**Rhombohedral**	**01-086-0174**	**80869**
Dolomite	**$CaMg(CO_3)_2$**	**Rhombohedral**	**01-075-1711**	**31277**
Siderite	**$Fe(CO_3)$**	**Trigonal**	**01-080-0502**	**68298**
Smithsonite	$Zn(CO_3)$	Trigonal	01-083-1765	100679
Strontianite	$Cr(CO_3)$	Orthorhombic	01-074-1491	27293
Malachite	$Cu_2(OH)_2(CO_3)$	Monoclinic	01-075-1163	30609
Anhydrite	$CaSO_4$	Orthorhombic	01-086-2270	40043
Barite	$BaSO_4$	Orthorhombic	01-072-1378	16904
Quartz	**SiO_2**	**Rhombohedral**	**00-046-1045**	**41414**
Cristobalite	SiO_2	Tetragonal	01-071-0785	9327
Hematite	Fe_2O_3	Trigonal	01-087-1166	82904
Spinel	Al_2MgO_4	Cubic	01-073-6120	22354
Willemite	$Zn_2(SiO_4)$	Tetragonal	01-070-2488	9147
Wollastonite	$Ca(SiO_3)$	Monoclinic	01-072-2297	20589
Diopside	**$CaMgSi_2O_6$**	**Monoclinic**	**01-071-1067**	**9672**
Clinochlore	$Mg_6(Si_4O_{10})(OH)_8$	Triclinic	01-073-2376	24950
Illite	$K(Al_4Si_2O_9(OH)_3)$	Monoclinic	01-070-3754	90144
Kaolinite	$Al_2(Si_2O_5)(OH)_4$	Triclinic	01-075-1593	31135
Mica	$KFe_3(Al_{0.24}Fe_{0.76}Si_3)O_{10}(OH)_2$	Monoclinic	01-073-9317	59843
Microcline	$K(AlSi_3O_8)$	Triclinic	01-071-0955	9542
Muscovite	$KAl_2((Si_3Al)O_{10}(OH)_2)$	Monoclinic	01-077-2255	60569
Fluorite	CaF_2	Cubic	01-075-0363	29008
Marcasite	FeS_2	Orthorhombic	01-089-2089	42726
Pyrite	FeS_2	Triclinic	01-071-1680	10422
Sphalerite	ZnS	Cubic	01-071-5976	77090

The structures used in the Rietveld refinement of limestones are indicated by the bold letters in Table 6-1.

For the crystalline and the amorphous/unidentified content determinations, as-received PLCs and limestone were each mixed with 20 wt.% of corundum as an internal-standard material [5], [8]–[12].

6.3.1 Limestone

6.3.1.1 L1

The phase search and match procedure and the Rietveld refinement analysis showed the presence of the following three crystalline phases in L1 limestone: calcite, quartz, and siderite. The weight fraction of the major crystalline phase, calcite, was about 98 wt.%. The amorphous/ unidentified content in L1 was less than 1 wt.%. The crystalline and amorphous/ unidentified contents in L1 are shown in Table 6-2.

Table 6-2: Mineralogical Analysis of L1 Limestone

	Wt. (%)			
Phase	P1-S1	P2-S1	P3-S1	AVERAGE (STDEV)
Calcite	97.9	98.2	98.3	98.1 (0.2)
Quartz	0.7	0.7	0.7	0.7 (0.0)
Siderite	0.4	0.4	0.4	0.4 (0.0)
A/uC	1.0	0.7	0.6	0.8 (0.2)

6.3.1.2 L2

The phase search and match procedure and the Rietveld refinement analysis showed that the L2 contains only two crystalline phases: calcite and quartz. The weight fraction of calcite was about 96 wt.%. The L2 has a higher amorphous/unidentified content, of about 4 wt.%. Phase analysis of L2 is shown in Table 6-3.

Table 6-3: Mineralogical Analysis of L2 Limestone

Phase	*Wt.* (%)			
	P1-S1	P2-S1	P3-S1	AVERAGE (STDEV)
Calcite	95.4	95.7	97.0	96.0 (0.9)
Quartz	0.3	0.3	0.3	0.3 (0.0)
A/uC	4.4	4.1	2.7	3.7 (0.9)

6.3.1.3 L3

The phase search and match procedure and Rietveld refinement showed the presence of the following four crystalline phases in L3 limestone: calcite, quartz, dolomite, and diopside. L3 had the lowest calcite content, about 82 wt.%. The amorphous/unidentified content in L3 was about 3 wt.% (see Table 6-4).

Table 6-4: Mineralogical Analysis of L3 Limestone

Phase	*W* (%)			
	P1-S1	P2-S1	P3-S1	AVERAGE (STDEV)
Calcite	81.6	81.9	82.0	81.8 (0.2)
Quartz	2.5	2.6	2.6	2.6 (0.1)
Dolomite	11.3	11.5	11.4	11.4 (0.1)
Diopside	1.7	1.7	1.5	1.6 (0.1)
A/uC	3.0	2.3	2.6	2.6 (0.4)

6.3.2 Portland-Limestone Cements

6.3.2.1 PCL1 Cement

The phase search and match procedure and the Rietveld refinement showed the presence of the following minor phases in PCL1 cement: portlandite, quartz, hemihydrate, and syngenite. The weight fractions of portlandite, quartz and hemihydrate were less than 1 wt.%, while the weight fraction of syngenite was about 1.4 wt.%. The weight fractions of calcite and gypsum in the cement, which come from grinding of the portland cement clinker with limestone and gypsum, were about 11 wt.% and 3.5 - 4.0 wt.%, respectively. The amorphous/unidentified content in PCL1 cement was about 10 wt.%. The amount of ferrite (almost 10 wt.%) was about three times that of the aluminate (about 3 wt.%), as can be seen in Table 6-5. The last column in Table 6-5, shows

the weight fractions of phases in the crystalline part of the cement; that is, without consideration of the amorphous content.

Table 6-5: Analyses of PCL1 Cement

	Wt. (%)				
	P1-S1	P2-S1	P3-S1	AVERAGE (STDEV)	AVERAGE(c) (STDEV)
Alite	36.5	35.4	35.6	35.8 (0.6)	39.9 (0.5)
Belite	23.8	23.7	23.5	23.7 (0.2)	26.3 (0.1)
Aluminate	3.0	2.8	2.9	2.9 (0.1)	3.2 (0.1)
Ferrite	9.9	9.8	9.5	9.7 (0.2)	10.8 (0.2)
Portlandite	0.3	0.4	0.5	0.4 (0.1)	0.4 (0.1)
Syngenite	1.4	1.4	1.3	1.4 (0.1)	1.5).1)
Quartz	0.6	0.5	0.5	0.5 (0.1)	0.6 (0.1)
Calcite	10.7	11.4	11.2	11.1 (0.4)	12.4 (0.5)
Gypsum	3.8	3.7	3.7	3.7 (0.1)	4.2 (0.0)
Hemihydrate	0.6	0.7	0.6	0.6 (0.1)	0.7 (0.1)
A/uC	9.6	10.3	10.6	10.2 (0.5)	-

6.3.2.2 PCL3 Cement

The phase search and match procedure and the Rietveld refinement analysis showed the presence of the following minor phases in PCL3: portlandite, arcanite, syngenite, potassium calcium sulfate, quartz, and diopside. The amounts of these phases were less than 1 wt.%. The calcite content was about 10 wt.%, and together with dolomite and diopside, corresponded to about 16 - 17 wt.% of limestone ground with the portland cement clinker. The total amount of gypsum and hemihydrate in the cement, stemming from the grinding of the clinker with gypsum, was about 2 wt.%. The alite content was over 3.5 times that of belite, 12 wt.% to 42 wt.%, respectively. In contrast to the other cements, the aluminate content was rather close to that of the ferrite, about 6.5 wt.% and 7 wt.%, respectively. The amorphous/unidentified content in PCL3 cement was about 8 - 9 wt.%. The crystalline and amorphous/unidentified contents for PCL3 cement are presented in Table 6-6.

Table 6-6: Analyses of PCL3 Cement

	Wt. (%)				
	P1-S1	P2-S1	P3-S1	AVERAGE (STDEV)	AVERAGE(c) (STDEV)
Alite	41.7	43.2	42.2	42.4 (0.8)	46.4 (0.5)
Belite	11.9	12.4	12.0	12.1 (0.3)	13.2 (0.2)
Aluminate	6.1	6.5	6.2	6.3 (0.2)	6.9 (0.2)
Ferrite	6.6	7.1	7.1	6.9 (0.3)	7.6 (0.2)
Periclase	1.4	1.6	1.5	1.5 (0.1)	1.6 (0.1)
Portlandite	0.1	0.1	0.1	0.1 (0.0)	0.1 (0.0)
Arcanite	0.6	0.6	0.6	0.6 (0.0)	0.7 (0.0)
Syngenite	0.7	0.6	0.8	0.7 (0.1)	0.8 (0.1)
K-Ca Sulfate	0.3	0.2	0.1	0.2 (0.1)	0.2 (0.1)
Quartz	0.1	0.1	0.1	0.1 (0.0)	0.1 (0.0)
Calcite	10.6	9.6	10.6	10.3 (0.6)	11.2 (0.7)
Dolomite	5.8	5.8	5.7	5.8 (0.1)	6.3 (0.1)
Diopside	0.4	0.4	0.5	0.4 (0.1)	0.5 (0.1)
Gypsum	1.2	1.0	1.3	1.2 (0.2)	1.3 (0.2)
Hemihydrate	0.8	0.8	0.9	0.8 (0.1)	0.9 (0.1)
Anhydrite	1.8	1.9	2.0	1.9 (0.1)	2.1 (0.1)
A/uC	9.8	8.0	8.1	8.6 (1.0)	-

6.4 Conclusions

(i) The limestones studied here were collected from different cement producers in the state of Florida. Phase analyses indicated that the limestones contained up to four crystalline phases. All limestones contained calcite as a major phase and quartz as a minor phase;

(ii) The calcite content in limestones varied from about 80 wt.% to 98 wt.%, while the amount of the amorphous/unidentified content varied from about 1 wt.% to 4 wt.%;

(iii) The weight fractions of the limestone and gypsum ground with the clinkers to produce the cements, were about 11 - 17 wt.% and 2 – 4 wt.%, respectively;

(iv) The amount of amorphous/unidentified content in the investigated portland cements-limestone blends varied from about 8 wt.% to about 11 wt.%;

(v) Quantification of calcite content in portland cement-limestone blends can be conducted with accuracy using x-ray diffraction coupled with Rietveld analysis.

6.5 References

[1] P. E. Stutzman, “Guide for X-Ray Powder Diffraction Analysis of Portland Cement and Clinker,” *NISTIR 5755*, 1996.

[2] C1365-06, “Standard Test Method for Determination of the Proportion of Phases in Portland Cement and Portland-Cement Clinker Using X-Ray Powder Diffraction Analysis,” *Annu. B. ASTM Stand. ASTM Int. West Conshohocken, PA*, vol. Vol. 4.01, pp. 1–10, 2011.

[3] J. M. Hammarstrom and P. L. Sibrell, “Characterization of limestone reacted with acid-mine drainage in a pulsed limestone bed treatment system at the Friendship Hill National Historical Site , Pennsylvania , in a pulsed limestone bed treatment system at the Friendship,” *Appl. Geochemistry*, no. September 2015, pp. 1705–1721, 2003.

[4] R. I. Iacobescu, D. Koumpouri, Y. Pontikes, R. Saban, and G. N. Angelopoulos, “Valorisation of electric arc furnace steel slag as raw material for low energy belite cements.,” *J. Hazard. Mater.*, vol. 196, pp. 287–94, Nov. 2011.

[5] R. Snellings, A. Bazzoni, and K. Scrivener, “The existence of amorphous phase in Portland cements: Physical factors affecting Rietveld quantitative phase analysis,” *Cem. Concr. Res.*, vol. 59, pp. 139–146, May 2014.

[6] “Rocks and Minerals Website.” [Online]. Available: www.rocksandminerals.com/finder/H1.HTM - www.rocksandminerals.com/finder/H3.HTM.

[7] R. D. Hooton, M. Nokken, and M. D. A. Thomas, “Portland-Limestone Cement : State-of-the-Art Report and Gap Analysis For CSA A 3000 Portland-Limestone Cement,” *Cem. Assoc. Canada*, no. July 17, 2007.

[8] M. A. G. Aranda, A. G. De la Torre, and L. Leon-Reina, “Rietveld Quantitative Phase Analysis of OPC Clinkers, Cements and Hydration Products,” *Rev. Mineral. Geochemistry*, vol. 74, no. 1, pp. 169–209, May 2012.

[9] V. Pecharsky and P. Zavalij, *Fundamentals of Powder Diffraction and Structural Characterization of Materials.*, Second Edi. Springer, 2009.

[10] N. V. Y. Scarlett, I. C. Madsen, L. M. D. Cranswick, T. Lwin, E. Groleau, G. Stephenson,

M. Aylmore, and N. Agron-Olshina, “Outcomes of the International Union of Crystallography Commission on Powder Diffraction Round Robin on Quantitative Phase Analysis: samples 2, 3, 4, synthetic bauxite, natural granodiorite and pharmaceuticals,” *J. Appl. Crystallogr.*, vol. 35, no. 4, pp. 383–400, Jul. 2002.

[11] J. P. Cline, R. B. Von Dreele, R. Winburn, P. W. Stephens, and J. J. Filliben, “Addressing the amorphous content issue in quantitative phase analysis: the certification of NIST standard reference material 676a.,” *Acta Crystallogr. A.*, vol. 67, no. Pt 4, pp. 357–67, Jul. 2011.

[12] G. Álvarez-Pinazo, A. Cuesta, M. García-Maté, I. Santacruz, E. R. Losilla, A. G. De la Torre, L. León-Reina, and M. A. G. Aranda, “Rietveld quantitative phase analysis of Yeelimite-containing cements,” *Cem. Concr. Res.*, vol. 42, no. 7, pp. 960–971, Jul. 2012.

Chapter 7. Supplementary Cementitious Materials

7.1 Introduction

In this chapter, the mineralogical and chemical analyses of the supplementary cementitious materials, class F fly ash and slag (ground granulated blast furnace slag), will be conducted and the protocol used for accurately determining their crystalline and amorphous content will be established.

Class F fly ash and ground granulated blast furnace slag are pozzolans that are traditionally blended with ordinary portland cement to enhance concrete fresh and hardened properties in addition to improving durability and service life of structural elements [1], [2]. To provide the required performance, the accurate characterization and quantification of the materials used is critical. In predicting the performance of blended cements, phase analysis and amorphous content quantification renders valuable information on the reactivity and effectiveness of the pozzolanic reaction, the strength evolution, and different durability aspects. It is therefore important to conduct phase analyses on SCMs to help understand and predict the properties of the blended cementitious system. Several authors reported on the mineralogical analysis of fly ash [3]–[7] and slag [4], [5]. Depending on the class, fly ash can contain several crystalline phases, such as hematite, anhydrite, magnetite, lime, periclase, melilite, merwinite, tricalcium aluminate, ye'elimite, mullite, and quartz, with a typical amorphous content of 60 – 90 weight percent (wt.%), [3]–[5]. The main crystalline phases in slag cements are akermanite, gehlenite, melilite, merwinite, and quartz, with an amorphous content of about 65 – 98 wt.% [4], [5]. The mineralogical analyses of cementitious materials, from the approved list of supplementary cementitious materials of the Florida Department of Transportation, will be reported here, and the protocols established for the analyses of SCMs will be provided for future adoption.

7.2 Methodology and Analysis Protocol

The following commonly used and approved pozzolans in the state of Florida were selected to conduct mineralogical and chemical oxide analyses and are designated: FA1 fly ash, SL1 and SL2 slag. For the mineralogical analyses of the SCMs, the following mixtures were selected: 80 wt.% FA1 + 20 wt.% SRM 676*a* corundum, 90 wt.% SL1 + 10 wt.% SRM 676*a* corundum and 90

wt.% SL2 + 10 wt.% SRM 676*a* corundum. The specific amount of the internal standard, SRM 676*a* corundum, used in the mixtures was selected according to Westphal et al. [8]. They indicated that about 20 wt.% of internal standard material is optimum when the amorphous content in the investigated material is about 70 wt.%, and about 10 wt.% of internal standard when the amorphous content is more than 90 wt.%.

The sample preparation, x-ray data collection and Rietveld refinement analysis of SCMs were conducted according to the methodologies previously described in Chapter 2. The search and match procedures [9], [10] were used to identify the crystalline phases commonly present in Class F fly ash and ground granulated blast furnace slag. Typical minerals present in SCMs studied here are presented in Table 7-1 and Table 7-2 , [3-5], [10].

Table 7-1: Fly Ash Common Minerals

Phase	Formula	PDF codes	ICSD Code
Mullite	**Al_4SiO_8**	**01-073-1389**	**23867**
Aluminate	$Ca_3Al_2O_6$	01-070-0839	1841
	$Ca_{8.5}NaAl_6O_{18}$	01-083-1359	100220
	$Ca_{8.5}NaAl_6O_{18}$	00-032-0150	1880
	$Ca_{8.25}Na_{1.5}Al_6O_{18}$	01-083-1360	100221
Yeelimite	$Ca_4Al_6SO_{16}$	00-042-1478	80361
	$Ca_4Al_6SO_{16}$	01-071-0969	9560
Melilite	$Ca_8\ (Al_6Mg_1Si_5)\ O_{28}$	00-004-0689	158173
	$Ca_8\ (Al_4Mg_2Si_6)\ O_{28}$	00-004-0683	158174
	$Ca_8(Al_2Mg_3Si_7)O_{28}$	00-004-0682	158175
Merwinite	$Ca_3Mg(SiO_4)_2$	01-089-2432	43078
Lime	**CaO**	**01-071-4121**	**52783**
	CaO	00-043-1001	75785
Anhydrite	**$CaSO_4$**	**01-086-2270**	**40043**
Anhydrite-III	$CaSO_4$	01-073-1942	24473
Anhydrite-II	$CaSO_4$	01-072-0916	16382
Quartz	**SiO_2**	**00-046-1045**	**41414**
	SiO_2	01-083-2465	200721
Periclase	**MgO**	**01-071-1176**	**9863**
	MgO	00-045-0946	104844
Hematite	**Fe_2O_3**	**01-087-1166**	**82904**
Magnetite	**Fe_3O_4**	**01-077-1545**	**49549**

Table 7-2: Slag Common Minerals

Phase	Formula	PDF codes	ICSD Code
Gehlenite	$Ca_2Al_2SiO_7$	01-089-5917	87144
Melilite	$Ca_8\ (Al_6Mg_1Si_5)\ O_{28}$	00-004-0689	158173
	$Ca_8\ (Al_4Mg_2Si_6)\ O_{28}$	**00-004-0683**	**158174**
	$Ca_8(Al_2Mg_3Si_7)O_{28}$	**00-004-0682**	**158175**
Akermanite	$Ca_2Mg(Si_2O_7)$	00-035-0592	158177
Merwinite	$Ca_3Mg(SiO_4)_2$	01-089-2432	43078
Calcite	**$CaCO_3$**	**01-086-0174**	**80869**
	$CaCO_3$	01-083-0577	79673
Quartz	**SiO_2**	**00-046-1045**	**41414**
	SiO_2	01-083-2465	200721
Hematite	Fe_2O_3	01-087-1166	82904
Magnetite	**Fe_3O_4**	**01-077-1545**	**49549**

The structures used in the Rietveld refinement of slags are indicated by the bold letters.

7.3 Rietveld Refinement Procedures

For materials with high amorphous content, the Chebyshev polynomial [11]–[17] with a relatively high number of refined coefficients should be used in Rietveld refinement. Analysis of the background refinement showed that for fly ash with approximately 70 wt.% of amorphous content, the 20-coefficient Chebyshev polynomial gave a good background fit, while for slag, where the amorphous content was more than 90 wt.%, the number of coefficients was increased to 23. It was observed that better fitting of the slag crystalline phase parameters can be obtained when slag is first analyzed without an internal standard. In the case of fly ash, refinement can be started directly from the mixture of as-received fly ash with internal standard. The refinement procedure for slag and fly ash is outlined below.

(i) Insert crystal structures from a database for the phases identified in the SCM during the Search and Match procedure. For SCM mixtures with internal standard, add a crystal structure for the internal standard as well.

(ii) Select ***Chebyshev I*** polynomial for the ***Background Method*** on the background ***Object Inspector*** pane. Click the option ***Use Extended Background Terms*** to expand the number of Chebyshev polynomial coefficients from 6 to 23.

(iii) Refine the flat background.

(iv) Refine scale factors for all phases.

(v) Refine zero shift.

(vi) Refine Chebyshev I polynomial coefficients. The number of Chebyshev coefficients depends on amorphous content in the SCM. The number of background coefficients should be selected to obtain good fitting of the SCM amorphous hump. However, it was observed that the number of coefficients can vary by 1-2 coefficients without a significant effect on the quantification results.

(vii) Refine lattice parameters of phases. This step should be accompanied by visual observation of peak positions, as peak positions of some phases may shift compared to the collected pattern since all phases in SCMs are present in relatively low quantities. If the peak shift is observed for some phases, the lattice parameters for these phases should be excluded from the refinement in this step and can be refined individually.

(viii) Successive refinement should be carried out for the phases with the largest phase content to the smallest. When refinement is performed for an SCM with internal standard, the internal standard phase parameters *W*, *V*, and *U* should be refined last.

(ix) Refine the *W* parameter. This should be accompanied by visual observation of the peak shapes. If peak broadening beyond the collected pattern is observed, undo this refinement step and limit the ***Set Value Range (%)*** for the *W* parameter in the ***Object Inspector*** pane. This may be repeated several times until good agreement between the simulated and the collected pattern is observed. This should be done during *V* and *U* refinement as well.

(x) Refine the *V* parameter.

(xi) Refine the *U* parameter.

(xii) Refine preferred orientation if necessary.

(xiii) Uncheck the *W*, *V*, *U*, and preferred orientation parameters for the refined phase.

(xiv) Repeat steps *(ix) – (xiii)* for the next most dominant phase.

(xxiii) After refinement of the internal standard, open the ***Object Inspe***ctor pane for the internal standard phase, and enter the actual crystalline content of the internal standard under ***Standard Weight Percentage*** in order to calculate amorphous/unidentified content. If the wt.% of internal standard is displayed with

the rest of the phases in the ***Analyze View***, select ***Program Settings*** from the ***Customize*** menu, select ***Fitting/Rietveld*** tab and change the ***Show Weight Percentages*** drop-down menu to ***As Received***. The program will then recalculate the wt.% for the as-received material without the internal standard and the internal standard phase will no longer be visible in the ***Analyze View***.

(xv) Uncheck all refined parameters for all phases and save the refined structures as a .cry file.

(xvi) After analyzing as-received slag without an internal standard, analyze the slag with internal standard by repeating steps *(i) – (xv)*, except in step *(i)* the refined structures obtained for the as-received slag should be used instead of the database structures.

7.4 Results and Discussion

7.4.1 Mineralogical Analyses of Fly Ash and Slag

The phase search and match procedure and the Rietveld analyses identified the presence of the following crystalline phases in FA1: mullite, quartz, magnetite, periclase, hematite, anhydrite, and free lime. The major crystalline phases are mullite and quartz. The amorphous/unidentified content in FA1 was about 74 wt.%. The details of the crystalline and amorphous/unidentified content in FA1 are presented in Table 7-3.

Table 7-3: Mineralogical Analyses of FA1

Phase	*Wt.* (%)			
	P1-S1	P2-S1	P3-S1	AVERAGE (STDEV)
Mullite	17.6	17.9	17.6	17.7 (0.2)
Quartz	6.3	6.0	6.1	6.1 (0.2)
Magnetite	0.6	0.6	0.6	0.6 (0.0)
Periclase	0.5	0.6	0.6	0.6 (0.1)
Hematite	0.6	0.6	0.6	0.6 (0.0)
Anhydrite	0.3	0.2	0.2	0.2 (0.1)
Lime	0.1	0.1	0.1	0.1 (0.0)
A/uC	73.9	74.0	74.1	74.0 (0.1)

Quantitative x-ray analysis identified the presence of fewer crystalline phases in slags compared to fly ash. Table 7-4 shows that for SL1, the crystalline phases present in minor amounts are: melilite, quartz and calcite. The analysis indicates that the amorphous/unidentified content in SL1 is high, about 99 wt.%. However, for SL2 an additional phase, magnetite, was present as indicated in Table 7-5. The major crystalline phase of the SL2 is calcite at about 2 - 2.5 wt.%. The amorphous/unidentified content in SL2 is about 2 wt.% lower than that in the SL1.

Table 7-4: Mineralogical Analysis of SL1

Phase	*Wt.* (%)			
	P1-S1	P2-S1	P3-S1	Average (STDEV)
Melilite	1.0	0.9	1.0	1.0 (0.1)
Quartz	0.1	0.1	0.1	0.1 (0.0)
Calcite	0.4	0.3	0.3	0.3 (0.1)
A/uC	98.5	98.7	98.6	98.6 (0.1)

Table 7-5: Mineralogical Analysis of SL2

Phase	*Wt.* (%)			
	P1-S1	P2-S1	P3-S1	Average (STDEV)
Melilite	0.5	0.4	0.5	0.5 (0.1)
Quartz	0.3	0.2	0.3	0.3 (0.1)
Calcite	2.2	2.3	2.2	2.2 (0.1)
Magnetite	0.1	0.2	0.2	0.2 (0.1)
A/uC	96.9	97.0	96.9	96.9 (0.1)

7.5 Elemental Oxide Analyses of SCMs

Elemental oxide composition determined using x-ray fluorescence (XRF) analyses for the supplementary materials studied here are presented in Table 7-6 through Table 7-8. The distribution of the elemental oxides in the crystalline or amorphous content of fly ash was determined using x-ray diffraction analysis, the chemical formulas of the crystalline phases, and

the molar weights of the crystalline phases and elemental oxides. The last two columns in the presented data show the oxide distribution in the crystalline (W_{Cry}) and amorphous (W_{Am}) constituents of the supplementary material. The results indicate that for FA1, the major elemental oxide is silica, of which 20% is contained in the crystalline material, while 80% is present in the amorphous material. However, alumina and magnesia appear to be equally distributed in the amorphous and crystalline form. The remaining major oxides, CaO and Fe_2O_3, were predominately distributed in the amorphous phase. All other oxides did not show a distinctive presence in the crystalline phases, but that does not preclude their presence as impurity oxides. The results depicted in Table 7-6 indicate the predominance of silica and alumina in the amorphous content, along with some lime, iron oxide, and magnesia. This indicates that the glass content in this fly ash is predominately aluminosilicate, calcium aluminosilicate, or a combination of both with some presence of magnesia.

Table 7-6: Elemental Oxide Distribution in FA1

Oxide	W_{XRF} (1) (wt.%)	W_{Cry} (2) (wt.%)	W_{Am} (3) (wt.%)
SiO_2	51.51	10.21	41.30
Al_2O_3	26.97	13.29	13.68
Fe_2O_3	5.05	1.43	3.62
CaO	5.91	0.24	5.67
MgO	2.13	0.67	1.46
SO_3	0.55	0.16	0.39
Na_2O	0.5	0.00	0.50
K_2O	1.35	0.00	1.35
TiO_2	1.39	0.00	1.39
P_2O_5	0.83	0.00	0.83
Mn_2O_3	0.06	0.00	0.06
SrO	0.04	0.00	0.04
Cr_2O_3	0.03	0.00	0.03
ZnO	0.06	0.00	0.06
BaO	0.2	0.00	0.20
LOI	2.82	0.00	2.82

The elemental oxide analysis for SL1 indicates the presence of the following major oxides: lime, silica, alumina, and magnesia. Most of the oxides are present in the amorphous form as indicated by the high amorphous content in SL1 shown in Table 7-7. The amorphous content of

SL1 was predominately calcium aluminosilicate with some magnesia. Similar to SL1, SL2 had an abundance of silica, lime, magnesia and alumina as shown in Table 7-8. However, it is interesting to note that silica was higher than lime in the SL2, and magnesia was substantially higher in the SL2 compared to the SL1. The latter is almost 3 times higher than in SL1, while the alumina content is substantially lower in SL2 compared to SL1. Alumina content of the slag has been identified as potentially detrimental to performance of cementitious systems exposed, during their service life, to an aggressive sulfate environment.

Table 7-7: Elemental Oxide Distribution in SL1

Oxides	W_{XRF} (wt.%)	W_{Cry} (wt.%)	W_{Am} (wt.%))
SiO_2	34.81	0.41	34.40
Al_2O_3	14.4	0.16	14.24
Fe_2O_3	0.44	0.00	0.44
CaO	42.87	0.59	42.28
MgO	4.57	0.07	4.50
SO_3	1.3	0.00	1.30
Na_2O	0.2	0.00	0.20
K_2O	0.35	0.00	0.35
TiO_2	0.54	0.00	0.54
P_2O5	0.01	0.00	0.01
Mn_2O_3	0.19	0.00	0.19
SrO	0.03	0.00	0.03
Cr_2O_3	0.01	0.00	0.01
ZnO	0.06	0.00	0.06
BaO	0.07	0.00	0.07
LOI	0.15	0.15	0.00

Table 7-8: Elemental Oxide Distribution in SL2

Oxides	W_{XRF} (wt.%)	W_{Cry} (wt.%)	W_{Am} (wt.%)
SiO_2	39.84	0.38	39.46
Al_2O_3	7.28	0.06	7.22
Fe_2O_3	0.32	0.10	0.22
CaO	35.53	1.50	34.03
MgO	12.05	0.03	12.02
SO_3	0.98	0.00	0.98
Na_2O	0.13	0.00	0.13
K_2O	0.4	0.00	0.40
TiO_2	0.28	0.00	0.28
P_2O_5	0.01	0.00	0.01
Mn_2O_3	0.48	0.00	0.48
SrO	0.03	0.00	0.03
Cr_2O_3	0.01	0.00	0.01
ZnO	0.05	0.00	0.05
BaO	0.04	0.00	0.04
LOI	2.51	1.07	1.44

7.6 Conclusions

(i) The findings indicate the presence of a higher crystalline phase content in fly ash compared to the slags.

(ii) While the amorphous content of the two analyzed slags was similar, their oxide constituents were substantially different. This indicates the importance and significance of characterizing supplementary materials through x-ray fluorescence and quantitative x-ray diffraction for proper prediction of cementitious systems performance and durability.

7.7 References

[1] J. C. Taylor, L. P. Aldridge, C. E. Matulis, and I. Hinczak, “X-ray powder diffraction analysis of cements,” in *Structure and Performance of Cements*, Second edi., J. Bensted and P. Barnes, Eds. Spon Press, 2002, pp. 420–441.

[2] S. Mindess, J. F. Young, and D. Darwin, *Concrete.*, Second Edi. Prentice Hall, 2003.

[3] R. S. Winburn, D. G. Grier, G. J. McCarthy, and R. B. Peterson, “Rietveld quantitative X-ray diffraction analysis of NIST fly ash standard reference materials,” *Powder Diffr.*, vol. 15, no. September, pp. 163–172, 2000.

[4] T. Westphal, G. Walenta, T. Füllmann, M. Gimenez, E. Bermejo, K. L. Scrivener, and H. Pöllmann, “Characterisation of cementitious materials,” *Int. Cem. Rev.*, pp. 47–51, 2002.

[5] G. Walenta and T. Füllmann, “Advances in quantitative XRD analysis for clinker, cements, and cementitious additions,” *Powder Diffr.*, vol. 19, no. 1, pp. 40–44, Mar. 2004.

[6] C. Ward and D. French, “Determination of glass content and estimation of glass composition in fly ash using quantitative X-ray diffractometry,” *Fuel*, vol. 85, no. 16, pp. 2268–2277, Nov. 2006.

[7] M. Criado, A. Fernández-Jiménez, A. G. de la Torre, M. A. G. Aranda, and A. Palomo, “An XRD study of the effect of the SiO_2/Na_2O ratio on the alkali activation of fly ash,” *Cem. Concr. Res.*, vol. 37, no. 5, pp. 671–679, May 2007.

[8] T. Westphal, T. Füllmann, and H. Pöllmann, “Rietveld quantification of amorphous portions with an internal standard—Mathematical consequences of the experimental approach,” *Powder Diffr.*, vol. 24, no. 3, pp. 239–243, Feb. 2009.

[9] C1365-06, “Standard Test Method for Determination of the Proportion of Phases in Portland Cement and Portland-Cement Clinker Using X-Ray Powder Diffraction Analysis,” *Annu. B. ASTM Stand. ASTM Int. West Conshohocken, PA*, vol. Vol. 4.01, pp. 1–10, 2011.

[10] M. A. G. Aranda, A. G. De la Torre, and L. Leon-Reina, “Rietveld Quantitative Phase Analysis of OPC Clinkers, Cements and Hydration Products,” *Rev. Mineral. Geochemistry*, vol. 74, no. 1, pp. 169–209, May 2012.

[11] V. K. Peterson, A. S. Ray, and B. A. Hunter, “A comparative study of Rietveld phase analysis of cement clinker using neutron, laboratory X-ray, and synchrotron data,” *Powder Diffr.*, vol. 21, no. 1, pp. 12–18, Mar. 2006.

[12] N. Marinoni, A. Pavese, M. Voltolini, and M. Merlini, “Long-term leaching test in concretes: An X-ray powder diffraction study,” *Cem. Concr. Compos.*, vol. 30, no. 8, pp.

700–705, Sep. 2008.

[13] J. P. Cline, R. B. Von Dreele, R. Winburn, P. W. Stephens, and J. J. Filliben, “Addressing the amorphous content issue in quantitative phase analysis: the certification of NIST standard reference material 676a.,” *Acta Crystallogr. A.*, vol. 67, no. Pt 4, pp. 357–67, Jul. 2011.

[14] M. L. Gualtieri, M. Romagnoli, P. Miselli, M. Cannio, and A. F. Gualtieri, “Full quantitative phase analysis of hydrated lime using the Rietveld method,” *Cem. Concr. Res.*, vol. 42, no. 9, pp. 1273–1279, Sep. 2012.

[15] R. Snellings, A. Bazzoni, and K. Scrivener, “The existence of amorphous phase in Portland cements: Physical factors affecting Rietveld quantitative phase analysis,” *Cem. Concr. Res.*, vol. 59, pp. 139–146, May 2014.

[16] W. Wilson, K. J. Krakowiak, and F.-J. Ulm, “Simultaneous assessment of phase chemistry, phase abundance and bulk chemistry with statistical electron probe micro-analyses: Application to cement clinkers,” *Cem. Concr. Res.*, vol. 55, pp. 35–48, Jan. 2014.

[17] M. De Schepper, K. De Buysser, I. Van Driessche, and N. De Belie, “A Hydration Study by XRD / Rietveld Analysis of Cement Regenerated from Completely Recyclable Concrete,” *IJRET*, vol. 3, no. 13, pp. 129–134, 2014.

Chapter 8. Characterization of Portland Cement-SCM Binary Systems

8.1 Introduction

One of the main objective of this research is to quantify and characterize the SCM content in commercially blended cements. Based on the previous findings of the study, x-ray diffraction coupled with Rietveld refinement was adopted for the quantification of the SCM content in blended system. First, the analysis was conducted on laboratory-prepared binary mixtures of known proportions of portland cements with slag and portland cement with fly ash. A new approach using a modified PONKCS method was developed to determine the contribution of SCMs to the total amorphous content in the system. The procedure was established on laboratory-prepared mixtures and then tested on commercially-blended cement-slag and cement-fly ash systems. A total of three commercial blends were studied here; namely, PC1-1P (cement-fly ash), PC1-1S (cement-slag) and PC3-1S (cement-slag). The modified PONKCS approach was successful in quantifying the SCM content in commercially blended systems, in addition to determining the individual amorphous contribution of each SCM to the total amorphous/unidentified content of the blended system.

Class F fly ash and ground granulated blast furnace slag (slag) SCMs are materials that are traditionally blended with portland cements to enhance concrete durability [1], [2]. To provide the required performance, the accurate quantification of SCM content in the mixture is important. The main difficulty of such quantification is the fact that SCMs are largely amorphous in nature with about 60 – 90 wt.% amorphous content in fly ash [3]–[5] and 65 – 98 wt.% amorphous content in slags [4], [5]. Therefore, an accurate quantification of the amorphous content in each SCM material is necessary. Scarlet and Madsen developed a method for the quantification of phases with **p**artial **o**r **n**o **k**nown **c**rystal **s**tructure, referred to as the PONKCS method [6]. The PONKCS method was adopted here for the direct determination of the amorphous content in the blended mixtures [7], [8].

The intensity contribution of PONKCS amorphous (or crystalline) phases to the sample diffraction pattern can be characterized by empirical structure factors that can be calculated via Pawley [9] or Le Bail et al. [10] curve-fitting methods. In the procedure, the *ZMV* calibration constants [11] must be first empirically determined [6], [12]. Here, *Z*, *M*, and *V* are the number of

formula units per unit cell, the mass of the formula unit, and the unit-cell volume for each phase, respectively. This can be achieved by using the internal-standard method for the respective amorphous or crystalline phase [6], [12]. Once determined, the calibration constant can then be used in the Rietveld refinement of the PONKCS (amorphous or crystalline) phase.

The direct determination of the amorphous content by the PONKCS method was conducted by Madsen et al. [7] using crystalline quartz – amorphous silica flour mixtures and Snellings et al. [8] in the mixture of portland cement – amorphous slag and metakaolin mixtures. In their research, the precision and accuracy of the amorphous phase determination were within several weight percent. The authors mainly gave general descriptions of the developed approaches without details of refinement, which can significantly affect the quantification of the amorphous phase content. Therefore, further development of the PONKCS method for amorphous phase determination, with higher precision and accuracy, is of importance.

8.2 Materials

To distinguish between laboratory-mixed cementitious materials and commercial blended cementitious systems, the following terminology was used throughout this chapter: samples formulated by mixing cement with an SCM in our laboratory are referred to as **mixtures** or **mixed** materials, whereas the commercial blended cement is referred to as **blends**, **blended** materials, or **blended** cements.

The following cements and SCMs were used to prepare laboratory mixtures: PC1 and FA1, PC1 and SL1, and PC3 and SL2. These as-received materials are the components used in manufacturing of the commercially blended systems studied here: PC1-1P (30) blended cement (cement-fly ash), PC1-1S (30) blended cement (cement-slag), and PC3-1S (20) blended cement (cement-slag). For phase analyses and the determination of the weight fractions of the crystalline phases and amorphous contents in SCMs, the following mixtures were selected: 80 wt.% FA1 + 20 wt.% SRM 676*a* corundum, 90 wt.% SL1 + 10 wt.% SRM 676*a* corundum, and 90 wt.% SL2 + 10 wt.% SRM 676*a* corundum. The amount of the internal-standard SRM 676*a* corundum was chosen according to the recommendations of Westphal et al. [13]: about 20 wt.% of internal-standard material should be used when the amorphous content in the investigated material is about

70 wt.%, and about 10 wt.% of internal-standard material should be used when the amorphous content in the investigated material is more than 90 wt.%.

In order to assess the procedures for the quantification of the SCM constituents in blended portland cement systems, sixteen laboratory mixtures were prepared. They are:

- PC1 - FA1 Mixtures:

(i) 5% FA1 + 95% PC1 (labelled 5FA1-PC1);
(ii) 10% FA1 + 90% PC1 (labelled 10FA1-PC1);
(iii) 20% FA1 + 80% PC1 (labelled 20FA1-PC1);
(iv) 30% FA1 + 70% PC1 (labelled 30FA1-PC1) ;

- **PC1 - SL1 Mixtures:**

(v) 5% SL1 + 95% PC1 (labelled 5SL1-PC1);
(vi) 10% SL1 + 90% PC1 (labelled 10SL1-PC1) ;
(vii) 20% SL1 + 80% PC1 (labelled 20SL1-PC1);
(viii) 30% SL1 + 70% PC1 (labelled 30SL1-PC1);
(ix) 50% SL1 + 50% PC1 (labelled 50SL1-PC1);
(x) 70% SL1 + 30% PC1 (labelled 70SL1-PC1);

- **PC3-SL2 Mixtures:**

(xi) 5% SL2 + 95% PC3 (labelled 5SL2-PC3);
(xii) 10% SL2 + 90% PC3 (labelled 10SL2-PC3) ;
(xiii) 20% SL2 + 80% PC3 (labelled 20SL2-PC3);
(xiv) 30% SL2 + 70% PC3 (labelled 30SL2-PC3);
(xv) 50% SL2 + 50% PC3 (labelled 50SL2-PC3);
(xvi) 70% SL2 + 30% PC3 (labelled 70SL2-PC3);

To determine the amorphous content by the internal-standard PONKCS method, the above materials were mixed with 20% of the standard SRM 676*a* corundum. The same amount of corundum was used in studying the blended commercial systems.

8.3 Methodology

A detailed study was conducted using a modified PONKCS method on SCMs and their mixtures as well as blended portland cements. The technique developed here uses a **strict order of parameter refinement**. The use of an external standard was not attempted; however, it is expected that the method could be adapted for use with an external standard. The modified method developed for this investigation is called the **Iterative Rietveld-PONKCS** technique. The as-

received SCMs, cements, and blended cements were each mixed with an internal-standard material (corundum). This allows the amorphous contribution of SCM to be separated from the amorphous/unidentified content in cement.

The **Iterative Rietveld-PONKCS** technique used for analysis of blended cements and laboratory-prepared mixtures can be divided into three steps:

1. Rietveld analysis of as-received materials (SCMs, unblended cements, if any, and blended cements) to determine their crystalline phase content. The refined crystal structure parameters obtained in this step are fixed in the following steps to reduce the number of refined parameters, thus simplifying the refinement.
2. Refinement of a PONKCS pseudo-structure for the amorphous phase present in the unblended SCM.
3. Refinement of the blended cements or laboratory-prepared mixtures with the refined PONKCS pseudo-structure to determine the SCM content.

8.3.1 Step 1: Rietveld Refinement of As-Received Materials

8.3.1.1 Refinement of SCMs

The crystalline phase content of the two SCMs investigated in this study was significantly different, with slag having approximately 1-3 wt.% of crystalline material, while Class F fly ash crystalline content was approximately 26 wt.%. It was observed that better fitting of the slag crystalline phase parameters can be obtained when slag is first analyzed without an internal standard. In the case of fly ash, refinement can be started directly from the mixture of as-received fly ash with internal standard.

(i) Insert crystal structures from a database for the phases identified in the SCM during the Search and Match procedure. For SCM mixtures with internal standard, add a crystal structure for the internal standard as well.

(ii) Select ***Chebyshev I*** polynomial for the ***Background Method*** on the background object inspector pane. Click the option ***Use Extended Background Terms*** to expand the number of Chebyshev polynomial coefficients from 5 to 23.

(iii) Refine the flat background.

(iv) Refine scale factors for all phases.

(v) Refine zero shift.

(vi) Refine Chebyshev I polynomial coefficients. The number of Chebyshev coefficients depends on amorphous content in the SCM. For example, 23 coefficients were used for slag refinement, while 20 coefficients were used for fly ash. The number of background coefficients should be selected to obtain good fitting of the SCM amorphous hump. However, it was observed that the number of coefficients can vary by 1-2 coefficients without a significant effect on the quantification results.

(vii) Refine lattice parameters of phases. This step should be accompanied by visual observation of peak positions, as peak positions of some phases may shift compared to the collected pattern since all phases in SCMs are present in relatively low quantities. If the peak shift is observed for some phases, the lattice parameters for these phases should be excluded from the refinement in this step and can be refined individually.

(viii) Successive refinement should be carried out for the phases with the largest content to the smallest. When refinement is performed for an SCM with internal standard, the internal standard phase parameters *W, V, U* should be refined last.

(ix) Refine the *W* parameter. This should be accompanied by visual observation of the peak shapes. If peak broadening beyond the collected pattern is observed, undo this refinement step and limit the ***Set Value Range (%***) for the *W* parameter in the ***Object Inspector*** pane. This may be repeated several times until good agreement between the simulated and the collected pattern is observed. This should be done during *V* and *U* refinement as well.

(x) Refine the *V* parameter.

(xi) Refine the *U* parameter.

(xii) Refine preferred orientation if necessary. Care should be taken to enter the correct hkl value for the direction of the preferred orientation in the ***Object Inspector*** pane.

(xiii) Uncheck the *W, V, U* and preferred orientation parameters for the refined phase.

(xiv) Repeat steps *(ix) – (xiii)* for the next most dominant phase.

(xv) After refinement of the internal standard, open the ***Object Inspector*** pane for the internal standard phase, and enter the actual crystalline content of the internal standard under ***Standard Weight Percentage*** in order to calculate amorphous/unidentified content. If the wt.% of internal standard is displayed with the rest of the phases in the ***Analyze View***, select ***Program Settings*** from the ***Customize*** menu, select ***Fitting/Rietveld*** tab and change the ***Show Weight Percentages*** drop-down menu to ***As Received***. The program will then recalculate the wt.% for the as-received material without the internal standard and the internal standard phase will no longer be visible in the ***Analyze View***.

(xvi) Uncheck all refined parameters for all phases and save the refined structures as a .cry file.

(xvii) After analyzing as-received slag without an internal standard, analyze the slag with internal standard by repeating steps *(i) – (xv)*, except in step *(i)* the refined structures obtained for the as-received slag should be used instead of the database structures.

8.3.1.2 Refinement of As-Received OPC and Blended Cement

Both OPC and blended cements contain a number of phases that suffer from peak overlap as well as minor phases present in small quantities. In order to aid identification of the minor phases and selection of the appropriate crystal structure for the overlapped phases, it is recommended to perform selective dissolutions. In this study, KOSH and SAM extractions were used to refine crystal structures of silicates, aluminates, ferrites, and minor phases, which were then used in the refinement of the as-received cements. Since OPC samples were used to prepare the laboratory mixtures with various amounts of SCMs, they were analyzed in this step without an internal standard. However, since no additional SCMs were added to commercial blended cements, they were analyzed with an internal standard.

8.3.1.2.1. Refinement of the SAM and KOSH Extraction Residues

(xxiv) Insert crystal structures from a database for the phases identified in the SCM during the Search and Match procedure.

(xxv) For refinement of extraction residues of OPC, polynomial was selected as the profile function in the background ***Object Inspector*** pane. For blended cements,

Chebyshev I was selected as the profile function due to higher amorphous content in blended cements.

(xxvi) Refine the flat background.

(xxvii) Refine scale factors for all phases.

(xxviii) Refine zero shift.

(xxix) For OPC, refine background coefficients 1-4. For blended cements, refine Chebyshev I polynomial coefficients. A sufficient number of refined Chebyshev coefficients should be selected in order to obtain a good agreement between the fitted and collected background. It was observed that for refinement of blended cement containing fly ash, refinement of coefficients 1-8 provided a good fit, while for blended cements containing slag it was necessary to refine coefficients 1-14.

(xxx) Refine lattice parameters. Minor phases, especially those with peak overlap, should be excluded from refinement in this step. The lattice parameters for these phases can be refined individually.

(xxxi) Refinement of *W, V, U,* and preferred orientation parameters should first be performed for the major phases with strong peak overlap, for example, for alite and belite in the KOSH residue, and for aluminate and ferrite in the SAM residue.

(xxxii) Simultaneously refine the *W* parameters for the major phases with strong peak overlap.

(xxxiii) Simultaneously refine the *V* parameters.

(xxxiv) Simultaneously refine the *U* parameters.

(xxxv) Refine preferred orientation if necessary.

(xxxvi) Uncheck the *W, V, U,* and preferred orientation parameters for the refined phases.

(xxxvii) Consider the next most dominant phase. If refinement of lattice parameters for this phase was omitted in step *(vii),* refine all the lattice parameters with visual observation. If peak shift beyond the collected pattern is observed, the lattice parameters for this phase should be excluded from refinement.

(xxxviii) If the phase considered in step *(xiv)* is present in amounts above 5 wt.%, repeat steps *(viii) – (xiii).* For phases present in weight fractions of approximately 5-20%, this step should be accompanied by visual observation. If during refinement

of one of the parameters, the value of this parameter increases dramatically and the shape of the calculated profile broadens beyond the collected profile, undo this refinement step and limit the ***Set Value Range (%)*** for the *W* parameter in the ***Object Inspector*** pane. This may be repeated several times until good agreement between the simulated and the collected pattern is observed. This should be done during *V* and *U* refinement as well. For phases present in amounts of approximately 1-5%, only refine the *W* parameter. However, if a strong, non-overlapped peak of this minor phase can be clearly observed in the collected pattern, *V* and *U* parameters can be refined as well with visual observation. For phases present in amounts below 1%, refinement of *W*, *V*, *U*, and preferred orientation parameters can be omitted.

(xxxix) Repeat steps *(xiv)* and *(xv)* until all the phases have been considered.

(xl) Uncheck all refined parameters for all phases and save the refined structures as a .cry file.

8.3.1.2.2. Refinement of OPC and Blended Cements

(xli) Insert the refined crystal structures obtained from the KOSH and SAM residue refinement (step *(xvii)*). For blended cement mixtures with internal standard, add a crystal structure for the internal standard as well. It was observed that although a gypsum structure is refined as part of the SAM extraction residue, the gypsum is altered by the extraction process, and the use of this refined gypsum structure results in overestimation of the gypsum content in as-received cement. Therefore, the gypsum structure should be added from the database. The calcite structure was taken from the KOSH residue refinement as formation of additional calcite was observed during SAM extraction. The periclase structure was taken from the SAM residue refinement since there is less peak overlap compared to the KOSH residue.

(xlii) Repeat steps *(ii) – (vii)*, except in step *(vi)* the number of refined Chebyshev I coefficients should be increased for blended cements to obtain a good fitting with the collected background.

(xliii) Repeat steps *(viii) – (xiii)* first for alite and belite, then for aluminate and ferrite.

(xliv) Repeat steps *(xiv)* – *(xvi)* for calcite and gypsum. It may not be necessary to further refine the rest of the phases. This decision is based on the quality of the fitting of the calculated pattern of such phases. If poor fitting is noted, further refinement should be done.

(xlv) When refinement is performed for blended cements with an internal standard, the internal standard phase parameters should be refined last. After refinement of the internal standard, open the ***Object Inspector*** pane for the internal standard phase, and enter the actual crystalline content of the internal standard under ***Standard Weight Percentage*** in order to calculate amorphous/unidentified content.

(xlvi) Uncheck all refined parameters for all phases.

(xlvii) For OPC, save the refined structures as a .cry file. For blended cements, it is sufficient to save the analysis as a .hpf file. The .cry file created after OPC refinement will be used in the quantification of the OPC_SCM blends. Since the refinement of the blended cements will be further used in Step 3 of the **Iterative Rietveld-PONKCS** techniques, the refinement results should be saved as a .hpf file.

8.3.1.2.3. Refinement of Laboratory Mixtures

(xlviii) Insert the refined crystal structures obtained in step *(xxiv)* above for OPC and in step *(xvi)* of the procedure for SCM refinement above. In the case of mixtures containing phases that may be shared between the OPC and SCM, for example calcite, insert these structures from the database. Add a crystal structure for the internal standard as well.

(xlix) Select ***Chebyshev I*** as the profile function.

(l) Refine the flat background.

(li) Refine scale factors for all phases.

(lii) Refine zero shift.

(liii) Refine Chebyshev I polynomial coefficients. Sufficient number of coefficients should be selected to obtain a good fitting of the background.

(liv) Repeat steps *(xix)* – *(xxii)* above.

8.3.2 Step 2: Refinement of a PONKCS Pseudo-Structure for SCMs

The accuracy of the amorphous phase determination using the PONKCS refinement depends on background refinement for both the SCM and the blended material. Madsen et al. [7] used a third-order Chebyshev polynomial with a $1/2\theta$ term (1/x in HighScore Plus v4.5 software) for background fitting, while Snellings et al. [8] recommended the use of a first-order Chebyshev polynomial with a $1/2\theta$ term. Based on the results of the current study, the latter approach gave better refinement results. This could be explained as follows: the first-order Chebyshev polynomial with the $1/2\theta$ term is the highest order of Chebyshev polynomial that is concave-upward in any 2θ range for any experimental scan. Though higher order Chebyshev polynomials gave a better background fit, especially for the calibration SCM, it gave less accurate results for amorphous phase determination.

Quantification of the amorphous phase depends on the choice of the crystal system and space group used in the Pawley [9] or Le Bail et al. [10] curve-fitting step for each SCM (within the PONKCS refinement procedure). The amorphous hump is treated as a phase that will be referred to as the "SCM amorphous phase" or SCMAP. During curve fitting, the approximate Bragg position of the SCM amorphous hump maximum is determined, and an appropriate space group is chosen to represent the amorphous phase.

For the choice of the space group for the SCMAP, preference should be given to the cubic crystal system. This minimizes the number of lattice parameters that need to be refined in the Pawley or Le Bail fitting, which makes the analysis simpler. In principle, the space group of the SCMAP could be arbitrary, but choosing a space group corresponding to a cubic crystal system reduces the number of lattice parameters to one ($a = b = c$).

For the choice of the cubic space group of the amorphous phase, preference should be given to a space group that has only one peak within the 2θ range of the amorphous hump being fitted by the Pawley or Le Bail method. The presence of more peaks lowers the quality of the background fit, making the amorphous phase determination less accurate. In the current study, the cubic structure with the space group $Fm\bar{3}m$ (space group number 225) gave good fit for the slag hump, while a cubic structure with the space group $Fd\bar{3}m$ (space group number 227) gave good fit for the fly ash hump.

After fitting the amorphous SCM hump, the *ZMV* calibration constant of the SCMAP should be determined. *V* is the unit-cell volume obtained at the end of the curve fitting procedure, while *Z* is the formula mass, which is unknown in this case since the material is x-ray amorphous and the crystal structure and space group are arbitrarily chosen to enable fitting of the amorphous hump. Therefore, the *ZM* formula mass is absent in the Pawley or Le Bail fitting mode. However, the *ZM* value can be artificially introduced into the "hkl-file" fitting mode as the ZM_{PFM} "Pseudo Formula Mass" and calibrated for the SCMAP. This calibration is based on the assumption that all amorphous content of the SCM belongs to the SCMAP; therefore, the correct value of *ZM* will transfer all the amorphous content to the fitted SCMAP.

The main difference between traditional Rietveld refinement procedures described earlier in this chapter and the **Iterative Rietveld-PONKCS** refinement is the separation of the background refinement from the refinement of amorphous hump.

8.3.2.1.1. Iterative Refinement of the PONKCS Pseudo-Structure

(i) Open the .hpf file of the SCM-internal standard mixture obtained at the end of the SCMs refinement procedure discussed previously in section 8.3.1.

(ii) Turn off all refinement parameters.

(iii) Zero all the background Chebyshev polynomial parameters

(iv) Create an SCMAP structure. In the ***Analysis*** menu, select ***Fitting***, then click on ***Enter New Structure***. In the new window, choose the cubic space group in the ***Enter Space Group*** drop-down menu (space group 225 for slag and 227 for fly ash), and enter lattice parameter *a* under ***Enter Unit Cell***. The lattice parameter value should be chosen to obtain a 2θ position of the first peak close to the maximum position of the SCM amorphous hump. Choose the ***Pawley Fit*** in the ***Fitting Mode*** of the ***Object Inspector*** pane. Unclick Use ***Min/Max Values*** for shape parameters to allow these parameters to change in the infinite range.

(v) Refine scale factors for all crystalline phases.

(vi) Refine the flat background parameter.

(vii) Refine the 1/x background parameter.

(viii) Refine the background coefficient 1.

(ix) Uncheck all the refined background parameters.

(x) Refine the lattice parameter *a* and the *W* parameter for the SCMAP.

(xi) Refine the *V* parameter for the SCMAP.

(xii) Refine the *U* parameter for the SCMAP.

(xiii) Refine the shape parameter 1, η_1, for the SCMAP.

(xiv) Refine the shape parameter 2, η_2, for the SCMAP.

(xv) Refine the shape parameter 3, η_3, for the SCMAP.

(xvi) Turn off all parameters for the SCMAP.

(xvii) Perform next iteration of the SCMAP fitting by repeating the steps *(iii), (v) – (xvi)* to stabilize refinement results. Typically, 10-20 iterations are sufficient to obtain good fitting of the amorphous hump.

8.3.2.1.2. ZM Formula Mass Calibration of SCMAP

(xviii) Open the ***Object Inspector*** pane for the internal standard phase, and enter the actual crystalline content of the internal standard under Standard Weight Percentage in order to calculate the amorphous content.

(xix) Change the ***Fitting Mode*** of the SCMAP in the ***Object Inspector*** pane from the ***Pawley Fit*** to the ***HKL-File Fit*** mode.

(xx) Enter a value for the ***Pseudo Formula Mass*** for the SCMAP that will convert all the amorphous content into the SCMAP weight percentage. The resulting amorphous content will be equal to zero.

8.3.3 Step 3: Refinement Using PONKCS

(i) Open the .hpf file of the blended cements or laboratory-prepared mixture obtained in Step 1 discussed previously.

(ii) Turn off all refinement parameters;

(iii) Zero all the coefficients of the Chebyshev background polynomial;

(iv) Insert the refined SCMAP obtained in Step 2. In contrast to the crystalline phases with known structures, the refined SCMAP with the ***HKL-File Fit*** mode cannot be saved to any file for further use in refinement. However, this phase can be directly

copied from one refined .hpf file to another one. Therefore, in addition to the .hpf file with current refinement, the second file with refined SCMAP structure should be opened and the refined SCMAP structure should be copied to the first file by right-clicking on the SCMAP in the ***Refinement Control*** pane using the ***Copy To mode***.

(v) Refine the scale factors for major phases. Exclude minor phases from refinement at this step.

(vi) Refine the flat background parameter.

(vii) Refine the 1/x term parameter of background.

(viii) Refine background coefficient 1.

(ix) Refine scale factors for minor phases one phase at a time while observing the change in its wt.%. If there is a significant change, undo the refinement and fix the scale factor before proceeding to the next phase.

(x) Repeat step *(ix)* for the remainder of the phases.

(xi) Repeat the refinement several times until the weight fractions of the SCMAP and the amorphous content are stabilized.

8.4 Results and Discussion

8.4.1 SCM Amorphous Content Analysis

The Rietveld refinement results of FA1, SL1 and SL2 were presented earlier in Chapter 7. From the Pawley fit of the FA1 amorphous hump, Figure 8-1, where the measured pattern, fitted background, corundum, crystalline, and amorphous phases of the fly ash are superimposed. The formula mass calibration of the fly ash SCMAP and the following fit parameters were obtained:

Table 8-1: Fit Parameters of FA1

Crystal System	Cubic
Space Group Name	$Fd\bar{3}m$
Space Group Number	227
Lattice Parameters	
$a = b = c$ (A)	6.14619
$\alpha = \beta = \gamma$ (deg)	90
Peak Shape Parameters	
Caglioti U	-33.79836
Caglioti V	110.4921
Caglioti W	155.1914
Peak Shape 1, η_1	-0.1
Peak Shape 2, η_2	-0.020412
Peak Shape 3, η_3	-0.000137
Pseudo Formula Mass (g/mol)	4.365

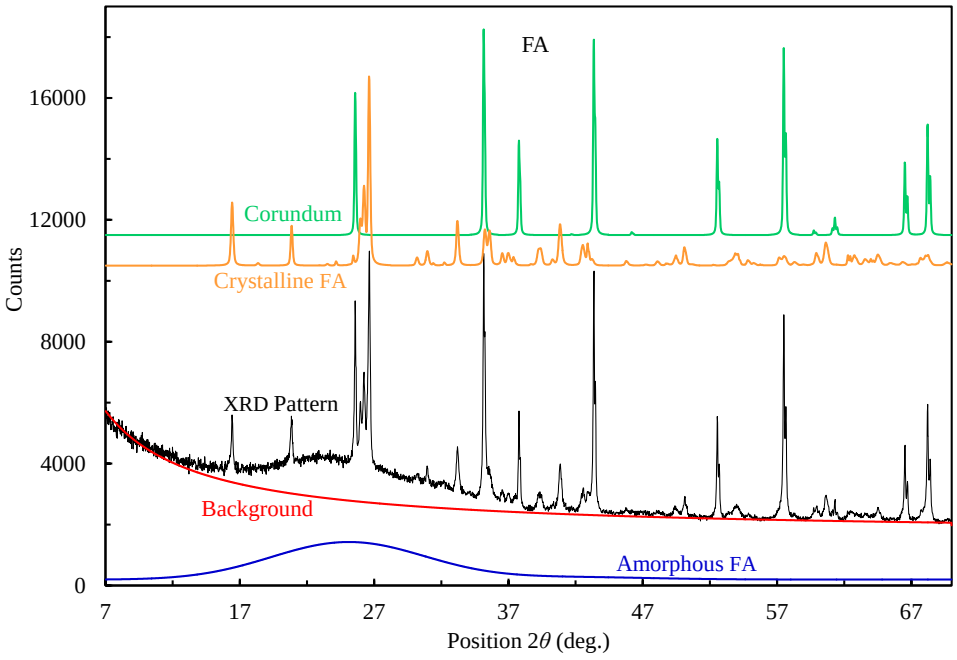

Figure 8-1: Iterative Rietveld-PONKCS analysis of FA1

The Pawley fit for the SL1 amorphous hump, Figure 8-2, and the formula mass calibration results for the slag SCMAP and the determined fit parameters are presented in Table 8-2. For SL2, the formula mass for the SCMAP and the fit parameters are presented in Table 8-3.

Table 8-2: Fit Parameters of SL1

Crystal System	Cubic
Space Group Name	$Fm\bar{3}m$
Space Group Number	225
Lattice Parameters	
$a = b = c$ (A)	5.130387
$\alpha = \beta = \gamma$ (deg)	90
Peak Shape Parameters	
Caglioti U	748.1456
Caglioti V	-26.92349
Caglioti W	0.000578
Peak Shape 1, η_1	-0.1
Peak Shape 2, η_2	0.064082
Peak Shape 3, η_3	-0.001858
Pseudo Formula Mass (g/mol)	6.905

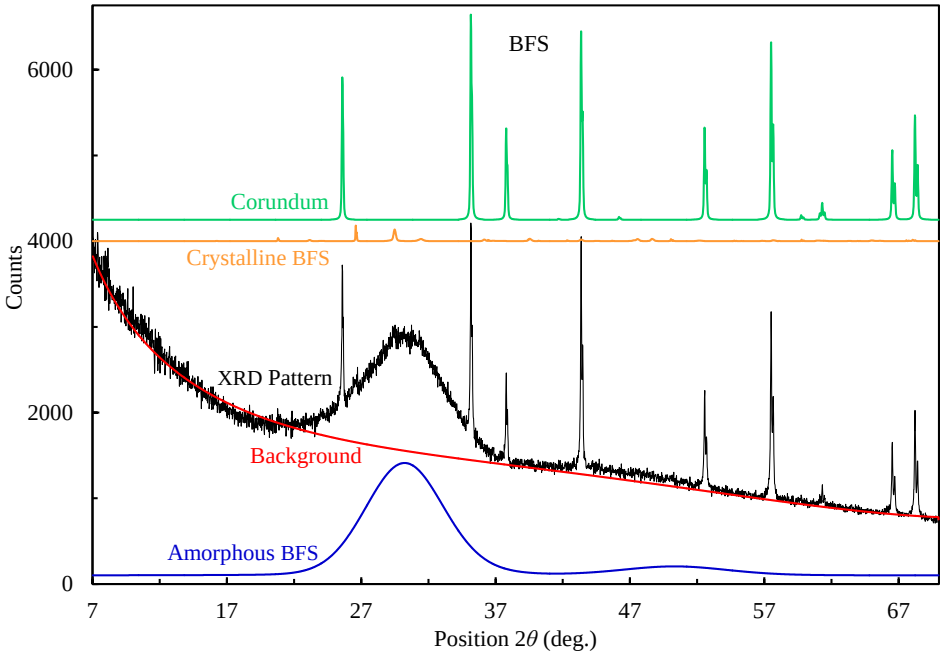

Figure 8-2: Iterative Rietveld-PONKCS Analysis of SL1

Table 8-3: Fit Parameters of HC Slag SL2

Crystal System	Cubic
Space Group Name	$Fm\bar{3}m$
Space Group Number	225
Lattice Parameters	
$a = b = c$ (*A*)	5.113546
$\alpha = \beta = \gamma$ (deg)	90
Peak Shape Parameters	
Caglioti *U*	555.1889
Caglioti *V*	-5.368256
Caglioti *W*	15.20484
Peak Shape 1, η_1	-0.036446
Peak Shape 2, η_2	-0.000183
Peak Shape 3, η_3	0.000122
Pseudo Formula Mass (g/mol)	8.6262

8.4.2 Refinement of Portland Cement-SCM Mixtures within PONKCS Method

The results of mixtures analyses will be presented in this section. The data analyses for FA1- PC1 mixtures, using the internal-standard **Iterative Rietveld-PONKCS** method, are presented in Table 8-4 through Table 8-7. The determined weight fractions of FA1 SCMAPs are shown in the "Amorphous Fly Ash" row. The total (crystalline plus amorphous) fly ash contents in the mixtures (see the rows labelled "Part of Fly Ash in Mixture"), were determined by normalizing the weight fraction of the fly ash SCMAP in the mixture by the amorphous content in the fly ash, that is, by 0.74 (see Chapter 7). The last row in the Tables gives the difference between this value and the actual amount (in wt.%) of fly ash in each mixture. As can be seen from the results presented here, the PONKCS method developed in this study gave better that 1 wt.% precision and accuracy in the determination of the fly ash content in the prepared mixtures.

In principle, the crystalline phase with the strongest peaks in FA1, mullite, can also be used for quantifying the fly ash content in the mixture. This is because the weight fraction of mullite in fly ash is rather high, about 17 wt.%, and the strongest mullite peaks do not overlap with any peak

in portland cement. Using this approach, the accuracy of fly ash content determination in mixtures was about 1 – 3 wt.%, which is lower than the accuracy obtained by using the SCMAP approach.

Table 8-4: Analysis of 5 FA1-PC1 Mixture

Phase	*Wt.* (%)				
	P1-S1	P2-S1	P3-S1	AVERAGE	STDEV
Alite	42.6	42.4	42.0	42.3	0.3
Belite	23.9	23.1	23.4	23.5	0.4
Aluminate	4.4	4.5	4.6	4.5	0.1
Ferrite	8.9	9.1	8.9	9.0	0.1
Calcite	5.0	4.9	4.7	4.9	0.2
Syngenite	0.9	0.9	0.8	0.9	0.1
Portlandite	1.1	0.8	0.9	0.9	0.2
Gypsum	4.8	4.9	4.8	4.8	0.1
Hemihydrate	1.2	1.3	1.3	1.3	0.1
Mullite	1.0	1.0	1.0	1.0	0.0
Quartz	0.3	0.4	0.3	0.3	0.1
Magnetite	0.0	0.0	0.0	0.0	0.0
Periclase	0.0	0.0	0.0	0.0	0.0
Fly Ash SCMAP	**3.7**	**4.4**	**4.2**	**4.1**	**0.4**
Amorphous Phase - Other	2.2	2.3	3.0	2.5	0.4
Total Amorphous Phase	5.9	6.7	7.2	6.6	0.7
Part of Fly Ash in Mixture				**5.5**	
Difference Between Measured and Actual Amount of Fly Ash in Mixture				**-0.5**	

Table 8-5: Analysis of 10 FA1-PC1 Mixture

Phase	*Wt.* (%)				
	P1-S1	P2-S1	P3-S1	AVERAGE	STDEV
Alite	40.9	40.6	40.9	40.8	0.2
Belite	22.7	22.5	21.8	22.3	0.5
Aluminate	4.7	4.6	4.6	4.6	0.1
Ferrite	8.9	8.5	8.8	8.7	0.2
Calcite	4.2	4.3	4.3	4.3	0.1
Syngenite	0.8	0.7	0.8	0.8	0.1
Portlandite	0.8	0.7	0.7	0.7	0.1
Gypsum	4.5	4.4	4.6	4.5	0.1
Hemihydrate	1.2	1.1	1.3	1.2	0.1
Mullite	1.8	1.7	1.6	1.7	0.1
Quartz	0.6	0.6	0.6	0.6	0.0
Magnetite	0.0	0.0	0.0	0.0	0.0
Periclase	0.0	0.0	0.0	0.0	0.0
Fly Ash SCMAP	**7.6**	**7.6**	**7.9**	**7.7**	**0.2**
Amorphous Phase - Other	1.4	2.8	2.0	2.1	0.7
Total Amorphous Phase	9.0	10.4	9.9	9.8	0.7
Part of Fly Ash in Mixture				**10.4**	
Difference Between the Measured and Actual Amount of Fly Ash in Mixture				**-0.4**	

Table 8-6: Analysis of 20FA1-PC1 Mixture

Phase	*Wt.* (%)				
	P1-S1	P2-S1	P3-S1	AVERAGE	STDEV
Alite	36.4	35.9	36.0	36.1	0.3
Belite	18.9	18.6	18.8	18.8	0.2
Aluminate	4.0	3.9	3.9	3.9	0.1
Ferrite	7.4	7.5	7.2	7.4	0.2
Calcite	3.8	4.0	3.9	3.9	0.1
Syngenite	0.8	0.7	0.7	0.7	0.1
Portlandite	0.7	0.6	0.6	0.6	0.1
Gypsum	4.1	4.1	4.3	4.2	0.1
Hemihydrate	0.7	0.9	1.0	0.9	0.2
Mullite	3.8	3.9	3.8	3.8	0.1
Quartz	1.3	1.3	1.3	1.3	0.0
Magnetite	0.3	0.3	0.4	0.3	0.1
Periclase	0.2	0.2	0.2	0.2	0.0
Fly Ash SCMAP	**15.2**	**15.5**	**15.3**	**15.3**	**0.2**
Amorphous Phase - Other	2.3	2.5	2.6	2.5	0.2
Total Amorphous	17.5	18.0	17.9	17.8	0.3
Part of Fly Ash in Mixture				**20.7**	
Difference Between the Measured and Actual Amount of Fly Ash in Mixture				**-0.7**	

Table 8-7: Analysis of 30 FA1-PC1 Mixture

Phase	*Wt.* (%)				
	P1-S1	P2-S1	P3-S1	AVERAGE	STDEV
Alite	31.6	31.7	31.4	31.6	0.2
Belite	16.1	15.5	16.3	16.0	0.4
Aluminate	3.7	3.7	3.5	3.6	0.1
Ferrite	7.0	6.8	7.0	6.9	0.1
Calcite	3.5	3.5	3.5	3.5	0.0
Syngenite	0.3	0.6	0.5	0.5	0.2
Portlandite	0.5	0.6	0.5	0.5	0.1
Gypsum	3.0	3.0	2.9	3.0	0.1
Hemihydrate	0.9	1.1	0.9	1.0	0.1
Mullite	5.5	5.4	5.1	5.3	0.2
Quartz	2.0	2.0	2.0	2.0	0.0
Magnetite	0.3	0.4	0.4	0.4	0.1
Periclase	0.2	0.2	0.3	0.2	0.1
Fly Ash SCMAP	**22.5**	**22.9**	**22.6**	**22.7**	**0.2**
Amorphous Phase - Other	2.9	2.6	3.1	2.9	0.3
Total Amorphous	25.4	25.5	25.7	25.5	0.2
Part of Fly Ash in Mixture				**30.6**	
Difference Between the Measured and Actual Amount of Fly Ash in Mixture				**-0.6**	

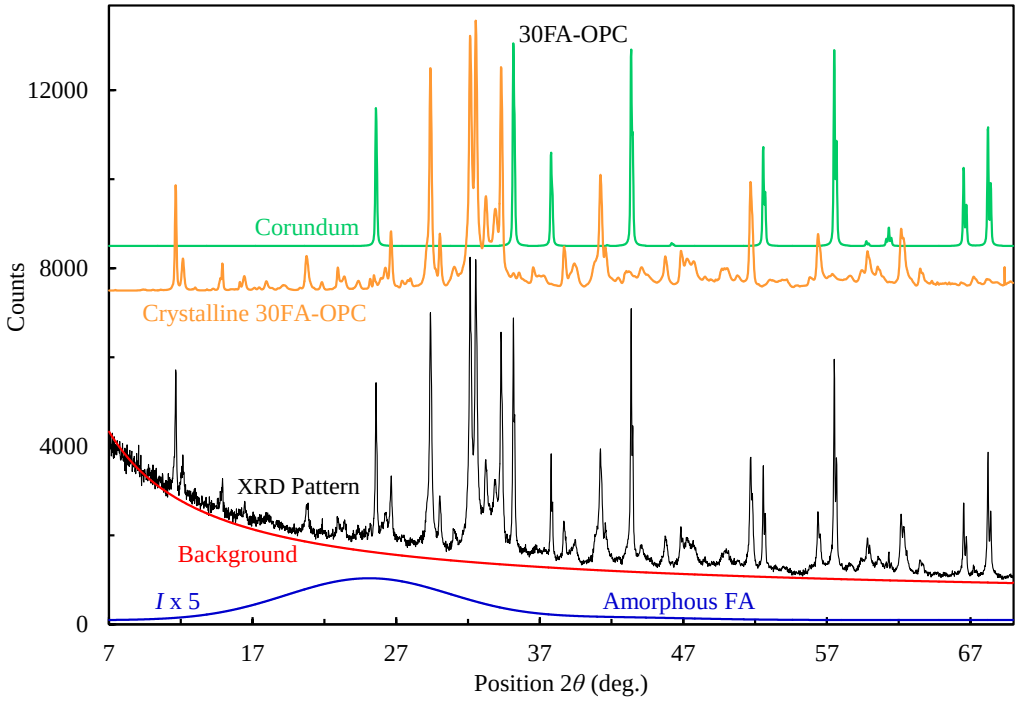

Figure 8-3: Iterative Rietveld-PONKCS analysis of the 30FA1-PC1 mixture

The results of the analyses of PC1-SL1 mixtures by the internal-standard **Iterative Rietveld-PONKCS** method are shown in Table 8-8 through Table 8-13, Figure 8-4, and Figure 8-5. Similar to PC1-FA1 mixtures, the precision and accuracy of the determination of SL1 in mixtures within the PONKCS method was high, (about 1 wt.%). In contrast to PC1-FA1 mixtures, the crystalline phases in SL1 are very low and therefore could not be successfully used to determine the slag content in the mixture as the weight fraction of the strongest crystalline phase, melilite, was less than 1 wt.%.

Table 8-8: Analysis of 5 SL1-PC1 Mixture

Phase	*Wt.* (%)				
	P1-S1	P2-S1	P3-S1	AVERAGE	STDEV
Alite	44.8	43.5	44	44.1	0.7
Belite	24.5	23.7	23	23.7	0.8
Aluminate	4.9	4.7	4.9	4.8	0.1
Ferrite	9.4	9	9.1	9.2	0.2
Calcite	4.6	4.6	4.6	4.6	0.0
Syngenite	0.3	0.1	0.2	0.2	0.1
Portlandite	0.8	0.8	0.7	0.8	0.1
Gypsum	3.6	4	3.7	3.8	0.2
Hemihydrate	1.3	1.2	1.2	1.2	0.1
Melilite	0	0	0	0.0	0.0
Slag SCMAP	**4.6**	**5.4**	**5.2**	**5.1**	**0.4**
Amorphous Phase - Other	1.2	2.9	3.4	2.5	1.2
Total Amorphous Phase	5.8	8.3	8.6	7.6	1.5
Part of Slag in Mixture				**5.1**	
Difference Between the Measured and Actual Amount of Slag in Mixture				**-0.1**	

Table 8-9: Analysis of 10 SL1-PC1Mixture

Phase	*Wt.* (%)				
	P1-S1	P2-S1	P3-S1	AVERAGE	STDEV
Alite	41.4	42.3	41.8	41.8	0.5
Belite	23.2	23.7	23.2	23.4	0.3
Aluminate	4.5	4.5	4.5	4.5	0.0
Ferrite	8.6	8.9	8.8	8.8	0.2
Calcite	4.5	4.6	4.7	4.6	0.1
Syngenite	0.3	0.1	0.2	0.2	0.1
Portlandite	0.7	0.5	0.6	0.6	0.1
Gypsum	3.2	3.3	3.3	3.3	0.1
Hemihydrate	1.2	1.2	1.2	1.2	0.0
Melilite	0	0	0	0.0	0.0
Slag SCMAP	**10.5**	**9.8**	**10.2**	**10.2**	**0.4**
Amorphous - Other	1.9	1	1.4	1.4	0.5
Total Amorphous Phase	12.4	10.8	11.6	11.6	0.8
Part of Slag in Mixture				**10.3**	
Difference Between the Measured and Actual Amount of Slag in Mixture				**-0.3**	

Table 8-10: Analysis of 20SL1-PC1 Mixture

Phase	*Wt.* (%)				
	P1-S1	P2-S1	P3-S1	AVERAGE	STDEV
Alite	36.7	37.1	37.9	37.2	0.6
Belite	20.9	21.2	21.1	21.1	0.2
Aluminate	4.1	4.0	4.2	4.1	0.1
Ferrite	7.4	7.7	7.7	7.6	0.2
Calcite	3.7	3.6	3.5	3.6	0.1
Syngenite	0.1	0.3	0.1	0.2	0.1
Portlandite	0.6	0.6	0.6	0.6	0.0
Gypsum	3.3	3.3	3.1	3.2	0.1
Hemihydrate	0.9	1.0	1.0	1.0	0.1
Melilite	0.1	0.1	0.1	0.1	0.0
Slag SCMAP	**19.8**	**19.4**	**19.9**	**19.7**	**0.3**
Amorphous Phase - Other	2.4	1.7	0.6	1.6	0.9
Total Amorphous Phase	22.2	21.1	20.5	21.3	0.9
Part of Slag in Mixture				**20.0**	
Difference Between the Measured and Actual Amount of Slag in Mixture				**0.0**	

Table 8-11: Analysis of 30SL1-PC1 Mixture

Phase	*Wt.* (%)				
	P1-S1	P2-S1	P3-S1	AVERAGE	STDEV
Alite	31.0	31.7	31.4	31.4	0.4
Belite	18.2	17.5	18.2	18.0	0.4
Aluminate	3.5	3.5	3.6	3.5	0.1
Ferrite	6.8	6.8	6.8	6.8	0.0
Calcite	4.6	4.6	4.5	4.6	0.1
Syngenite	0.2	0.3	0.1	0.2	0.1
Portlandite	0.6	0.5	0.4	0.5	0.1
Gypsum	2.8	2.9	3.2	3.0	0.2
Hemihydrate	0.5	0.7	0.7	0.6	0.1
Melilite	0.1	0.1	0.1	0.1	0.0
Slag SCMAP	**30.0**	**29.8**	**29.6**	**29.8**	**0.2**
Amorphous Phase - Other	1.8	1.6	1.4	1.6	0.2
Total Amorphous Phase	31.8	31.4	31.0	31.4	0.4
Part of Slag in Mixture				**30.2**	
Difference Between the Measured and Actual Amount of Slag in Mixture				**-0.2**	

Table 8-12: Analysis of 50SL1-PC1 Mixture

Phase	*Wt.* (%)				
	P1-S1	P2-S1	P3-S1	AVERAGE	STDEV
Alite	23.1	22.6	22.3	22.7	0.4
Belite	13.6	13.7	14.1	13.8	0.3
Aluminate	2.8	2.5	2.6	2.6	0.2
Ferrite	5.2	5.1	5.0	5.1	0.1
Calcite	3.5	3.5	3.7	3.6	0.1
Syngenite	0.2	0.2	0.2	0.2	0.0
Portlandite	0.2	0.2	0.3	0.2	0.1
Gypsum	2.0	2.3	2.1	2.1	0.2
Hemihydrate	0.3	0.4	0.4	0.4	0.1
Melilite	0.2	0.1	0.2	0.2	0.1
Slag SCMAP	**48.3**	**48.8**	**48.9**	**48.7**	**0.3**
Amorphous Phase - Other	0.6	0.6	0.3	0.5	0.2
Total Amorphous Phase	48.9	49.4	49.2	49.2	0.3
Part of Slag in Mixture				**49.4**	
Difference Between the Measured and Actual Amount of Slag in Mixture				**0.6**	

Table 8-13: Analysis of 70SL1-PC1 Mixture

Phase	*Wt.* (%)				
	P1-S1	P2-S1	P3-S1	AVERAGE	STDEV
Alite	13	13.1	12.7	12.9	0.2
Belite	9.8	9.2	10.4	9.8	0.6
Aluminate	1.6	1.5	1.6	1.6	0.1
Ferrite	3.1	3.3	3.1	3.2	0.1
Calcite	2.3	2.3	2.3	2.3	0.0
Syngenite	0	0	0	0.0	0.0
Portlandite	0	0	0	0.0	0.0
Gypsum	1.3	1.4	1.4	1.4	0.1
Hemihydrate	0.2	0.1	0.2	0.2	0.1
Melilite	0.2	0.2	0.1	0.2	0.1
Slag SCMAP	**68.2**	**68.6**	**68.1**	**68.3**	**0.3**
Amorphous Phase - Other	0.2	0.3	0.1	0.2	0.1
Total Amorphous Phase	68.4	68.9	68.2	68.5	0.4
Part of Slag in Mixture				**69.3**	
Difference Between the Measured and Actual Amount of Slag in Mixture				**0.7**	

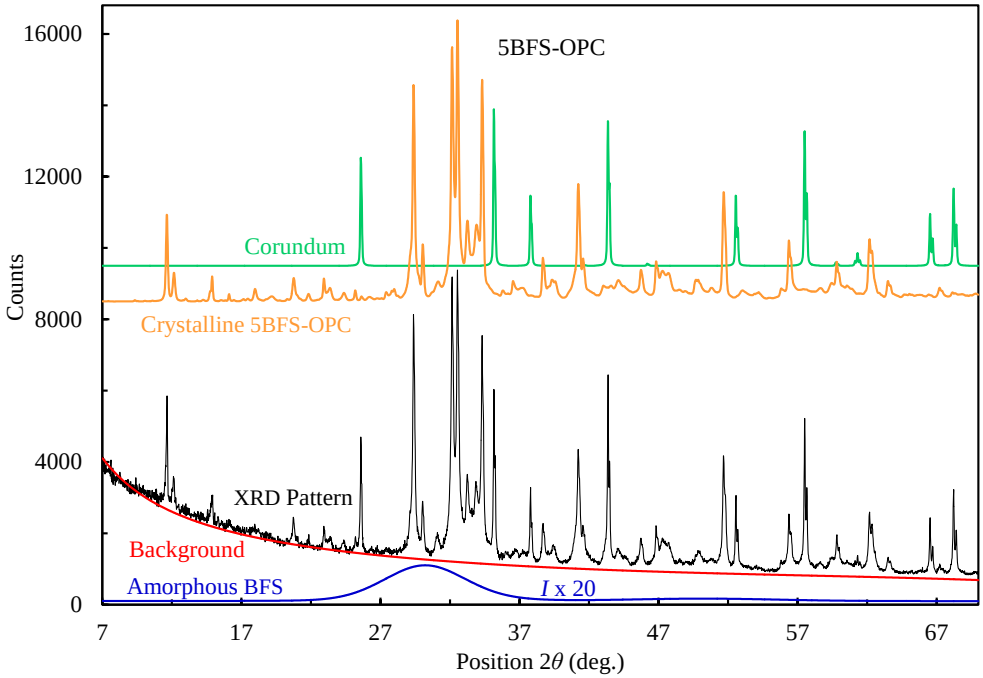

Figure 8-4: Iterative Rietveld-PONKCS analysis of the 5SL1-PC1 mixture

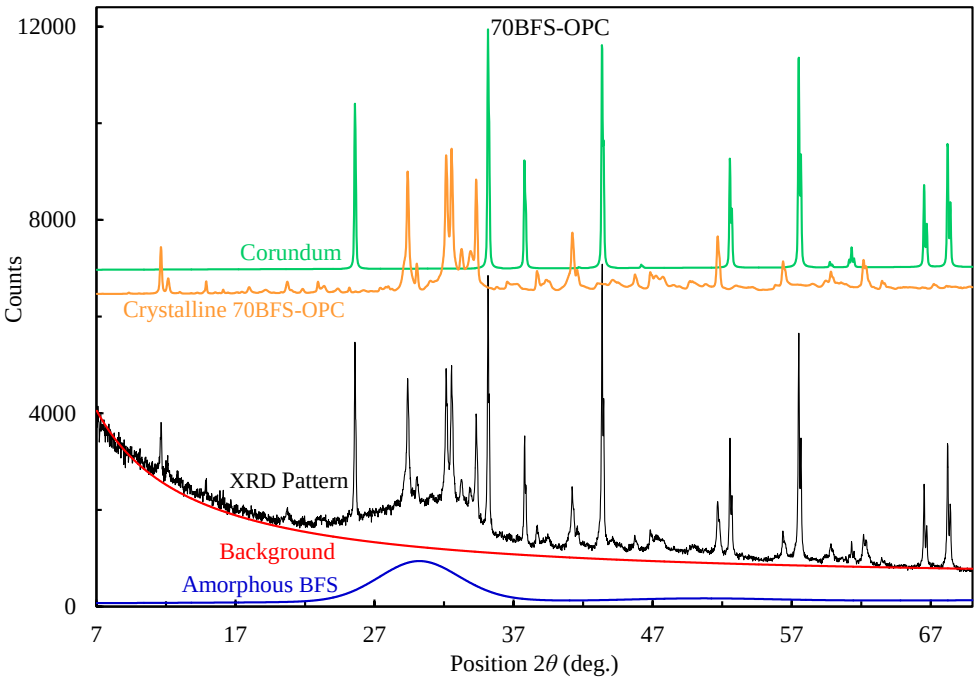

Figure 8-5: Iterative Rietveld-PONKCS analysis of the 70SL1-PC1 mixture

The results of the analysis of PC3-SL2 mixtures by the iterative internal-standard PONKCS method are shown in Table 8-14 through Table 8-19. Similar to PC1-SL1 mixtures, the precision and accuracy of slag quantification in SL2 mixtures using the PONKCS method was high, about 1 wt.%. Additionally, the findings indicate that similar to PC1-SL1 mixtures, there is no crystalline phase in the SL2 that can be successfully used for the determination of the SL2 content in its mixtures with PC3. The amorphous content in the SL2 was very high, about 97 wt.%, and the weight fraction of the SL2 crystalline phase, melilite, was less than 0.5 wt.%.

Table 8-14: Analysis of 5SL2-PC3 Mixture

	Wt. (%)				
Phase	P1-S1	P2-S1	P3-S1	AVERAGE	STDEV
Alite	49.6	49.4	49.7	49.6	0.2
Belite	13.8	13.0	13.0	13.3	0.5
Aluminate	1.5	1.4	1.4	1.4	0.1
Ferrite	10.9	11.0	11.2	11.0	0.2
Calcite	5.4	5.5	5.4	5.4	0.1
Aphthitalite	0.2	0.1	0.1	0.1	0.1
Syngenite	0.8	1.2	1.1	1.0	0.2
Periclase	0.2	0.3	0.3	0.3	0.1
Gypsum	2.4	2.5	2.5	2.5	0.1
Hemihydrate	1.1	1.2	1.1	1.1	0.1
Melilite	0.0	0.0	0.0	0.0	0.0
Magnetite	0.0	0.0	0.0	0.0	0.0
Quartz	0.0	0.0	0.0	0.0	0.0
Slag SCMAP	**5.6**	**5.2**	**5.6**	**5.5**	**0.2**
Amorphous Phase - Other	8.4	9.2	8.5	8.7	0.4
Total Amorphous Phase	14.0	14.4	14.1	14.2	0.2
Part of Slag in Mixture				**5.6**	
Difference Between the Measured and Actual Amount of Slag in Mixture				**-0.6**	

Table 8-15: Analysis of 10SL2–PC3 Mixture

Phase	*Wt.* (%)				
	P1-S1	P2-S1	P3-S1	AVERAGE	STDEV
Alite	47.9	48.6	46.9	47.8	0.9
Belite	11.7	12.0	11.7	11.8	0.2
Aluminate	1.4	1.4	1.4	1.4	0.0
Ferrite	10.7	10.8	10.3	10.6	0.3
Calcite	4.9	5.1	5.2	5.1	0.2
Aphthitalite	0.1	0.2	0.2	0.2	0.1
Syngenite	0.9	1.1	1.0	1.0	0.1
Periclase	0.3	0.3	0.2	0.3	0.1
Gypsum	2.2	2.3	2.4	2.3	0.1
Hemihydrate	1.0	1.0	1.1	1.0	0.1
Melilite	0.0	0.0	0.0	0.0	0.0
Magnetite	0.0	0.0	0.0	0.0	0.0
Quartz	0.0	0.0	0.0	0.0	0.0
Slag SCMAP	**10.4**	**9.3**	**10.1**	**9.9**	**0.6**
Amorphous Phase - Other	8.4	7.9	9.6	8.6	0.9
Total Amorphous Phase	18.8	17.2	19.7	18.6	1.3
Part of Slag in Mixture				**10.3**	
Difference Between the Measured and Actual Amount of Slag in Mixture				**-0.3**	

Table 8-16: Analysis of 20SL2-PC3Mixture

Phase	*Wt.* (%)				
	P1-S1	P2-S1	P3-S1	AVERAGE	STDEV
Alite	41.9	42.9	44.2	43.0	1.2
Belite	11.9	11.6	11.1	11.5	0.4
Aluminate	1.5	1.5	1.4	1.5	0.1
Ferrite	9.1	9.6	9.6	9.4	0.3
Calcite	4.9	4.8	4.8	4.8	0.1
Aphthitalite	0.1	0.0	0.0	0.0	0.1
Syngenite	0.5	0.4	0.3	0.4	0.1
Periclase	0.2	0.1	0.2	0.2	0.1
Gypsum	2.0	1.8	1.7	1.8	0.2
Hemihydrate	0.9	1.0	0.8	0.9	0.1
Melilite	0.0	0.0	0.0	0.0	0.0
Magnetite	0.0	0.0	0.0	0.0	0.0
Quartz	0.0	0.0	0.0	0.0	0.0
Slag SCMAP	**19.9**	**19.3**	**18.5**	**19.2**	**0.7**
Amorphous Phase - Other	7.3	7.0	7.4	7.2	0.2
Total Amorphous Phase	27.2	26.3	25.9	26.5	0.7
Part of Slag in Mixture				**19.8**	
Difference Between the Measured and Actual Amount of Slag in Mixture				**0.2**	

Table 8-17: Analysis of 30SL2-PC3 Mixture

Phase	*Wt.* (%)				
	P1-S1	P2-S1	P3-S1	AVERAGE	STDEV
Alite	36.7	37.6	35.8	36.7	0.9
Belite	10.2	10.1	10.3	10.2	0.1
Aluminate	1.2	1.3	1.2	1.2	0.1
Ferrite	8.2	8.3	8.3	8.3	0.1
Calcite	4.5	4.5	4.6	4.5	0.1
Aphthitalite	0.0	0.0	0.1	0.0	0.1
Syngenite	0.2	0.3	0.3	0.3	0.1
Periclase	0.1	0.1	0.2	0.1	0.1
Gypsum	1.6	1.6	1.6	1.6	0.0
Hemihydrate	0.8	0.7	0.9	0.8	0.1
Melilite	0.0	0.0	0.0	0.0	0.0
Magnetite	0.1	0.2	0.1	0.1	0.1
Quartz	0.1	0.1	0.1	0.1	0.0
Slag SCMAP	**29.7**	**29.4**	**29.7**	**29.6**	**0.2**
Amorphous Phase - Other	6.5	5.8	6.7	6.3	0.5
Total Amorphous Phase	36.2	35.2	36.4	35.9	0.6
Part of Slag in Mixture				**30.5**	
Difference Between the Measured and Actual Amount of Slag in Mixture				**-0.5**	

Table 8-18: Analysis of 50SL2-PC3 Mixture

Phase	*Wt.* (%)				
	P1-S1	P2-S1	P3-S1	AVERAGE	STDEV
Alite	26.3	25.3	25.6	25.7	0.5
Belite	7.2	7.9	7.6	7.6	0.4
Aluminate	0.8	0.9	0.9	0.9	0.1
Ferrite	5.9	5.9	5.7	5.8	0.1
Calcite	3.9	4.3	4.0	4.1	0.2
Aphthitalite	0.0	0.0	0.0	0.0	0.0
Syngenite	0.0	0,1	0.0	0.0	0.0
Periclase	0.1	0.0	0.1	0.1	0.1
Gypsum	1.3	1.1	1.3	1.2	0.1
Hemihydrate	0.4	0.7	0.7	0.6	0.2
Melilite	0.1	0.1	0.1	0.1	0.0
Magnetite	0.2	0,1	0.1	0.2	0.1
Quartz	0.1	0.2	0.1	0.1	0.1
Slag SCMAP	**48.3**	**48.9**	**48.7**	**48.6**	**0.3**
Amorphous Phase - Other	5.3	4.5	5.0	4.9	0.4
Total Amorphous Phase	53.6	53.4	53.7	53.6	0.2
Part of Slag in Mixture				**50.2**	
Difference Between the Measured and Actual Amount of Slag in Mixture				**-0.2**	

Table 8-19: Analysis of 70SL2-PC3 Mixture

Phase	*Wt.* (%)				
	P1-S1	P2-S1	P3-S1	AVERAGE	STDEV
Alite	15.6	15.5	15.3	15.5	0.2
Belite	4.7	4.9	5.1	4.9	0.2
Aluminate	0.5	0.5	0.6	0.5	0.1
Ferrite	3.5	3.6	3.4	3.5	0.1
Calcite	3.5	3.4	3.4	3.4	0.1
Aphthitalite	0.0	0.0	0.0	0.0	0.0
Syngenite	0.3	0.1	0.3	0.2	0.1
Periclase	0.1	0.1	0.1	0.1	0.0
Gypsum	0.8	0.7	0.6	0.7	0.1
Hemihydrate	0.4	0.3	0.2	0.3	0.1
Melilite	0.0	0.0	0.0	0.0	0.0
Magnetite	0.2	0.2	0.2	0.2	0.0
Quartz	0.2	0.2	0.2	0.2	0.0
Slag SCMAP	**67.9**	**68.0**	**67.9**	**67.9**	**0.1**
Amorphous Phase - Other	2.4	2.6	2.7	2.6	0.2
Total Amorphous Phase	70.3	70.6	70.6	70.5	0.2
Part of Slag in Mixture				**70.1**	
Difference Between the Measured and Actual Amount of Slag in Mixture				**-0.1**	

8.4.3 Refinement of Commercial SCM-Blended Cements using PONKCS Method

Analysis of PC1-1P(30) using the internal-standard **Iterative Rietveld-PONKCS** method is presented in Table 8-20. The fly ash content in PC1-1P(30) is about 30 – 31 wt.%. This is in good agreement with the manufacturer reported fly ash content of 30%. The presence of a relatively large amount of mullite, 17.7 wt.% in FA1 fly ash (Table 7-3) makes it possible to verify the fly ash content in PC1-1P(30) using mullite content. The determined amount of mullite in the blended PC1-1P(30), 5.2 wt.% (Table 8-20), gives about 29.4 wt.% of fly ash in the blended cement, which is in good agreement with the determined value of 30.6 wt.% (Table 8-20), determined through the **Iterative Rietveld-PONKCS** method. However, if fly ash substitution in the blended system is low, the latter would be the only reliable technique for studying the blended system.

Table 8-20: Mineralogical Analysis of PC1-1P(30) (wt.%)

Phase	P1	P2	P3	Average	STDEV
Alite	29.3	28.9	28.8	29.0	0.3
Belite	16.7	16.3	16.5	16.5	0.2
Aluminate	4.5	4.2	4.2	4.3	0.2
Ferrite	6.6	7.2	7.0	6.9	0.3
Calcite	3.8	3.7	3.7	3.7	0.1
Syngenite	0.5	0.7	0.7	0.6	0.1
Portlandite	0.5	0.6	0.6	0.6	0.1
Gypsum	1.3	1.3	1.2	1.3	0.1
Hemihydrate	2.0	2.1	2.0	2.0	0.1
Anhydrite	0.5	0.5	0.6	0.5	0.1
Mullite	5.4	5.1	5.2	5.2	0.2
Quartz	2.0	1.9	2.0	2.0	0.1
Magnetite	0.4	0.2	4.0	1.5	2.1
Periclase	0.3	0.3	0.3	0.3	0.0
Fly Ash SCMAP	**22.6**	**22.8**	**22.6**	**22.7**	**0.1**
Cement A/u	3.6	4.1	3.9	3.9	0.3
Blended cement A/u	26.2	26.9	26.5	26.5	0.4
Fly Ash content in blended cement				**30.6**	

For the blended slag systems, the results for PC1-1S(30) using the internal-standard **Iterative Rietveld-PONKCS** method are shown in Table 8-21. The analysis indicates that the slag content in the blended cement is about 30 wt.%, which is in agreement with the reported value by the blended cement manufacturer. In contrast to PC1-1P(30), the slag content in this blended cement cannot be accurately estimated using any of the crystalline phases reported here due to their very low amounts.

Table 8-21: Mineralogical Analysis of PC1-1S(30)

Phase	P1	P2	P3	Average	STDEV
Alite	29.3	29.3	29.4	29.3	0.1
Belite	20.9	20.3	20.8	20.7	0.3
Aluminate	3.3	3.3	3.3	3.3	0.0
Ferrite	7.2	7.3	7.3	7.3	0.1
Calcite	2.6	2.5	2.2	2.4	0.2
Syngenite	0.4	0.5	0.3	0.4	0.1
Portlandite	0.3	0.2	0.2	0.2	0.1
Gypsum	2.3	2.4	2.5	2.4	0.1
Hemihydrate	1.1	1.3	1.3	1.2	0.1
Anhydrite	0.3	0.4	0.3	0.3	0.1
Quartz	0.1	0.2	0.2	0.2	0.1
Melilite	0	0	0.1	0.0	0.1
Slag SCMAP	**29.4**	**29.6**	**29.9**	**29.6**	**0.3**
Cement A/u	2.7	2.9	2.3	2.6	0.3
Blended A/u	32.1	32.5	32.2	32.3	0.2
Slag content in Blended Cement				**30.1**	

The analysis of the third commercially blended cement, PC3-1S(20), conducted by the internal-standard **Iterative Rietveld-PONKCS** method is presented in Table 8-22. The slag content in PC3-1S(20) blend is about 19-20 wt.%. The slag content in the blended cement was indicated to be 20% by the producer.

Table 8-22: Mineralogical Analysis of PC3-1S(20)

Phase	P1-S1	P2-S1	P3-S1	AVERAGE	STDEV
Alite	43.4	43.5	43.7	43.5	0.2
Belite	14.6	15.1	15.1	14.9	0.3
Aluminate	1.2	1.2	1.3	1.2	0.1
Ferrite	10.4	10.7	10.5	10.5	0.2
Calcite	2.6	2.5	2.5	2.5	0.1
Aphthitalite	0.2	0.1	0.1	0.1	0.1
Syngenite	0.4	0.5	0.4	0.4	0.1
Periclase	0.1	0.2	0.1	0.1	0.1
Gypsum	1.6	1.6	1.6	1.6	0.0
Hemihydrate	2.0	1.9	1.9	1.9	0.1
Anhydrite	0.0	0.1	0.1	0.1	0.1
Melilite	0.0	0.0	0.0	0.0	0.0
Magnetite	0.0	0.0	0.0	0.0	0.0
Quartz	0.0	0.0	0.0	0.0	0.0
Slag SCMAP	**19.2**	**18.3**	**18.8**	**18.8**	**0.5**
Cement A/u	4.4	4.4	4.0	4.3	0.2
Blended A/u	23.6	22.7	22.8	23.0	0.5
Slag content in Blended Cement				**19.4**	

8.5 Conclusions

(i) The internal-standard **Iterative Rietveld-PONKCS** approach/method developed in this study, has high precision and accuracy (1 wt.%), for the quantification of the SCM content in blended systems;

(ii) The method is based on refinement of both the calibration SCM and the cement-SCM mixtures;

(iii) The method involves background refinement of the calibration SCMs and the cement-SCM mixtures, using first-order Chebyshev polynomials with a $1/2\theta$ term. The first-order polynomial gave the best refinement results for the determinations of the SCM contents in mixtures and blends. One probable reason for the effectiveness of the first-order Chebyshev polynomial is that it is the highest order of polynomial that is concave upward in the 2θ ranges studied here;

(iv) To get the best fit for the SCMAP, the iterative technique requires the separation of the amorphous hump refinement from background refinement.

8.6 References

[1] J. C. Taylor, L. P. Aldridge, C. E. Matulis, and I. Hinczak, “X-ray powder diffraction analysis of cements,” in *Structure and Performance of Cements*, Second edi., J. Bensted and P. Barnes, Eds. Spon Press, 2002, pp. 420–441.

[2] S. Mindess, J. F. Young, and D. Darwin, *Concrete.*, Second Edi. Prentice Hall, 2003.

[3] R. S. Winburn, D. G. Grier, G. J. McCarthy, and R. B. Peterson, “Rietveld quantitative X-ray diffraction analysis of NIST fly ash standard reference materials,” *Powder Diffr.*, vol. 15, no. September, pp. 163–172, 2000.

[4] T. Westphal, G. Walenta, T. Füllmann, M. Gimenez, E. Bermejo, K. L. Scrivener, and H. Pöllmann, “Characterisation of cementitious materials,” *Int. Cem. Rev.*, pp. 47–51, 2002.

[5] G. Walenta and T. Füllmann, “Advances in quantitative XRD analysis for clinker, cements, and cementitious additions,” *Powder Diffr.*, vol. 19, no. 1, pp. 40–44, Mar. 2004.

[6] N. V. Y. Scarlett and I. C. Madsen, “Quantification of phases with partial or no known crystal structures,” *Powder Diffr.*, vol. 21, pp. 278–284, 2006.

[7] I. C. Madsen, N. V. Y. Scarlett, and A. Kern, “Description and survey of methodologies for the determination of amorphous content via X-ray powder diffraction,” *Z. Krist.*, vol. 226, pp. 944–955, 2011.

[8] R. Snellings, A. Salze, and K. L. Scrivener, “Use of X-ray diffraction to quantify amorphous supplementary cementitious materials in anhydrous and hydrated blended cements,” *Cem. Concr. Res.*, vol. 64, pp. 89–98, Oct. 2014.

[9] G. S. Pawley, “Unit-cell refinement from powder diffraction scans,” *J. Appl. Crystallogr.*, vol. 14, pp. 357–361, 1981.

[10] A. Le Bail, H. Duroy, and J. L. Fourquet, “Ab-initio structure determination of LiSbWO6 by X-Ray powder diffraction,” *Mat. Res. Bull.*, vol. 23, pp. 447–452, 1988.

[11] R. J. Hill and C. J. Howard, “Quantitative phase analysis from neutron powder diffraction data using the Rietveld method,” *J. Appl. Crystallogr.*, vol. 20, pp. 467–474, 1987.

[12] A. Kern, I. C. Madsen, and N. V. Y. Scarlett, “Quantifying Amorphous Phases,” in *Uniting Electron Crystallography and Powder Diffraction*, U. Kolb, K. Shankland, L. Meshi, A.

Avilov, and W. I. David, Eds. Dordrecht: Springer Netherlands, 2012, pp. 219–231.

[13] T. Westphal, T. Füllmann, and H. Pöllmann, “Rietveld quantification of amorphous portions with an internal standard—Mathematical consequences of the experimental approach,” *Powder Diffr.*, vol. 24, no. 3, pp. 239–243, Feb. 2009.

[14] V. K. Peterson, A. S. Ray, and B. A. Hunter, “A comparative study of Rietveld phase analysis of cement clinker using neutron, laboratory X-ray, and synchrotron data,” *Powder Diffr.*, vol. 21, no. 1, pp. 12–18, Mar. 2006.

[15] N. Marinoni, A. Pavese, M. Voltolini, and M. Merlini, “Long-term leaching test in concretes: An X-ray powder diffraction study,” *Cem. Concr. Compos.*, vol. 30, no. 8, pp. 700–705, Sep. 2008.

[16] J. P. Cline, R. B. Von Dreele, R. Winburn, P. W. Stephens, and J. J. Filliben, “Addressing the amorphous content issue in quantitative phase analysis: the certification of NIST standard reference material 676a.,” *Acta Crystallogr. A.*, vol. 67, no. Pt 4, pp. 357–67, Jul. 2011.

[17] M. L. Gualtieri, M. Romagnoli, P. Miselli, M. Cannio, and A. F. Gualtieri, “Full quantitative phase analysis of hydrated lime using the Rietveld method,” *Cem. Concr. Res.*, vol. 42, no. 9, pp. 1273–1279, Sep. 2012.

[18] R. Snellings, A. Bazzoni, and K. Scrivener, “The existence of amorphous phase in Portland cements: Physical factors affecting Rietveld quantitative phase analysis,” *Cem. Concr. Res.*, vol. 59, pp. 139–146, May 2014.

[19] W. Wilson, K. J. Krakowiak, and F.-J. Ulm, “Simultaneous assessment of phase chemistry, phase abundance and bulk chemistry with statistical electron probe micro-analyses: Application to cement clinkers,” *Cem. Concr. Res.*, vol. 55, pp. 35–48, Jan. 2014.

[20] M. De Schepper, K. De Buysser, I. Van Driessche, and N. De Belie, “A Hydration Study by XRD / Rietveld Analysis of Cement Regenerated from Completely Recyclable Concrete,” *IJRET*, vol. 3, no. 13, pp. 129–134, 2014.

[21] V. K. Pecharsky and P. Y. Zavilij, *Fundamentals of Powder Diffraction and Structural Characterization of Materials*, 2nd ed. New York, NY, USA: Springer, 2009.

[22] G. Caglioti, A. Paoletti, and F. P. Ricci, “Choice of collimators for a crystal spectrometer for neutron diffraction,” *Nucl. Instruments*, vol. 3, pp. 223 – 228, 1958.

[23] Y. P. Stetsko, N. Shanahan, H. Deford, and A. Zayed, “Quantification of supplementary cementitious content in blended Portland cement using an iterative Rietveld–PONKCS technique,” *J. Appl. Crystallogr.*, vol. 50, no. 2, pp. 498–507, 2017.

Chapter 9. Conclusions and Recommendations

The findings of this study can be summarized as follows:

1. The main goal of this research project was achieved through the development of analysis procedures to quantify the phases present in portland cement-supplemental cementitious material combinations that are or may be used by FDOT.
2. An iterative Rietveld-PONKCS (IRP) method was developed that combines quantitative x-ray diffraction, Rietveld refinement, and PONKCS analyses. This method has been shown to determine the phase contents of anhydrous cementitious systems with high precision and accuracy.
3. The IRP protocol was developed and tested on laboratory-prepared portland cement-supplemental cementitious material mixtures with portland cement replacements ranging from 5 to 70% and was shown to be highly accurate compared to previous methods.
4. The method was used to analyze commercial limestone-blended portland cement, ground granulated blast furnace slag-blended portland cement, and Class F fly ash-blended portland cement. The phase contents in anhydrous portland cement clinker, the slag and fly ash contents in commercial blended cements, the limestone contents of portland-limestone cements, and the amorphous phase contents of each cementitious material were determined with a typical accuracy of about 1%.

The following recommendations are based on the findings of this study:

1. Adopt the IRP quantitative analysis method for blended cementitious systems for the verification of the constituents of blended portland cement-SCM systems. This should enable enhancement of the reliability and durability of concrete elements in the infrastructure system of the state of Florida.
2. Change FDOT specifications to require quantitative XRD analyses (QXRDA) of all cementitious materials as part of the acceptance program and for Quality Assurance procedures.
3. Arrange with the Construction Materials Group in the Department of Civil and Environmental Engineering of the University of South Florida to host workshops for

the characterization and phase analyses of portland cements and blended cementitious systems used by the state of Florida Department of Transportation. The training received would enable FDOT personnel to perform QXRDA on cementitious raw materials at the State Materials Office (SMO).

Appendix A. Certificate of Analysis SRM 676a

National Institute of Standards & Technology

Certificate of Analysis

Standard Reference Material® 676a

Alumina Powder
(Quantitative Analysis Powder Diffraction Standard)

This Standard Reference Material (SRM) consists of an alumina powder (corundum structure) intended primarily for use as an internal standard for quantitative phase analysis using powder diffraction methods. It is also suitable for determination of I/I_c values [1] (for a complete discussion of the I/I_c see [2]). A unit of SRM 676a consists of approximately 20 g of powder, bottled in an argon atmosphere.

Material Description: The alumina powder was produced via the alum [$NH_4Al(SO_4)_2 \cdot 12H_2O$] precursor route, calcined to 1400 °C, and jet milled to a fully disaggregated state. The alumina grains are sub-micrometer in size and equi-axial in shape. The high calcination temperature ensures high phase purity while the isometric form of the grains effectively eliminates preferred orientation effects in this powder. The disaggregated state of this material ensures the homogeneity of mixtures prepared by conventional methods.

An analysis of the phase fractions determined from X-ray powder diffraction data from mixtures of SRM 676a and silicon powder, SRM 640c [3], indicated that the SRM material was homogeneous with respect to diffraction properties.

Certified Values: A NIST certified value is a value for which NIST has the highest confidence in its accuracy in that all known or suspected sources of bias have been investigated or taken into account. The certified phase purity of the material expressed as a mass fraction is:

Crystalline Alumina: 99.02 % ± 1.11 %

The interval defined by the certified value and its uncertainty represents an expanded uncertainty using $k = 2$, in the absence of systematic error [4,5]. The certified value of the phase purity may not exceed 100 %, even though the uncertainty error bounds define a range in excess of 100 %. The measurand is the certified value for the phase purity of the material (alumina). Metrological traceability is to the SI unit for the derived unit of mass fraction (expressed as a percent). The measurands are the certified lattice parameters listed in Table 1. Metrological traceability is to the SI unit of length (expressed as nanometers).

Information Values: The analyses associated with certification of SRM 676a included the computation of the diffraction line positions shown in Table 2. Measured relative intensity values are shown in Table 3. These data are presented as information values. An information value is considered to be a value that will be of interest to the SRM user, but insufficient information is available to assess the uncertainty associated with the value. Information values cannot be used to establish metrological traceability.

Expiration of Certification: The certification of **SRM 676a** is valid indefinitely, within the measurement uncertainty specified, provided the SRM is stored and handled in accordance with instructions given in this certificate (See "Instructions for Storage"). Accordingly, periodic recalibration or recertification of this SRM is not required. The certification is nullified if the SRM is damaged, contaminated, or otherwise modified.

Overall coordination and technical direction of the certification of this SRM were performed by J.P. Cline of the NIST Materials Measurement Science Division.

John A. Small, Chief
Materials Measurement Science Division

Gaithersburg, MD 20899
Certificate Issue Date: 04 November 2015
Certificate Revision History on Page 6

Robert L. Watters, Jr., Director
Office of Reference Materials

The material preparation, measurements, and data analysis were provided by J.P. Cline, D. Black, D. Windover, and A. Henins of the NIST Materials Measurement Science Division; R.B. Von Dreele of Argonne National Laboratory, Argonne, IL; R. Winburn of Minot State University, Minot, ND; P.W. Stephens of the State University of New York, Stony Brook, NY, and the National Synchrotron Light Source, Brookhaven, NY.

Statistical analysis was provided by J.J. Filliben and A.M. Possolo of the NIST Statistical Engineering Division.

J. Evans of Durham University, Durham, UK developed a template for the input files used in data analysis procedures for certification of lattice parameters.

Support aspects involved in the issuance of this SRM were coordinated through the NIST Office of Reference Materials.

Maintenance of SRM Certification: NIST will monitor this SRM over the period of its certification. If substantive technical changes occur that affect the certification, NIST will notify the purchaser. Registration (see attached sheet or register online) will facilitate notification.

INSTRUCTIONS FOR STORAGE

Storage: SRM 676a was bottled in an argon atmosphere. While no long-term stability studies have been performed, no degradation of the diffraction properties of this SRM have been observed when stored and used under laboratory conditions. Furthermore, alumina is known to be a highly stable oxide and is expected to remain stable after exposure to atmospheric conditions. However, the unused portion of this SRM powder should be stored, tightly capped, in the original bottle or in one of analogous integrity.

SOURCE, PREPARATION, AND ANALYSIS[1]

Materials: The material used for this SRM was obtained from Baikowski International Corporation (Charlotte, NC).

Phase Purity: A long-count-time X-ray powder diffraction pattern of SRM 676a will offer data consistent with a high-purity alumina powder. However, the surface region of any crystalline material will not diffract as the bulk due to relaxation of the crystal structure and inclusion of surface reaction products. While this disordered, amorphous surface layer may only be on the order of a few crystallographic units in thickness, in a finely divided solid it can easily account for several percent of the total mass. Phase purity as discussed herein is a microstructural characteristic innate to a finely divided crystalline solid and influenced by the production history of the alumina powder used as the feedstock.

Certification Method: The certified measurement values of SRM 676a include the crystalline phase purity and the lattice parameters. The data that led to the certification of phase purity consisted of powder diffraction measurements performed on neutron time-of-flight (TOF) and synchrotron radiation equipment. The lattice parameters were certified with data from a NIST-built X-ray diffractometer [6] located in the temperature-controlled environment of the NIST Advanced Measurement Laboratory (AML).

The phase purity was certified through an analysis of the discrepancy between the results of powder diffraction experiments, which measure the mass ratio of material exhibiting Bragg diffraction, relative to weighing operations, which include all components. The procedure involved a comparison of the phase abundance measured from a series of mixtures of SRM 676a and hyper-pure silicon powder. The experimental design included the assumptions that (1) the silicon consists of single crystal particles, (2) the non-Bragg-diffracting material associated with the silicon was confined to the crystallite surface, and (3) the amorphous layer thickness was invariant with respect to crystallite size. Systematic variation in the amorphous content of the silicon was then effected within the aforementioned series of mixtures by the selection/variation of the particle size (hence specific surface area) of the silicon powder. The effects of extinction in the silicon, which lead to distortions in observed diffraction intensity, were addressed with use of the neutron TOF and synchrotron X-ray powder diffraction at energies of 25 keV and 67 keV, in conjunction with the Rietveld data analysis method [7]. For a complete discussion of the Rietveld method see references 8 and 9. The mass fractions of crystalline silicon, determined from the Rietveld refinements, were plotted relative to the surface areas of the silicon of each sample. An extrapolation of these data to a hypothetical (and physically impossible) silicon sample that would have no specific surface area and, therefore, no amorphous content yielded the mass fraction of SRM 676a that exhibited Bragg diffraction.

---

[1] Certain commercial equipment, instruments, or materials are identified in this certificate to adequately specify the experimental procedure. Such identification does not imply recommendation or endorsement by the National Institute of Standards and Technology, nor does it imply that the materials or equipment identified are necessarily the best available for the purpose.

The linkage of the certified lattice parameter values to the fundamental unit of length, as defined by the International System of Units (SI) [10], was established with use of the emission spectrum of Cu Kα radiation as the basis for constructing the diffraction profiles. Data were analyzed using a fundamental parameters approach (FPA) [11] wherein diffraction profiles are modeled as a convolution of functions that describe the wavelength spectrum, the contributions from the diffraction geometry, and the sample contributions resulting from microstructural features. A rigorous analysis of data from a divergent-beam instrument requires knowledge of both the diffraction angle and the effective source-sample-detector distance. Two additional models must therefore be included in the FPA analyses to account for the factors that affect the distances critical in the use of this geometry. Certification data were analyzed in the context of both Type A uncertainties, assigned by statistical analysis, and Type B uncertainties, based on knowledge of the nature of errors in the measurements, to result in the establishment of robust uncertainties for the certified values.

Certification Procedure: The procedure by which SRM 676a was certified with respect to phase purity is examined in Cline, *et al.* [12]. Additional information concerning the characteristics and use of SRM 676a, quantitative phase analysis, and the issue of amorphous content can also be found in this reference.

Data for the certification of lattice parameters were collected using a 2.2 kW copper X-ray tube of long fine-focus geometry operated at a power of 1.8 kW. The source size was approximately 12 mm × 0.04 mm. Axial divergence of the incident beam was limited by a 2.2° Soller slit. Scattered X-rays were filtered with a graphite post-sample monochromator, and detected with a scintillation detector. The variable divergence slit was set nominally to 0.8°. Also, a 2 mm anti-scatter slit was placed approximately 113 mm in front of the 0.2 mm (0.05°) receiving slit. The goniometer radius was 217.5 mm. Samples were spun at 0.5 Hz during data collection. The machine was located within a temperature-controlled laboratory space where the nominal short-range control of temperature was ± 0.1 K. The instrument was controlled via LabVIEW software. Data were recorded in true x-y format. The performance of the machine was qualified with the use of NIST SRM 660b Line Position and Line Shape Standard for Powder Diffraction [13,14] and SRM 676a Alumina Powder for Quantitative Analysis by X-Ray Diffraction using procedures discussed by Cline, *et al.* [6]. (Note: Use of SRM 676a, as referenced in Cline, *et al.* [6], takes advantage of the non-orientating nature of this alumina powder; it does not employ its certified values.)

Ten samples of SRM 676a were selected for certification measurements in a stratified random manner. The data were collected from 10 selected regions; run-time parameters for each region were adjusted with regards to observed full-width at half-maximum (FWHM) and diffraction intensity to optimize data quality per unit time. The scanned regions accessed all but two of the reflections with a relative intensity greater than 5 % and within the 2θ range of 20° to 154°. The angular widths of the scan ranges were 20 to 30 times the observed FWHM values of the profiles and were chosen to provide at least 0.3° 2θ of apparent background straddling each peak. The step width was chosen to include at least eight data points above the FWHM. The count time spent on each profile was inversely proportional to the observed diffraction intensity to realize constant counting statistics amongst the profiles. The total collection time for each sample was about 24 hours.

The certification data for lattice parameters were analyzed using the FPA method with a Rietveld refinement as implemented in TOPAS [15]. The analysis used the Cu Kα emission spectrum, including a satellite component, as characterized by G. Hölzer *et al.* and M. Maskil *et al.* [16,17]. Hölzer models the Cu $K\alpha_1/K\alpha_2$ doublet using four Lorentzian profiles, two primary ones, $K\alpha_{11}$ and $K\alpha_{21}$, and two secondary ones, $K\alpha_{12}$ and $K\alpha_{22}$; the latter two are of reduced intensity and only serve to account for the asymmetry, towards high energy, observed in the spectrum. During calibration of the instrument using high-quality data from SRM 660b, the four Lorentzian breadths of the Cu emission spectrum were refined with constraints to preserve the asymmetric profile shape as modeled by Hölzer. This analysis accounted for the reduction in the FWHM values of the emission spectrum due to the non-uniform band-pass of the of graphite monochromator. The wavelengths and intensities of the $K\alpha_2$ lines were also refined, again with the values of the $K\alpha_{21}$ and $K\alpha_{22}$ lines constrained to one another to preserve the asymmetric shape as modeled by Hölzer. Once this analysis had quantified the impact of the monochromator and yielded an appropriate set of breadths, they were fixed for the subsequent analyses of SRM 676a. The wavelengths and intensities of the $K\alpha_2$ and satellite lines were refined, with constraints applied to the $K\alpha_2$ lines as aforementioned. The other refined parameters included scale factors, second-order Chebyshev polynomial terms for modeling of the background, the lattice parameters, terms indicating the position and intensity of the "tube tails" [18], a Soller slit value in the "full" axial divergence model [19,20] (the axial divergence of the incident and diffracted beams was constrained to be identical), specimen displacement, an attenuation term, structural parameters, size-strain and micro-strain broadening terms of a Lorentzian profile, and a micro-strain broadening term of a Gaussian profile. The very slight level of texture was modeled with a 6th order spherical harmonic.

Examination of the fit to the individual profiles revealed a discrepancy between the model and the observations in the low-angle region. It is well known that low-angle profiles are more prone to error than high-angle lines as the optical aberrations affecting their position are more complex. Also, the reported lattice parameter is more strongly affected

by angular errors in the low-angle region. The (012) line was not used in obtaining the certified parameters. The thermal expansion of alumina as reported by Shvyd'ko *et al.* [21] was used to adjust the lattice parameter to 22.5 °C. A statistical model (bivariate Gaussian random effects model [22]) was used to evaluate the components of uncertainty that reflect differences between samples of the material, and the dispersion of the replicated values measured for each sample. The resulting estimates of the lattice parameters are a = 0.475 935 53 nm and c = 1.299 231 1 nm. The corresponding Type A evaluation of these components of measurement uncertainty was done in conformity with the GUM Supplement 2 [23], and yielded $k = 2$ expanded uncertainties of 0.000 000 61 nm and 0.000 002 7 nm for a and c, respectively. However, the components of uncertainty that were evaluated by Type B methods must also be taken into account, and these are roughly one order of magnitude larger than those that were evaluated using statistical methods (Type A). Data were considered in the context of the uniformity in lattice parameter as a function of 2θ angle; this, in turn, would reflect the functionality of the FPA model. This consideration leads to an assignment of Type B uncertainties of 0.000 008 0 nm and 0.000 015 nm for a and c, respectively. The certified lattice parameters and their expanded uncertainties, Type A compounded in quadrature with Type B, are shown in Table 1. Peak positions were computed from the certified lattice parameters for Cu Kα Radiation, λ = 0.154 059 29 nm, and are shown in Table 2.

Table 1. Certified Lattice Parameters of SRM 676a

	Lattice Parameter (nm)	Expanded Uncertainty ($k = 2$)
a	0.475 935 5	± 0.000 008 0
c	1.299 231	± 0.000 015

Data for relative intensity determinations were collected from 10 randomly selected specimens on a Siemens D500 diffractometer. This machine was equipped with a focusing Ge incident beam monochromator, sample spinner/changer, and a quartz-wire position-sensitive proportional detector (PSD). The divergence slit was of 0.67° while the receiving angle of the PSD was nominally 4.5°. The PSD was also fitted with a Soller slit of 2°. Calibration of the equipment was performed using SRM 660a [24] and SRM 676 [25] using methods outlined in Cline, *et al.* [6]. Data were collected from 20° to 154° 2θ with a step width of 0.01° and a scan rate of 1° per minute. Data were analyzed with two methods using two software packages, though the results from only one are reported. The first procedure was to fit the profiles using the split Pearson VII profile shape function (PSF) as implemented within TOPAS. The second involved Rietveld analyses via GSAS [26]. The background in both analyses was represented by a tenth-order Chebyshev polynomial with a $1/x$ term. The refined parameters of the Rietveld analyses included the scale factors, Gaussian and Lorentzian crystallite size, and strain broadening as represented by the GP, LX, and LY terms of the Thompson-Cox-Hastings "Type 3" profile shape model [27], the "Type 1" polarization factor, sample shift and transparency terms, and structural parameters. Profile terms GU, GV, GW, and the peak asymmetry parameters of the Finger model [28] were fixed at values obtained from an analysis of SRM 660a. Relative intensity data were extracted with the GSAS utility REFLIST, which uses the observed structure factors, corrected for multiplicity and Lorentz-polarization factor, to compute relative intensity values. The observed structure factors are determined from a background-subtracted summation of the counts in the peak region of the raw data. The Rietveld analyses served to fit the background, determine the peak cutoff angles, and the ratio of the intensity distributed between overlapping lines. Relative intensity data correlated to better than 1 % between the two methods, which served to validate the results. Data are reported from the Rietveld analyses as these are judged more accurate because no PSF is used. The relative intensities of SRM 676a and their expanded uncertainties, using the $k = 2$ factor, are shown in Table 3.

Table 2. Peak Position Information Values for SRM 676a,
Lines Listed with a Relative Intensity >5 %, Computed Using Cu Kα Radiation, λ = 0.154 059 29 nm

Reflection Indices, h k l	Peak Position (2θ, degrees)	Reflection Indices, h k l	Peak Position (2θ, degrees)
0 1 2	25.574	3 2 4	116.085
1 0 4	35.149	0 1 14	116.602
1 1 0	37.773	4 1 0	117.835
1 1 3	43.351	4 1 3	122.019
0 2 4	52.548	1 3 10	127.671
1 1 6	57.497	3 0 12	129.870
2 1 4	66.513	2 0 14	131.098
3 0 0	68.203	1 4 6	136.056
1 0 10	76.873	1 1 15	142.314
1 1 9	77.233	4 0 10	145.153
2 2 3	84.348	0 5 4	149.185
0 2 10	88.994	1 2 14	150.102
1 3 4	91.179	1 0 16	150.413
2 2 6	95.240	3 3 0	152.380
2 1 10	101.070		

Table 3. Information Values for Relative Intensity Data from SRM 676a

Reflection Indices, h k l	Relative Intensity	Expanded Uncertainty ($k = 2$)
0 1 2	57.06	± 0.122
1 0 4	88.41	± 0.254
1 1 0	37.75	± 0.112
1 1 3	100.0	------
0 2 4	47.33	± 0.075
1 1 6	95.78	± 0.250
2 1 4	37.74	± 0.101
3 0 0	57.49	± 0.157

REFERENCES

[1] Visser, J.W.; deWolff, P.M.; *Absolute Intensities*; Report No. 641.109; Technisch Physische Dienst: Delft, The Netherlands (1964).

[2] Snyder, R.L.; *The Use of Reference Intensity Ratios in X-ray Quantitative Analysis*; Powder Diff. J., Vol. 7, No. 4, pp. 186–192 (1992).

[3] SRM 640c; *Silicon Powder Line Position and Line Shape Standard for Powder Diffraction*; National Institute of Standards and Technology; U.S. Department of Commerce: Gaithersburg, MD (2000).

[4] JCGM 100:2008; *Guide to the Expression of Uncertainty in Measurement*; (GUM 1995 with Minor Corrections), Joint Committee for Guides in Metrology (JCGM) (2008); available at http://www.bipm.org/utils/common/documents/jcgm/JCGM_100_2008_E.pdf (accessed Nov 2015).

[5] Taylor, B.N.; Kuyatt, C.E.; *Guidelines for Evaluating and Expressing the Uncertainty of NIST Measurement Results*; NIST Technical Note 1297; U.S. Government Printing Office: Washington, DC (1994); available at http://www.nist.gov/pml/pubs/index.cfm (accessed Nov 2015).

[6] Cline, J.P.; Mendenhall, M.H.; Black, D.; Windover, D.; Henins, A.; *The Optics and Alignment of the Divergent Beam Laboratory X-ray Powder Diffractometer and its Calibration Using NIST Standard Reference Materials*; J. Res. Natl. Inst. Stand. Technol., Vol. 120, pp. 173–222 (2015).

[7] Rietveld, H.M.; *Line Profiles of Neutron Powder-Diffraction Peaks for Structure Refinement*; Acta Crystallogr., Vol. 22, pp. 151–152 (1967); and Rietveld, H.M.; *A Profile Refinement Method for Nuclear and Magnetic Structures*; J. Appl. Crystallogr., Vol. 2, pp. 65–71 (1969).

[8] *The Rietveld Method*; Young, R.A., Ed.; Oxford University Press: New York (1993).

[9] *Modern Powder Diffraction*; Bish, D.L.; Post, J.E., Eds.; Rev. Mineral., Vol. 20, p. 369 (1989).
[10] BIPM; *International System of Units (SI)*, Bureau International des Poids et Mesures; 8th ed., Sèvres, France (2006); available at http://www.bipm.org/utils/common/pdf/si_brochure_8_en.pdf (accessed Nov 2012)
[11] Cheary, R.W.; Coelho, A.A.; *A Fundamental Parameters Approach to X-Ray Line-Profile Fitting;* J. Appl. Crystallogr., Vol 25, pp. 109–121 (1992).
[12] Cline, J.P.; Von Dreele, R.B.; Winburn, R.; Stephens, P.W.; Filliben, J.J.; *Addressing the Amorphous Content Issue in Quantitative Phase Analysis: The Certification of NIST SRM 676a*; Acta Crystallographica Section A, Vol. A67, pp. 357–367 (2011).
[13] SRM 660b; *Line Position and Line Shape Standard for Powder Diffraction*; National Institute of Standards and Technology; U.S. Department of Commerce: Gaithersburg, MD (29 April 2010).
[14] Black, D.R.; Windover, D.; Henins, A.; Filliben, J.; Cline, J.P.; *Certification of Standard Reference Material 660B*; Powder Diff. J., Vol. 26, No. 2, pp. 155–159 (2011).
[15] TOPAS, *General Profile and Structure Analysis Software for Powder Diffraction Data*, V4.2, Bruker AXS GmbH, Karlsruhe, Germany.
[16] Hölzer, G.; Fritsch, M.; Deutsch, M.; Härtwig, J.; Förster, E.; *$K\alpha_{1,2}$ and $K\beta_{1,3}$ X-Ray Emission Lines of the 3d Transition Metals*; Phys. Rev. A, Vol. 56, No. 6, pp. 4554–4568 (1997).
[17] Maskil, M.; Deutsch, M.; *X-Ray Kα Satellites of Copper*; Phys. Rev. A, Vol. 38, pp. 3467–3472 (1988).
[18] Bergmann, J.; Kleeberg, R.; Haase, A.; Breidenstein, B.; *Advanced Fundamental Parameters Model for Improved Profile Analysis*; Proceedings of the 5th European Conference on Residual Stresses, Delft-Noordwijkerhout, The Netherlands, September 29-30; Böttger, A.J.; Delhez, R.; Mittemeijer, E.J., Eds.; Trans Tech Publications, Vol. 347–349, pp. 303–308 (2000).
[19] Cheary, R.W.; Coelho, A.A.; *Axial Divergence in a Conventional X-Ray Powder Diffractometer I. Theoretical Foundations;* J. Appl. Crystallogr., Vol. 31, pp. 851–861, (1998),
[20] Cheary, R.W.; Coelho, A.A.; *Axial Divergence in a Conventional X-Ray Powder Diffractometer II, Implementation and Comparison with Experiment;* J. Appl. Crystallogr., Vol. 31, pp. 862–868, (1998).
[21] Shvyd'ko, Yu.V.; Lucht, M.; Gerdaua, E.; Lerche, M.; Alp, E.E.; Sturhahn, W.; Sutter, J.; Toellner, T.S.; *Measuring Wavelengths and Lattice Constants with the Mossbauer Wavelength Standard;* J. of Synchrotron Radiat., Vol. 9, pp. 17–23 (2002).
[22] Berkey, C.S.; Hoaglin, D.C.; Antczak-Bouckoms; Mosteller, F.; Colditz, G.A.; *Meta-analysis of Multiple Outcomes by Regression with Random Effects*; Statistics in Medicine, Vol. 17, No. 22, pp. 2537–2550 (1998).
[23] JCGM 102:2011; *Evaluation of Measurement Data -- Supplement 2 to the Guide to the Expression of Uncertainty in Measurement -- Extension to any number of output quantities*; JCGM (2011); available at http://www.bipm.org/utils/common/documents/jcgm/JCGM_102_2011_E.pdf (accessed Nov 2015)
[24] SRM 660a; *Lanthanum Hexaboride Powder Line Position and Line Shape Standard for Powder Diffraction*; National Institute of Standards and Technology; U.S. Department of Commerce: Gaithersburg, MD (2000).
[25] SRM 676; *Alumina Internal Standard for Quantitative Analysis by X-ray Powder Diffraction*; National Institute of Standards and Technology; U.S. Department of Commerce: Gaithersburg, MD (2005).
[26] Larson, A.C.; Von Dreele, R.B.; *General Structure Analysis System (GSAS)*; Report LAUR 86–748; Los Alamos National Laboratory: Los Alamos, NM (2003).
[27] Thompson, P., Cox, D.E., Hastings, J.B.; *Rietveld Refinement of Debye-Scherrer Synchrotron X-ray Data from Al_2O_3;* J. Appl. Crystallogr., Vol. 20, pp. 79–83 (1987).
[28] Finger, L.W.; Cox, D.E.; Jephcoat, A.P.; *A Correction for Powder Diffraction Peak Asymmetry due to Axial Divergence*; J. Appl. Crystallogr., Vol. 27, pp. 892–900 (1994).

Certificate Revision History: 04 November 2015 (Editorial changes); 23 April 2012 (Lattice parameters reported as certified values; Discussion of lattice value certification procedure included; Reference to phase purity determination included; Editorial changes); 28 January 2008 (Original certificate date).

Users of this SRM should ensure that the Certificate of Analysis in their possession is current. This can be accomplished by contacting the SRM Program: telephone (301) 975-2200; fax (301) 948-3730; e-mail srminfo@nist.gov; or via the Internet at http://www.nist.gov/srm.

APPENDIX

Acknowledgements

We would like to thank Peter L. Lee for the collection of 25 keV data on Beamline 32IDB at the Advanced Photon Source, Argonne National Laboratory (Argonne, IL). Use of the Advanced Photon Source was supported by the U.S. Department of Energy, Office of Science, Office of Basic Energy Sciences, under Contract No. DE-AC02-06CH11357. Use of the National Synchrotron Light Source, Brookhaven National Laboratory (Upton, NY), was supported by the U.S. Department of Energy, Office of Science, Office of Basic Energy Sciences, under Contract No. DE-AC02-98CH10886.

Appendix B. Certificate of Analysis SRM 674b

National Institute of Standards & Technology

Certificate of Analysis

Standard Reference Material® 674b

X-Ray Powder Diffraction Intensity Set

(Quantitative Powder Diffraction Standard)

This Standard Reference Material (SRM) consists of four oxide powders (ZnO, TiO_2, Cr_2O_3, and CeO_2), intended primarily for use as internal standards for quantitative X-ray diffraction analysis. These four oxides offer a range of linear attenuations for Cu-Kα radiation: 279 cm^{-1} (ZnO, wurtzite structure), 536 cm^{-1} (TiO_2 rutile structure), 912 cm^{-1} (Cr_2O_3 corundum structure), and 2203 cm^{-1} (CeO_2 fluorite structure) that allow the user to nominally match the standard to the unknown in order to minimize the effects of microabsorption. A unit of SRM 674b consists of approximately 10 g of each powder, bottled in an argon atmosphere.

Material Description: The powders consist of fine-grained high-purity equi-axial grains that are not in an aggregated state. The isometric form of the grains effectively eliminates preferred orientation effects in these powders. The de-aggregated state of these materials ensures the homogeneity of test mixtures prepared by conventional methods.

An analysis of the lattice parameters and phase fractions determined from X-ray powder diffraction data collected from mixtures of SRM 674b and SRM 676 [1] indicated that the SRM material was homogeneous with respect to diffraction properties.

Certified Values and Uncertainties: The certified phase purity of these materials, expressed as a mass fraction is given in Table 1.

Table 1. Certified Phase Purity Mass Fractions

Crystalline Component	Phase Purity (%)
ZnO	95.28 ± 0.64
TiO_2	89.47 ± 0.62
Cr_2O_3	95.91 ± 0.60
CeO_2	91.36 ± 0.55

The interval defined by the certified value and its uncertainty represents an expanded uncertainty using $k = t$, where t is the appropriate 2-sided 95 % confidence interval coefficient, in the absence of systematic error [2,3]. The uncertainty reported does not include that of the phase purity determination of the standard used for this certification, SRM 676.

Expiration of Certification: The certification of **SRM 674b** is valid indefinitely, within the uncertainty specified, provided the SRM is handled and stored in accordance with the instructions given in this certificate (see "Instructions for Handling, Storage, and Use"). Accordingly, periodic recalibration or recertification of this SRM is not required. The certification is nullified if the SRM is damaged, contaminated, or otherwise modified.

Maintenance of SRM Certification: NIST will monitor this SRM over the period of its certification. If substantive technical changes occur that affect the certification, NIST will notify the purchaser. Registration (see attached sheet) will facilitate notification.

The technical direction and overall coordination on the certification of this SRM were provided by J.P. Cline of the NIST Ceramics Division.

Debra L. Kaiser, Chief
Ceramics Division

Gaithersburg, MD 20899
Certificate Issue Date: 13 March 2012
Certificate Revision History on Last Page
SRM 674b

Robert L. Watters, Jr., Chief
Measurement Services Division

The material preparation, measurements, and data analysis leading to the certification of this SRM were performed by R.S. Winburn of Minot State University (Minot, ND), J.P. Cline of the NIST Ceramics Division, and R.B. Von Dreele of Argonne National Laboratory (Argonne, IL).

Statistical analysis was provided by J.J. Filliben and I. Aviles of the NIST Statistical Engineering Division.

Support aspects involved in the issuance of this SRM were coordinated through the NIST Measurement Services Division.

PREPARATION AND ANALYSIS[1]

Materials: The ZnO and TiO_2 powders of SRM 674b were obtained from Alfa Aesar (Ward Hill, MA) and Cr_2O_3 and CeO_2 powders were obtained from Cerac Inc. (Milwaukee, WI).

Certification: The oxide powders of this SRM were certified with respect to the mass fraction of material that exhibits Bragg scattering in correspondence to their crystal structure, or phase purity. The certification procedure utilized Quantitative Rietveld Analyses (QRA) [4] (for a complete discussion of the Rietveld method, see [5,6]) of neutron time-of-flight (TOF) diffraction measurements in conjunction with the use of SRM 676 as the internal standard. This procedure referenced the phase purity of SRM 674b against that of SRM 676. The basis of the method rests on an analysis of the discrepancy between the results of powder diffraction experiments, which measure the mass of material exhibiting Bragg diffraction, relative to weighing operations, which include all components.

The consideration of a long-count-time X-ray powder diffraction pattern may indicate that the sample is a high-purity powder, i.e., no peaks from impurity phases and a background that is consistent with contributions of air scatter from the incident beam and thermal diffuse scatter from the sample. However, the surface region of any crystalline material will not diffract as the bulk due to relaxation of the crystal structure and inclusion of surface reaction products. While this surface layer may only be on the order of a few crystallographic units in thickness, in a finely divided solid it can easily account for several percent of the total mass. The characterization of "phase purity" or "amorphous content" discussed herein is not in the context of a mechanically separable impurity phase, but it is a microstructural characteristic innate to the chemistry and the production history of the SRM feedstock.

The QRA of laboratory, divergent beam X-ray powder diffraction (XRPD) data displayed a systematic bias of less than 2 %; however, these results were as precise as those determined from the TOF data. Therefore, the certified phase composition was determined from the TOF data while the homogeneity of the SRM material was verified with Rietveld analyses of XRPD data. It should be noted that the mechanism inducing this bias is not operative in Reference Intensity Ratio (RIR) based methods [7] (for a complete discussion of RIR methods, see [8]). The reported, non-certified, lattice parameters were from the aforementioned Rietveld analyses of the XRPD data. While the XRPD data suffer from cent ration and penetration errors and, therefore, are not metrological in nature; a linkage is nonetheless established between of the reported lattice parameters and the X-ray emission spectrum of Cu, establishing a qualified traceability to the International System of Units (SI) [9].

Ten bottles were selected from the population in accordance to a stratified random protocol. Samples taken from two bottles were combined and admixed with SRM 676 at the 50 % level to yield a total of five samples for TOF neutron diffraction analysis. TOF data were obtained on the High Intensity Powder Diffractometer (HIPD) at the Manuel Lujan, Jr., Neutron Scattering Center (LANSCE) (Los Alamos, NM). The samples were contained in 9.5 mm diameter by 50 mm long vanadium cans during the analysis. Each sample was exposed to the neutron beam for 1.3 h with the LANSCE source operating at 70 μA proton beam current. Data used for this certification were obtained from detector banks positioned at $\pm$ 153° 2Θ covering a d-space range of 0.05 nm to 0.48 nm. The run order was randomized on an informal basis. Rietveld refinements using the General Structure Analysis System (GSAS) [10] of the phases in these samples included: scale factors, lattice parameters of the SRM 674b materials (those of SRM 676 were fixed at the certified values) a profile shape function term representing Lorentzian peak broadening [11], atomic positional and thermal parameters, a term for the diffractometer (DIFC), an absorption correction term, and six terms of a background function describing the effects of thermal diffuse and incoherent scattering. The amorphous phase content was determined from the mass fraction ratio determined from the diffraction experiment relative to that of the weighing operation, with the latter ratio being corrected for the known phase purity of SRM 676.

X-ray diffraction data for homogeneity testing and lattice parameter determination were collected on two specimens removed from each of the ten aforementioned bottles. These specimens also had SRM 676 admixed with them in a

[1] Certain commercial equipment, instrumentation or materials are identified in this certificate to adequately specify the experimental procedure. Such identification does not imply recommendation or endorsement by NIST, nor does it imply that the materials or equipment identified are necessarily the best available for the purpose.

50:50 mass ratio. These XRPD data were collected on a Siemens D5000 diffractometer equipped with a sample spinner, graphite post monochromator and scintillation detector. Copper $K\alpha_1$ radiation ($\lambda = 0.154\ 059\ 29$ nm) was used [12]. The scan range was from 20° to 155° 2Θ with a step width of 0.02° and a count time of 3.5 s/step. The divergence slit width was 0.85°; 2.3° incident Soller slits and a 0.05° receiving slit were used. The instrument was calibrated using SRM 660a [13] in conjunction with the *Fundamental Parameters Approach* [14] prior to data collection. For homogeneity testing, lattice parameter determination and microstructural characterization, the XRPD data were analyzed via the *Fundamental Parameters Approach* for Rietveld analyses as implemented in TOPAS, Bruker AXS GmbH [15]. Data analysis used the copper $K\alpha_1/K\alpha_2$ doublet described by G. Hölzer, et al. [12] with a satellite component. Axial divergence was accounted for in using the "full" axial divergence model [16]. The refined parameters included the scale factors, a background represented by a fifth order Chebyshev polynomial with a 1/x term, the lattice parameters of the SRM 674b materials, the intensities and position of the $K\alpha_2$ and satellite components of the copper $K\alpha$ emission spectrum, terms indicating the position and intensity of the "tube tails" [17], the secondary Soller slit value in the "full" axial divergence model, specimen displacement, attenuation, and size and strain (when relevant) terms. The reported crystallite size is a volume-weighted dimension, i.e., Scherrer equation, determined from the breadth of a Lorentzian profile following the $1/\cos\Theta$ relation convoluted with the instrument component. The reported strain value, $(\Delta d/d)_{hkl}$, was determined from the breadth of a Lorentzian profile following the $\tan\Theta$ relation convoluted with the instrument component. Assuming the major source of strain is dislocations, the root-mean-square (RMS) strain is 80 % of the quoted strain value [18]. Additional data, using the aforementioned instrument and configuration, were collected from three unaltered specimens of each of the SRM materials for determination of the relative intensity values. The I/I_0 [19] (for a complete discussion see [8]) and relative intensity values were determined by profile fitting of all peaks within the angular range of 20° to 70° 2Θ using the *Fundamental Parameters Approach* refinement of the non-structural terms as described above.

INSTRUCTIONS FOR HANDLING, STORAGE, AND USE

Storage: SRM 674b was bottled under an argon atmosphere to protect against humidity. Although there have been no long-term stability studies on this SRM, the oxides of which it is composed are known to be a stable in the ambient conditions of a typical laboratory. It is, therefore, believed that this SRM is stable after exposure to atmosphere. It is, nonetheless, recommended that the unused portion of the powder be stored in a tightly capped container such as the original bottle or in a manner to afford similar or greater protection against humidity.

Information Values and Uncertainties: NIST information values are considered to be of interest to the SRM user, but are not certified because the measurements are not traceable to the SI, or only a limited number of analyses were performed which disallowed imparting plausible uncertainties to the measured values. The information values determined from the aforementioned analyses of XRPD data are presented in Tables 2 through 5. The particle size distributions, determined from a disc centrifuge analyzer, are given in Table 6. The interval defined by a value and its uncertainty is a 95 % confidence interval for the true value of the mean in the absence of systematic error.

Table 2. Information Values of Lattice Parameters of SRM 674b

Component	a (nm)	c (nm)
ZnO	0.324 989 7 ± 0.000 000 38	0.520 653 ± 0.000 035
TiO_2	0.459 392 7 ± 0.000 004 4	0.295 887 5 ± 0.000 003 2
Cr_2O_3	0.495 897 9 ± 0.000 002 7	1.359 592 ± 0.000 010
CeO_2	0.541 165 1 ± 0.000 000 59	---

Table 3. Microstructural Parameters for SRM 674b

Component	Crystallite Size L (nm)	Microstrain
ZnO	201.4 ± 2.5	---
TiO_2	281.6 ± 9.9	0.064 ± 0.002
Cr_2O_3	380.2 ± 14.4	0.045 ± 0.001
CeO_2	380.6 ± 4.5	---

Table 4. I/I_c Values for SRM 674b

Component	I/I_c
ZnO	4.95 ± 0.01
TiO_2	3.44 ± 0.01
Cr_2O_3	1.97 ± 0.02
CeO_2	12.36 ± 0.09

Table 5. Relative Intensity Values of SRM 674b

ZnO

h k l	Angle	Rel I (%)
1 0 0	31.76	61.30 ± 2.34
0 0 2	34.41	37.24 ± 2.10
1 0 1	36.25	100.0 ----
1 0 2	47.53	22.29 ± 0.66
1 1 0	56.59	37.72 ± 1.44
1 0 3	62.85	30.28 ± 1.14
2 0 0	66.37	5.25 ± 0.24
1 1 2	67.94	27.13 ± 0.12
2 0 1	69.08	14.12 ± 0.32

TiO_2

h k l	Angle	Rel I (%)
1 1 0	27.45	100.0 ----
1 0 1	36.09	37.70 ± 1.50
2 0 0	39.20	5.96 ± 0.12
1 1 1	41.25	18.70 ± 0.48
2 1 0	44.05	7.46 ± 0.25
2 1 1	54.32	55.14 ± 1.58
2 2 0	56.63	17.48 ± 0.31
0 0 2	62.76	6.94 ± 0.40
3 1 0	64.05	8.03 ± 0.21
3 0 1	69.00	19.41 ± 0.62
1 1 2	69.80	8.96 ± 0.58

Cr_2O_3

h k l	Angle	Rel I (%)
0 1 2	24.52	66.71 ± 1.71
1 0 4	33.62	100.0 ----
1 1 0	36.22	81.27 ± 4.78
0 0 6	39.77	7.36 ± 0.93
1 1 3	41.50	31.64 ± 0.60
2 0 2	44.22	5.24 ± 0.25
0 2 4	50.24	39.64 ± 1.10
1 1 6	54.86	96.42 ± 0.64
1 2 2	58.42	8.17 ± 0.74
2 1 4	63.48	31.06 ± 1.55
3 0 0	65.13	39.31 ± 1.43
1 0 10	72.95	20.88 ± 1.53

CeO_2

h k l	Angle	Rel I (%)
1 1 1	28.61	100.0 ----
2 0 0	33.14	27.21 ± 0.46
2 2 0	47.54	54.21 ± 0.56
3 1 1	56.39	43.58 ± 0.60
2 2 2	59.14	8.29 ± 0.38
4 0 0	69.46	8.03 ± 0.25

Table 6. Particle Size Data for SRM 674b Determined Using a Disk Centrifuge Analyzer

Mass Percent Less Than (µm)	Components			
	ZnO	TiO_2	Cr_2O_3	CeO_2
10 %	0.22	0.41	0.34	0.53
16 %	0.28	0.55	0.38	0.65
50 %	0.58	0.93	0.56	1.13
84 %	1.15	1.38	1.05	1.91
90 %	1.55	1.66	1.45	2.18

REFERENCES

[1] SRM 676; *Alumina Internal Standard for Quantitative Analysis by X-ray Powder Diffraction*; National Institute of Standards and Technology; U.S. Department of Commerce: Gaithersburg, MD (20 September 2005).

[2] JCGM 100:2008; *Evaluation of Measurement Data — Guide to the Expression of Uncertainty in Measurement* (ISO GUM 1995 with Minor Corrections); Joint Committee for Guides in Metrology (JCGM) (2008); available at http://www.bipm.org/utils/common/documents/jcgm/JCGM_100_2008_E.pdf (accessed Mar 2012).

[3] Taylor, B.N.; Kuyatt, C.E.; *Guidelines for Evaluating and Expressing the Uncertainty of NIST Measurement Results*; NIST Technical Note 1297; U.S. Government Printing Office: Washington, DC (1994); available at http://www.nist.gov/pml/pubs/index.cfm (accessed Mar 2012).

[4] Rietveld, H.M.; *Line Profiles of Neutron Powder Diffraction Peaks for Structure Refinement*; Acta Crytsallogr., Vol. 22, pp. 151–152 (1967); and Rietveld, H.M.; *A Profile Refinement Method for Nuclear and Magnetic Structures*; J. Appl. Crystallogr., Vol. 2, pp. 65–71 (1969).

[5] *The Rietveld Method*; Young, R.A., Ed.; Oxford University Press (1993).

[6] *Modern Powder Diffraction*; Bish, D.L.; Post, J.E., Eds.; Rev. Mineral., Vol. 20 (1989).

[7] Chung, F.H.; *Quantitative Interpretation of X-ray Diffraction Patterns. I. Matrix-Flushing Method of Multi Component Analysis*; J. Appl. Crystallogr., Vol. 7, pp. 519–525 (1974); and Chung, F.H.; *Quantitative Interpretation of X-ray Diffraction Patterns. II. Adiabatic Principle of X-ray Diffraction Analysis of Mixtures*; J. Appl. Crystallogr., Vol. 7, pp. 526–531 (1974).

[8] Snyder, R.L.; *The Use of Reference Intensity Ratios in X-ray Quantitative Analysis*; Powder Diff. J., Vol. 7, No. 4, pp. 186–192 (1992).

[9] *International System of Units (SI)*, 7th ed.; Bureau International des Poids et Mesures, Sèvres, France (1998).

[10] Larson, A.C.; Von Dreele, R.B.; *General Structure Analysis System (GSAS)*; Report LAUR 86-748; Los Alamos National Laboratory: Los Alamos, NM (2003).

[11] Von Dreele, R.B.; Jorgensen, J.D.; Windsor, C.G.; *Rietveld Refinement with Spallation Neutron Powder Diffraction Data*; J. Appl. Crystallogr., Vol. 15, pp. 581–589 (1982).

[12] Hölzer, G.; Fritsch, M.; Deutsch, M.; Härtwig, J.; Förster, E.; *$K\alpha_{1,2}$ and $K\beta_{1,3}$ X-ray Emission Lines of the 3d Transition Metals*; Phys. Rev. A, Vol. 56, No. 6, pp. 4554–4568 (1997).

[13] SRM 660a; *Lanthanum Hexaboride Powder Line Position and Line Shape Standard for Powder Diffraction*; National Institute of Standards and Technology; U.S. Department of Commerce: Gaithersburg, MD (13 September 2000).

[14] Cheary, R.W.; Coelho, A.A.; *A Fundamental Parameters Approach to X-ray Line-Profile Fitting*; J. Appl. Crystallogr., Vol. 25, pp. 109–121 (1992).

[15] TOPAS; *General Profile and Structure Analysis Software for Powder Diffraction Data*, V2.1; Bruker AXS GmbH: Karlsruhe, Germany.

[16] Cheary, R.W.; Coelho, A.A.; *Axial Divergence in a Conventional X-ray Powder Diffractometer I, Theoretical Foundations*; J. Appl. Crystallogr., Vol. 31, pp. 851–861 (1998); and Cheary, R.W.; Coelho, A.A.; *Axial Divergence in a Conventional X-ray Powder Diffractometer II, Implementation and Comparison with Experiment*; J. Appl. Crystallogr., Vol. 31, pp. 862–868 (1998).

[17] Bergmann, J.; Kleeberg, R.; Haase, A.; Breidenstein, B.; *Advanced Fundamental Parameters Model for Improved Profile Analysis*; In Proceedings of the 5th European Conference on Residual Stresses: Delft-Noordwijkerhout, The Netherlands, September 29–30 (1999); Böttger, A.J.; Delhez, R.; Mittemeijer, E.J., Eds.; Trans Tech Publications; Materials Science Forum, Vol. 347–349, pp. 303–308 (2000).

[18] Klug, H.P.; Alexander, L.E.; *X-ray Diffraction Procedures*; ISBN 0-471-49369-4; John Wiley & Sons: New York (1974).

[19] Visser, J.W.; deWolff, P.M.; *Absolute Intensities*; Report No. 641.109; Technisch Physische Dienst: Delft, The Netherlands (1964).

Certificate Revision History: 13 March 2012 (Corrected ZnO c lattice parameter and uncertainty; corrected the ZnO and TiO_2 relative intensity values; editorial changes); 21 November 2011 (Updated title; editorial changes); 27 September 2011 (Updated title; editorial changes); 29 January 2007 (Correction of datum for the angle at hkl_{222} in Table 5 for CeO_2; Restatement of datum applicable to the receiving slit used in the scan range; editorial changes); 21 September 2005 (Original certificate date).

Users of this SRM should ensure that the Certificate of Analysis in their possession is current. This can be accomplished by contacting the SRM Program: telephone (301) 975-2200; fax (301) 926-4751; e-mail srminfo@nist.gov; or via the Internet at http://www.nist.gov/srm.

Appendix C. Certificate of Analysis SRM 2686 Clinker

National Institute of Standards & Technology

Certificate of Analysis

Standard Reference Material® SRM 2686

Portland Cement Clinker

This Standard Reference Material (SRM) is intended for use in evaluating methods of phase abundance analysis of major phases in cement clinkers: the percentages of alite (C_3S)[1], belite[2] (β-C_2S), aluminate (C_3A), ferrite (C_4AF), and periclase (M). Each unit consists of three hermetically-sealed containers of approximately 10 g each of crushed portland cement clinker. The materials selected for SRMs 2686, 2687, and 2688 differ widely in phase abundance, crystal sizes, and distribution of crystals [1,2].

Certified Values: The certified values for SRM 2686, expressed as mass fractions, are provided in Table 1. A NIST certified value is a value for which NIST has the highest confidence in its accuracy, in that all known or suspected sources of bias have been investigated or accounted for by NIST. The certified values listed are based on the results of analyses performed at NIST using quantitative X-ray powder diffraction (QXRD) and from optical microscopy point count analyses conducted by both Construction Technology Laboratories, Inc. (CTL)[3] and ASTM C 1.23 Microscopy Task Group (MPC) [3,4]. The MPC analyses followed ASTM C 1356M [5] and the QXRD used Reitveld refinement of powder diffraction data [6,7].

Sampling for the X-ray study allowed assessment of within and between vial homogeneity and found the materials to be homogeneous. The uncertainty listed with each value is an expanded uncertainty, with coverage factor 2, calculated by combining a between-method variance [8,9] with a pooled, within-method variance following the ISO/NIST Guide [10].

Informational Values: Information values for SRM 2686, expressed as mass fractions on an as-received basis, are provided in Table 2. Information values are noncertified values with no uncertainty assessed that are provided for information purposes only.

Expiration of Certification: The certification of this SRM is valid, within the measurement uncertainties specified, until **01 December 2007**, provided the SRM is handled and stored in accordance with the instructions given in this certificate (see Use and Handling). However, the certification will be nullified if the SRM is damaged, contaminated, or otherwise modified.

Coordination of technical measurements for certification was accomplished under the direction of P.E. Stutzman of the NIST Building Materials Division. Analytical measurements for certification of this SRM were performed by P.E. Stutzman of the NIST Building Materials Division, D. Campbell of CTL, Skokie, IL, and ASTM C 1.23.01 Task Group on Microscopy Methods.

Statistical consultation for this SRM was provided by S.D. Leigh of the NIST Statistical Engineering Division.

Support aspects involved in the preparation, certification, and issuance of this SRM were coordinated through the NIST Standard Reference Materials Program by B.S. MacDonald.

Geoffrey Frohnsdorff, Chief
Building Materials Division

Gaithersburg, MD 20899
Certificate Issue Date: 04 February 2002

John Rumble, Jr., Acting Chief
Standard Reference Materials Program

---

[1] Cement chemist's notation: C = CaO, S = SiO_2, A = Al_2O_3, F = Fe_2O_3, M = MgO.

[2] Belite is the β crystalline form of dicalcium silicate, C_2S.

[3] Certain commercial organizations, services, equipment, or materials are identified in this certificate to specify adequately the experimental procedure. Such identification does not imply recommendation or endorsement by the National Institute of Standards and Technology, nor does it imply that the organizations, services, materials, or equipment identified are necessarily the best available for the purpose.

Stability: This material is considered to be stable during the period of certification. NIST will monitor this material and will report any significant changes in certification to the purchaser as mentioned at the end of this document.

Source and Processing: A portion of the bulk material used for SRM 2686 had been used to make approximately 2500 vials of RM 8486 Portland Cement Clinker released in 1989. Details of the original processing of this bulk material are provided in the Report of Investigation for RM 8486 [1]. In 2000, the remaining bulk material was divided by the spinning riffler technique into vials containing approximately 10 g each and capped. Each vial was sealed in a foil bag and subsequently issued in sets of three vials as SRM 2686.

Use and Handling: Cement clinker is hygroscopic and storage over desiccant is recommended to minimize the effects of exposure to humidity. Changes in the appearance of the etched surface of polished sections, particularly the appearance of free lime, if present, which hydrates to epezite (calcium hydroxide) indicate change due to moisture exposure. Epezite exhibits a popcorn-like texture and high topographic relief. For XRD analysis, the presence of calcium hydroxide or calcium carbonate may be taken as an indication that moisture has altered the free lime. For XRD powders, heat-treating to 450 °C converts calcium hydroxide back to free lime without other alteration.

Table 1. Certified Values for SRM 2686

Major phases in cement clinker, expressed as mass fractions (in %), with mean and expanded uncertainty ($U = 2\,u_c$) at an approximate confidence level at 95 % [9,10].

Phase	Mass Fraction (%)		
Alite	58.6	±	4.0
Belite	23.3	±	2.8
Ferrite	14.1	±	1.4
Aluminate	2.3	±	2.1
Periclase	3.3	±	1.9

Table 2. Informational Values for SRM 2686

Elemental constituents determined by X-ray fluorescence spectrometry [1] and expressed as the chemical forms and in the order given in ASTM C 114-00, Section 3, Table 1 [12].

Constituent	Mass Fraction (%)	Constituent	Mass Fraction (%)	Constituent	Mass Fraction (%)
SiO_2	22.48	MgO	4.73	TiO_2	0.25
Al_2O_3	4.70	SO_3	0.27	P_2O_5	0.06
Fe_2O_3	3.60	Na_2O	0.10	Mn_2O_3	0.10
CaO	63.36	K_2O	0.42	SrO	0.05
				L.O.I.	0.16

Free Lime (mass fraction): 0.3 %*

*Based on optical microscopy and atomic absorption analysis of an ethyl acetoacetate extraction

Calculated Compounds (per ASTM C 150-98)	Mass Fraction (%)
C_3S	50
C_2S	27
C_3A	6
C_4AF	11

REFERENCES

[1] Report of Investigation, Reference Materials (RM) 8486, 8487, 8488, Portland Cement Clinkers, NIST, Gaithersburg, MD, (22 May 1989).

[2] Stutzman, P. and Leigh, S., "Phase Composition Analysis of the NIST Reference Clinkers by Optical Microscopy and X-ray Powder Diffraction," NIST Technical Note 1441.

[3] Struble, L., "A Review of Clinker Analysis by QXRD," in Characterization and Performance Prediction of Cement and Concrete, J.F. Young, Ed., New York, Engineering Foundation, pp. 31-37, (1982).

[4] Campbell, D.H., Microscopical Examination and Interpretation of Portland Cement and Clinker, 2nd Ed., The Portland Cement Association Research and Development Serial No. 1754, p. 202 (1999).

[5] ASTM C 1356M-96, "Standard Test Method for Quantitative Determination of Phases in Portland Cement Clinker by Microscopical Point-Count Procedure," ASTM Standards, **Vol. 4.01**, American Society for Testing and Materials, West Conshohocken, PA, (1999).

[6] Young, R.A., Ed., The Rietveld Method, International Union of Crystallography Monographs on Crystallography 5, Oxford University Press.

[7] ASTM C 1365 - 98, "Standard Test Method for Determination of the Proportions of Phases in Portland Cement and Portland Cement Clinker Using X-ray Powder Diffraction Analysis," ASTM Standards, **Vol. 04.01**, American Society for Testing and Materials, West Conshohocken, PA, (1999).

[8] Rukhin, A.L. and Vangel, M.G., "Estimation of a Common Mean and Weighted Means Statistics," Journal of the American Statistical Association, **Vol. 93**, No. 441, pp. 303-308, (March 1998).

[9] Levenson, M.S., Banks, D.L., Eberhardt, K.R., Gill, L.M., Guthrie, W.F., Liu, H.K., Vangel, M.G., Yen, J.H., and Zhang, N.F., "An Approach to Combining Results from Multiple Methods Motivated by the ISO GUM," J. Res. Natl. Inst. Stand. Technol., **Vol. 105**, No. 4, p. 571, (2000).

[10] *Guide to the Expression of Uncertainty in Measurement*, ISBN 92-67-10188-9, 1st Ed., ISO, Geneva, Switzerland, (1993); see also Taylor, B.N. and Kuyatt, C.E., "Guidelines for Evaluating and Expressing the Uncertainty of NIST Measurement Results," NIST Technical Note 1297, U.S. Government Printing Office, Washington, DC, (1994); available at http://physics.nist.gov/Pubs/.

[11] ASTM C 150-98, "Standard Specification for Portland Cement," ASTM Standards, **Vol. 04.01**, American Society for Testing and Materials, West Conshohocken, PA, (1999).

[12] ASTM C 114-00, "Test Methods for Chemical Analysis of Hydraulic Cement," **Vol. 04.01**, American Society for Testing and Materials, West Conshohocken, PA, (1999).

Users of this SRM should ensure that the certificate in their possession is current. This can be accomplished by contacting the SRM Program at: telephone (301) 975-6776; fax (301) 926-4751; e-mail srminfo@nist.gov; or via the Internet http://www.nist.gov/srm.

Appendix D. Certificate of Analysis SRM 2687 Clinker

National Institute of Standards & Technology

Certificate of Analysis

Standard Reference Material® 2687

Portland Cement Clinker

This Standard Reference Material (SRM) is intended for use in evaluating methods of phase abundance analysis of major phases in cement clinkers: the percentages of alite (C_3S)[1], belite (C_2S), aluminate (C_3A), ferrite (C_4AF), and arcanite (K_2SO_4). A unit of SRM 2687 consists of three hermetically sealed vials, each containing approximately 10 g of crushed portland cement clinker. The materials selected for SRMs 2686a, 2687, and 2688 differ widely in phase abundance, crystal sizes, and distribution of crystals [1,2].

Certified Values: The certified values for SRM 2687, expressed as mass fractions, are provided in Table 1. A NIST certified value is a value for which NIST has the highest confidence in its accuracy, in that all known or suspected sources of bias have been investigated or taken into account [3]. The certified values listed are weighted averages, the results of analyses performed at NIST using quantitative X-ray powder diffraction (QXRD), point-counting of scanning electron microscope backscattered electron images, and data from an ASTM interlaboratory study that used the SRM clinkers [4]. The QXRD used Reitveld refinement of powder diffraction data [5,6].

Sampling for the X-ray study allowed assessment of within-and between-vial homogeneity and found the materials to be homogeneous. The uncertainty listed with each value is an expanded uncertainty, $U = ku_c$, with coverage factor $k = 2$, calculated by combining a between-method variance [7] with a pooled, within-method variance following the ISO Guide [8].

Information Values: An information value is considered to be a value that will be of interest to the SRM user, but insufficient information is available to assess the uncertainty associated with the value [3]. Bulk oxide values determined by X-ray fluorescence and loss on ignition are provided in Table 2. Calculated compounds per ASTM C 150-07 are provided in Table 3.

Expiration of Certification: The certification of **SRM 2687** is valid, within the measurement uncertainty specified, until **01 December 2015**, provided the SRM is handled in accordance with instructions given in this certificate (see "Instructions for Use"). The certification is nullified if the SRM is damaged, contaminated, or otherwise modified.

Maintenance of SRM Certification: NIST will monitor this SRM over the period of its certification. If substantive technical changes occur that affect the certification before expiration, NIST will notify the purchaser. Registration (see attached sheet) will facilitate notification.

The overall direction and coordination of the analytical measurements leading to certification were performed by P.E. Stutzman and G. Lespinasse of the NIST Construction Materials Division.

Statistical consultation for this SRM was provided by S.D. Leigh of the NIST Statistical Engineering Division.

Support aspects involved with the certification and issuance of this SRM were coordinated through the NIST Measurement Services Division.

Jonathan W. Martin, Chief
Materials and Construction Research Division

Gaithersburg, MD 20899
Certificate Issue Date: 14 December 2010
Certificate Revision History on Last Page

Robert L. Watters, Jr., Chief
Measurement Services Division

[1] Cement chemist's notation: C = CaO, S = SiO_2, A = Al_2O_3, F = Fe_2O_3.

INSTRUCTIONS FOR USE

Use and Handling: Cement clinker is hygroscopic, so storage over desiccant is recommended to minimize the effects of exposure to humidity. Changes in the appearance of the etched surface of polished sections, particularly the appearance of free lime, which hydrates to epezite (calcium hydroxide), indicate change due to moisture exposure. Epezite exhibits a popcorn-like texture and high topographic relief. For XRD analysis, the presence of calcium hydroxide or calcium carbonate may be taken as an indication that moisture has altered the free lime. For XRD powders, heat-treating to 450 °C converts calcium hydroxide back to free lime without other alteration.

Table 1. Certified Values for Phase Abundance (Mass Fraction in %) of SRM 2687 [2–8].

SRM 2687	Alite	Belite	Aluminate	Ferrite	Arcanite
Mean	71.24	12.57	11.82	2.81	0.92
U	1.27	1.22	1.03	0.68	0.15

Table 2. Information Values for Bulk Chemistry Mass Fractions by X-Ray Fluorescence [1] and Loss on Ignition (LOI).

SiO_2	Al_2O_3	Fe_2O_3	CaO	MgO	SO_3	Na_2O	K_2O	TiO_2	P_2O_5	Mn_2O_3	SrO	LOI
21.43	5.53	1.98	67.20	1.48	0.83	0.14	0.72	0.27	0.29	0.04	0.11	0.17

Free Lime (Mass Fraction)[a]
2.2 %

[a] Based on optical microscopy and atomic absorption analysis of an ethyl acetoacetate extraction.

Table 3. Information Values for Calculated Compounds per ASTM C 150-07.

Phase	Mass Fraction (%)
alite	68.3
belite	9.9
aluminate	11.3
ferrite	6.0

REFERENCES

[1] Kanare, H.; *Production of Portland Cement Clinker Phase Abundance Standard Reference Materials (SRMs 2686, 2687, 2688)*; Final Report, Construction Technology Laboratories (1987).

[2] Stutzman, P.; Lespinasse, G.; Leigh, S.; *Compositional Analysis and Certification of NIST Reference Material Clinker 2686a*; NIST Technical Note 1602; U.S. Government Printing Office: Washington, DC (2008).

[3] May, W.; Parris, R.; Beck II, C.; Fassett, J.; Greenberg, R.; Guenther, F.; Kramer, G.; Wise, S.; Gills, T.; Colbert, J.; Gettings, R.; MacDonald, B.; *Definition of Terms and Modes Used at NIST for Value-Assignment of Reference Materials for Chemical Measurements*; NIST Special Publication 260-136 (2000); available at http://ts.nist.gov/MeasurementServices/ReferenceMaterials/PUBLICATIONS.cfm (accessed Arp 2010).

[4] ASTM C 1356M, *Standard Test Method for Quantitative Determination of Phases in Portland Cement Clinker by Microscopical Point-Count Procedure*; Annul. Book of ASTM Stand., Vol. 4.01 (2006).

[5] Stutzman, P; S. Leigh; *Phase Analysis of Hydraulic Cements by X-Ray Powder Diffraction: Precision, Bias and Qualification*; Journal of ASTM International, Vol. 4, No. 5, JAI Paper 101085 (2007).

[6] R.A. Young; *The Rietveld Method*; IUCr Monographs on Crystallography, Vol. 5, Oxford Science Publications, Oxford University (1995).

[7] Rukhin, A.L.; Vangel, M.G.; *Estimation of a Common Mean and Weighted Means Statistics*; J. Am. Stat. Assoc., Vol. 93, No. 441, pp. 303–308 (1998).

[8] JCGM 100:2008; *Evaluation of Measurement Data — Guide to the Expression of Uncertainty in Measurement* (ISO GUM 1995 with Minor Corrections); Joint Committee for Guides in Metrology (2008); available at http://www.bipm.org/utils/common/documents/jcgm/JCGM_100_2008_E.pdf (accessed Apr 2010); see also Taylor, B.N.; Kuyatt, C.E.; *Guidelines for Evaluating and Expressing the Uncertainty of NIST Measurement Results*; NIST Technical Note 1297; U.S. Government Printing Office: Washington, DC (1994); available at http://www.nist.gov/physlab/pubs/index.cfm (accessed Apr 2010).

Certificate Revision History: 14 December 2010 (Minor editorial changes); 15 April 2010 (Updated certified values and extended the certification period); 04 February 2002 (Original certificate date).

Users of this SRM should ensure that the Certificate of Analysis in their possession is current. This can be accomplished by contacting the SRM Program: telephone (301) 975-2200; fax (301) 926-4751; e-mail srminfo@nist.gov; or via the Internet at http://www.nist.gov/srm.

Appendix E. Certificate of Analysis SRM 2688 Clinker

National Institute of Standards & Technology

Certificate of Analysis

Standard Reference Material® 2688

Portland Cement Clinker

This Standard Reference Material (SRM) is intended for use in evaluating methods of phase abundance analysis of major phases in cement clinkers: the percentages of alite (C_3S)[1], belite (C_2S), aluminate (C_3A), and ferrite (C_4AF). A unit of SRM 2688 consists of three hermetically sealed vials, each containing approximately 10 g of crushed portland cement clinker. The materials selected for SRMs 2686a, 2687, and 2688 differ widely in phase abundance, crystal sizes, and distribution of crystals [1,2].

Certified Values: The certified values for SRM 2688, expressed as mass fractions, are provided in Table 1. A NIST certified value is a value for which NIST has the highest confidence in its accuracy, in that all known or suspected sources of bias have been investigated or taken into account [3]. The certified values listed are weighted averages, the results of analyses performed at NIST using quantitative X-ray powder diffraction (QXRD), point-counting of scanning electron microscope backscattered electron images, and data from an ASTM interlaboratory study that used the SRM clinkers [4]. The QXRD used Reitveld refinement of powder diffraction data [5,6].

Sampling for the X-ray study allowed assessment of within-and between-vial homogeneity and found the materials to be homogeneous. The uncertainty listed with each value is an expanded uncertainty, $U = ku_c$, with coverage with coverage factor $k = 2$, calculated by combining a between-method variance [7] with a pooled, within-method variance following the ISO Guide [8].

Information Values: An information value is considered to be a value that will be of interest to the SRM user, but insufficient information is available to assess the uncertainty associated with the value [3]. Bulk oxide values by X-ray fluorescence and loss on ignition are provided in Table 2. Calculated compounds per ASTM C 150-07 are provided in Table 3.

Expiration of Certification: The certification of **SRM 2688** is valid, within the measurement uncertainty specified, until **01 December 2015**, provided the SRM is handled in accordance with instructions given in this certificate (see "Instructions for Use"). The certification is nullified if the SRM is damaged, contaminated, or otherwise modified.

Maintenance of SRM Certification: NIST will monitor this SRM over the period of its certification. If substantive technical changes occur that affect the certification before expiration, NIST will notify the purchaser. Registration (see attached sheet) will facilitate notification.

The overall direction and coordination of the analytical measurements leading to certification were performed by P.E. Stutzman and G. Lespinasse of the NIST Construction Materials Division.

Statistical consultation for this SRM was provided by S.D. Leigh of the NIST Statistical Engineering Division.

Support aspects involved with the certification and issuance of this SRM were coordinated through the NIST Measurement Services Division.

Jonathan W. Martin, Chief
Materials and Construction Research Division

Gaithersburg, MD 20899
Certificate Issue Date: 16 April 2010
See Certificate Revision History on Last Page

Robert L. Watters, Jr., Chief
Measurement Services Division

[1] Cement chemist's notation: C = CaO, S = SiO_2, A = Al_2O_3, F = Fe_2O_3.

INSTRUCTIONS FOR USE

Use and Handling: Cement clinker is hygroscopic, so storage over desiccant is recommended to minimize the effects of exposure to humidity. Changes in the appearance of the etched surface of polished sections, particularly the appearance of free lime, which hydrates to epezite (calcium hydroxide), indicate change due to moisture exposure. Epezite exhibits a popcorn-like texture and high topographic relief. For XRD analysis, the presence of calcium hydroxide or calcium carbonate may be taken as an indication that moisture has altered the free lime. For XRD powders, heat-treating to 450 °C converts calcium hydroxide back to free lime without other alteration.

Table 1. Certified Values for Phase Abundance (Mass Fraction in %) of SRM 2688.

SRM 2688	Alite	Belite	Aluminate	Ferrite
Mean	64.95	17.45	4.99	12.20
U	1.04	0.96	0.50	0.84

Table 2. Information Values for Bulk Chemistry Mass Fractions by X-Ray Fluorescence (XRF) [1] and Loss on Ignition (LOI).

SiO_2	Al_2O_3	Fe_2O_3	CaO	MgO	SO_3	Na_2O	K_2O	TiO_2	P_2O_5	Mn_2O_3	SrO	LOI
22.68	4.90	4.07	66.50	0.98	0.31	0.11	0.35	0.24	0.08	0.03	0.13	0.21

Free Lime (Mass Fraction)[a]
0.2 %

[a] Based on optical microscopy and atomic absorption analysis of an ethyl acetoacetate extraction.

Table 3. Information Values for Calculated Compounds per ASTM C 150-07.

Phase	Mass Fraction (%)
alite	58.7
belite	20.7
aluminate	6.1
ferrite	12.4

REFERENCES

[1] Kanare, H.; *Production of Portland Cement Clinker Phase Abundance Standard Reference Materials (SRMs 2686, 2687, 2688)*; Final Report, Construction Technology Laboratories (1987).

[2] Stutzman, P.; Lespinasse, G.; Leigh, S.; *Compositional Analysis and Certification of NIST Reference Material Clinker 2686a*; NIST Technical Note 1602; U.S. Government Printing Office: Washington, DC (2008).

[3] May, W.; Parris, R.; Beck II, C.; Fassett, J.; Greenberg, R.; Guenther, F.; Kramer, G.; Wise, S.; Gills, T.; Colbert, J.; Gettings, R.; MacDonald, B.; *Definition of Terms and Modes Used at NIST for Value-Assignment of Reference Materials for Chemical Measurements*; NIST Special Publication 260-136 (2000); available at http://ts.nist.gov/MeasurementServices/ReferenceMaterials/PUBLICATIONS.cfm (accessed Apr 2010).

[4] ASTM C 1356M, *Standard Test Method for Quantitative Determination of Phases in Portland Cement Clinker by Microscopical Point-Count Procedure*; Annul. Book of ASTM Stand., Vol. 4.01 (2006).

[5] Stutzman, P; S. Leigh; *Phase Analysis of Hydraulic Cements by X-Ray Powder Diffraction: Precision, Bias and Qualification*; Journal of ASTM International, Vol. 4, No. 5, JAI Paper 101085 (2007).

[6] R.A. Young; *The Rietveld Method*; IUCr Monographs on Crystallography, Vol. 5, Oxford Science Publications, Oxford University (1995).

[7] Rukhin, A.L.; Vangel, M.G.; *Estimation of a Common Mean and Weighted Means Statistics*; J. Am. Stat. Assoc., Vol. 93, No. 441, pp. 303-308 (1998).

[8] JCGM 100:2008; *Evaluation of Measurement Data — Guide to the Expression of Uncertainty in Measurement* (ISO GUM 1995 with Minor Corrections); Joint Committee for Guides in Metrology (2008); available at http://www.bipm.org/utils/common/documents/jcgm/JCGM_100_2008_E.pdf (accessed Mar 2010); see also Taylor, B.N.; Kuyatt, C.E.; *Guidelines for Evaluating and Expressing the Uncertainty of NIST Measurement Results*; NIST Technical Note 1297; U.S. Government Printing Office: Washington, DC (1994); available at http://www.nist.gov/physlab/pubs/index.cfm (accessed Apr 2010).

Certificate Revision History: 16 April 2010 (The certified values for alite, belite, aluminate and ferrite were updated and the arcanite value was decertified. The certification period was extended.); 04 February 2002 (Original certificate date).

Users of this SRM should ensure that the Certificate of Analysis in their possession is current. This can be accomplished by contacting the SRM Program: telephone (301) 975-2200; fax (301) 926-4751; e-mail srminfo@nist.gov; or via the Internet at http://www.nist.gov/srm.